Experimental study of vertical jets in JONSWAP random waves

A thesis submitted in partial fulfillment of the requirements for the Degree of Master of Philosophy

by
TAM Ying Fan Barry

Department of Civil and Structural Engineering
The Hong Kong Polytechnic University
August 2005

CERTIFICATE OF ORIGINALITY

I hereby declare that this thesis is my own work and that, to the best of my knowledge and belief, it reproduces no material previously published or written nor material which has been accepted for the award of any other degree or diploma, except where due acknowledgement has been made in the text.

TAM, Ying Fan Barry

Abstract: The most common practice for wastewater disposal is to discharge the treated effluent into a large water body, such as oceans and streams. This is because the large volume of fluid provides a very good environment for dilution of the treated effluent. Consequently, an initial lower level of treatment scheme is sufficient before the discharge. Wastewater discharged into ambient fluid, thus, offers an economically attractive form of disposal.

Waves appear in all open coastal areas around the world. Waves are usually generated by wind and distant swell and normally have various frequencies and are random. The effect of regular surface waves on jets has been studied before and the results show that the jet fluid mixing process will be enhanced. Similar effect is expected for jet discharge in natural random wave environments.

The jet-wave interaction process has been investigated for many years with most studies focusing on the interaction between jet and regular waves. However, an investigation of the jet characteristics in the presence of random waves has received less attention. In an attempt to fill this knowledge gap and deepen the understanding of jet behaviour, an experimental study on a round jet in random surface waves is carried out in a laboratory wave flume.

A submerged turbulent jet, fed from a constant head water tank, discharges vertically at the bottom of the flume in which random waves are generated by a DHI

random-wave maker. An acoustic Doppler velocimeter (ADV) is employed to measure the jet velocity as well as the associated velocity fluctuation within the jet body for time-averaged analysis.

Wave-induced characteristic velocities and wave-induced momentum characteristic lengths are developed based on the wave energy spectrum. Those developed scaled parameters are then used in the data analysis.

The time-varying experimental data are collected. The jet characteristics such as the declining rate of jet centerline velocity, the jet spread rate, cross-sectional velocity profiles and the turbulence intensity are investigated. The results show that the jet centerline velocity in the random wave environment, in general, decays faster than that in the stagnant environment. With the use of dimensional analysis, the velocity variation is similar to that in the pure jet condition when the non-dimensional jet distance is short (i.e. $z/l_w \le 0.1$) while the degree of data scattering increases when $z/l_w > 0.1$. This result can be explained by the existence of transition region between the jet-momentum governed region and the wave momentum governed region. A non-linear jet half-width spread rate is also observed. This can be explained by that more ambient water is entrapped into the jet body due to the additional turbulent entrainment contributed by the wave-induced cross-current. Empirical formulas are proposed to predict the velocity decay rate and

the jet width spread rate. The cross-sectional velocity profiles, in general, follow the normal distribution curves while multi-peak velocity profiles occasionally appear. The occurrence of multi-peak profiles in an Eulerian frame is possibly due to the periodic lateral movement of the jet trajectory arising from the wave motion. The experimental results show that waves cause a shift of the location of peak turbulence towards the jet outlet. The extent of shift in location depends on the wave properties, showing that the jet turbulence is generated by both the wave motion and jet motion.

A Lagrangian integral model of jets in random waves has been proposed. With the use of appropriate entrainment coefficients, the results obtained from the integral model are in good agreement with the experimental results. Both the integral model and the empirical formulas are also extended to prototype situation. The results show that the jet centerline dilution can be increased by 25%.

Acknowledgements

I would like to thank and acknowledge the followings:

- Professor C.W. Li for his supervision of this research and thesis writing.
- Mr. K.H. Leung, the technician of the Hydraulic Laboratory, for his assistance in the experimental setup and laboratory observations.
- Mr. Y.P. Chen for his advices in the experimental data analysis.

NOTATION

The following symbols are used in this paper:

A	=	jet nozzle area;
a	=	wave amplitude;
a_p	=	amplitude of the oscillating velocity component;
b	=	$\sqrt{R_1 R_2}$;
b, R_1, R_2	=	jet half-width, defined as the distance from the jet centerline to the velocity ratio of 1/*e;*
c	=	concentration;
d	=	jet nozzle diameter;
E	=	wave energy;
f	=	wave frequency;
f_p	=	peak wave frequency;
g	=	acceleration due to gravity;
H	=	wave height;
H_{rms}	=	root mean square wave height;
H_s	=	significant wave height;
h	=	water depth;
k, k_a	=	wave number;
L	=	wave length;
l_m, l_{sig} , l_w	=	wave length scale;
M_0	=	jet momentum;
N	=	number of data;
Q_0	=	jet discharge rate;

R	=	W_0/u_w, ratio of initial jet velocity to crossflow velocity;
r	=	radial distance from jet center;
T	=	wave period;
T_p	=	peak wave period;
T_{total}	=	total sampling time;
U_a	=	ambient flow velocity;
u_c	=	horizontal velocity at jet centerline;
u_p	=	wave-induced fluid particle velocity;
u_{sig}	=	wave-induced significant velocity;
u_w	=	wave-induced characteristic velocity;
u_{wave}	=	horizontal wave-induced velocity;
v_ξ	=	centerline velocity of the jet element relative to the ambience
v_j	=	jet velocity relative to the ambience
W_0	=	jet discharge velocity;
w	=	measured vertical velocity;
$\tilde{w}$	=	measured vertical velocity fluctuation;
w'	=	jet velocity fluctuation;
$\overline{w}$	=	mean vertical velocity;
w_c	=	vertical velocity at jet centerline;
w_w	=	wave induced velocity fluctuation;
w_{wave}	=	horizontal wave-induced velocity;
w_ξ	=	vertical component of v_j;
X	=	horizontal coordinate;
x	=	distance along horizontal jet axis;
Z, Z_a	=	flow depth measured from bottom to free surface;

z = distance along vertical jet axis;

σ_-, σ_+ = JONSWAP spectrum shape factor;

ω = angular wave frequency;

α = entrainment coefficient;

β = forced entrainment coefficient;

β_g = $\frac{\partial b}{\partial z}$, jet spread rate;

γ = angle that v_ξ makes with the jet axis;

γ_j = JONSWAP peak enhancement factor;

ε = random number;

ξ = axial direction ordinate;

κ = Phillips constant; and

λ = ratio of concentration width to velocity width

CONTENT

LIST OF FIGURES

LIST OF PHOTOS

LIST OF TABLES

1 INTRODUCTION

1.1 Background

In recent decades, people have paid more attention to environmental protection because of the realization that the environment provides the most valuable resources for human life. The wastewater disposal method is one of the current environmental protection issues. Effluent from low level wastewater treatment usually contains high level of chemical and organic contents. There is the possibility that wastewater may contain a few viable pathogens even after extensive treatment, both disposal and reuse must be accomplished with due caution. Selecting the wrong strategy for wastewater disposal may have serious consequences such as the occurrence of red tide, which damages the ecological cycle and harms our natural resources. Numerous environmental regulations, criteria and policies have been implemented to ensure that the environmental impacts of treated wastewater discharges are acceptable. This regulatory framework affects not only the selection of discharge locations and the outfall design, but also the level of treatment required. Hence, treatment and disposal are strongly linked. Selecting the right approach of wastewater disposal scheme becomes the determinant issue in the public.

1.1.1 *Water disposal in coastal areas*

The most common practice for water disposal is discharge of the treated effluent into a massive amount of fluid, i.e. oceans, streams. For cities located near coastal areas, lake and ocean disposal offer cost effective scheme for engineers when selecting a disposal scheme. The effluent is transported out to sea by pipelines along the ocean floor and discharged at multiple points through a manifold. The effluent is then diluted by the large volume of water. For wastewater discharge into the ocean, the dilution will be affected by the ocean currents and waves. The length of the pipeline and manifold required depends on the quantity of waste and the magnitude of the ocean current. The required initial dilution ratio is normally 50 times the original treated effluent for effluent discharge into the stagnant ambience.

1.1.2 *Discharge tools – water jets*

Jets and plumes are usually used as mixing devices. A jet is a fluid motion whose primary source of kinetic energy and momentum flux is a pressure drop through an orifice. A plume is a fluid motion whose main source of kinetic energy and momentum flux is the body force. This means that the fluid is discharged into another fluid of different density. Since most wastewater has a fluid density which differs from the surrounding fluid, turbulent buoyant jets or forced plumes are usually encountered wastewater disposal. The mechanics of jets, although has been studied for

ages, is still receiving a good deal of research attention. Many studies show that the use of jets can enhance the rate of mixing and the initial dilution under different conditions. A good understanding of the processes by which a jet expands in volume by entraining the surrounding fluid thus has been achieved in the literature.

1.1.3 *Surface waves in coastal areas*

Waves appear in all open coastal areas around the world. Waves are usually generated by wind and distant swell. Normally they are random in shape and have a wide range of frequencies. When wastewater is discharged into the coastal area, it is always subjected to random wave conditions. It is expected that the wave induced motion will interact with the discharge, and the wave induced oscillation will generate a bodily swaying motion while discharging. So jet-wave interaction is possibly one of the parameters which affect the wastewater entrainment process. Although the presence of waves is believed to be an additional mechanism to affect the wastewater discharge, the degree of influence on the mixing mechanism between the discharge fluid and the receiving fluid is not fully understood.

Research with regard to the jet-wave interaction has been investigated for nearly three decades. Most works examined the jet discharge under the regular wave situation and concluded that wave motions provide a positive effect in the mixing process. As mentioned above, waves in nature are in random forms and with various frequencies.

Those reported studies, considering the jets in regular waves, may not be appropriate in determining the jet characteristics in the presence of random waves in nature.

1.2 Objectives

In order to fill the knowledge gap and deepen the understanding of jet behaviour, the present study aims to identify the effect on jet discharge under the presence of random waves. Flow visualization is conducted to examine the difference of mixing behaviour between the jet discharge in stagnant ambient water and that in random wave environment.

An understanding of the hydrodynamic behaviour of outfall discharge in random waves is achieved through velocity measurement using a 10MHz acoustic Doppler velocimeter (ADV). The jet parameters obtained in the presence of JONSWAP random waves is compared with those measured in stagnant ambient environment. Previous experimental results for jets discharge in regular wave environments are also analyzed. The objective of this is to better understand the jet characteristics under different form of surface waves. An attempt is also made to derive some empirical formulas for jet parameters such as the declining rate of jet centerline velocity and the jet width spread rate under the presence of random waves.

The results generated by a Lagrangian integral model of jets discharge in regular waves are used to compare with the results of jets discharge in random

waves. In addition, the centerline dilution of the outfall discharge in Hong Kong coastal areas is estimated based on the Lagrangian integral model and the developed empirical formulas.

1.3 Scope

The research is experimentally based. The experiments were carried out in a 27m long, 1.5m wide & 1.5m deep random wave flume located in the hydraulic laboratory of the Department of Civil and Structural Engineering of the Hong Kong Polytechnic University.

This study focuses on the submerged non-buoyant jet discharge vertically towards the water surface. A steel tube of 13.5mm diameter, mounted vertically in the bottom of a tank, was used as the jet nozzle in this study. Water of depth (h) of either 0.5m or 0.8m was contained in the wave flume to represent the large receiving fluid body. A constant head tank was installed to provide the driving force of the jet and the whole discharge system was connected by PVC pipes. Jet discharge velocities (W_0) of 0.137, 0.53, 0.75 (h=0.8m), 0.8 and 1.038m/s were adjusted with the inline flow meter connected in series with the PVC pipes.

Waves in the form of mean JONSWAP spectra (Hasselmann et al. 1973, i.e. peak enhancement factor γ_j =3.3, shape factors σ_- =0.07 and σ_+ =0.09) are generated in the wave flume to simulate the real coastal situation. JONSWAP waves

with peak wave periods (T_p) of 0.5, 1, 2 and 3s were generated by the DHI random-wave maker located at one edge of the wave flume in the hydraulic laboratory. Two wave gauges located inside the wave flume were used to monitor the free surface fluctuation. Wave energy density spectra were computed by the recorded time-series surface elevation fluctuations. The wave spectra were then used to reproduce the irregular wave condition and to calculate the wave-induced velocity at various depths.

The jet hydrodynamic characteristics such as the jet centreline velocity, the cross-sectional velocity distribution, jet widths and also the jet turbulence intensity are investigated in this study. A 10MHz acoustics Doppler velocimeter (ADV) by Sontek was employed to measure velocities at those pre-select points within the jet body in wave and stagnant ambient conditions. The sampling frequency was set to 20Hz while the sampling time was at least 120 times of the selected peak wave periods throughout the experiments. Time-averaged analysis was used to calculate the mean value of jet velocities and the associated turbulence intensities. The collected data were then used to analyse the hydrodynamic behaviour of jets in random waves.

The jet fluid was marked with a coloured dye tracer (Rhodamine B) and discharged into the receiving water. The jet dispersion pattern was then observed from

one side of the glass wall of the wave flume. A 3-CCD digital video camera was placed to record the flow pictures for flow visualization.

The collected data in random wave conditions are used to compare with those obtained in stagnant environments and previous results obtained in regular wave environments.

1.4 Organization of the thesis

A brief literature review about the research on jets is contained in Chapter 2. The literature review is limited to jets in stagnant ambient condition and in moving fluid such as currents and waves.

The apparatus used in this study is introduced in Chapter 3. The experimental methodology supplemented with schematic diagrams of the experimental setup and the ADV sampling points are presented in that chapter. In addition, a table summarizing the experimental conditions is also included.

The theoretical analysis including a short discussion on the general jet mixing mechanisms and the dimensional analysis used in this study is presented in Chapter 4. The derivations of the wave momentum characteristic length and the wave characteristic velocity are also discussed.

The experimental results are given in Chapter 5. Images captured from the digital video camera are displayed to show the difference of jets discharge in

stagnant ambient water and random wave environments. The images also demonstrate the jet-wave interaction and the formation of different jet motions. There are sub-sections in Chapter 5 discussing the hydrodynamic jet behaviour: Jet centerline velocity, radial velocity profiles, potential core and velocity ratio, jet widths and turbulence intensity. Formulas describing the jet flow behaviour such as the centerline velocity decay rate and the jet width spreading rate are proposed in this study. The jet discharge properties obtained in random wave conditions are briefly discussed. Previous results of jets in regular waves are also included for discussions.

A modified Lagrangian integral model for jets in a random wave environment is presented in Chapter 6. The equations used in this model are outlined. The model results are supplemented with the experimental results achieved in this study for comparison. The limitation of this integral model is also discussed. The extension of the results to prototype is also illustrated in this chapter. The developed empirical formulas and the Lagrangian integral model are used to estimate the centerline diluton under the typical Hong Kong sea waves. The computation results are also presented in that chapter.

The overall conclusions of this study are mentioned in Chapter 7. The issues required for further investigation are also outlined.

2 LITERATURE REVIEW

2.1 Introduction

A jet is a fluid motion whose primary source of kinetic energy and momentum flux is a pressure drop through an orifice. The research on jets has already been carried out for nearly two hundred years. At the earliest stage, the investigation of jet discharge was mainly based on visual observation. Until the advancement in the development of the equipment, more accurate experimental measurements were achieved. Some theoretical relationships with respect to the jet behaviour began to be reported in the last century (i.e. Albertson et al. 1950; Morton et al. 1956; Ricou and Spalding 1961; Wright 1977). Fluid discharged in the form of a jet is noticed to have better mixing and higher dilution. Thus, jets are commonly used in diffusers or discharge ports for environmental discharge. Numerical simulation is broadly employed in all industries recently. Based on the solution of the governing equations of fluid flow or the semi-analytical equations, many commercial or academic computer softwares [i.e. FLUENT (i.e. Xia and Lam 1997; Kwan and Swan 1998), VISJET (Lee and Chu 2003; Yu, Ali and Lee 2003)] have been developed with an accurate prediction of dilution and water quality inside the fluid body.

As the literature on jet is vast, the present study only concentrates on the literature related to non-buoyant jet discharged into stagnant or moving fluid. A brief review of the work on jet in stagnant ambience will be conduced first. The review on jet discharged into current will then be followed. Finally the review on jet under regular waves will be presented.

2.2 Jets in stagnant fluid

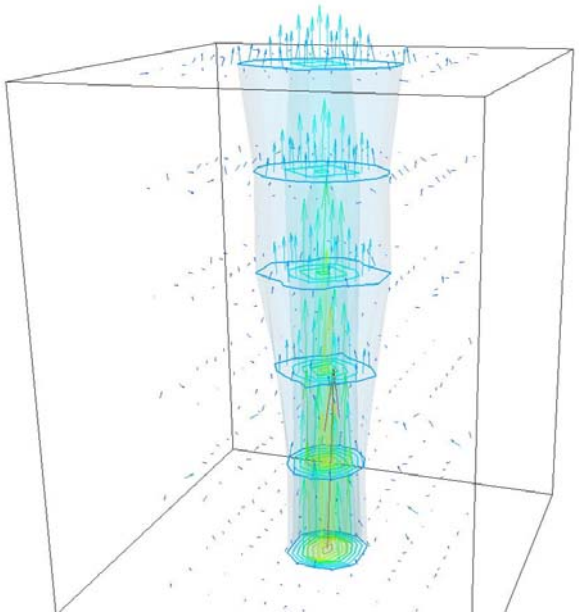

Figure 2.1. A round jet discharges in stagnant ambience.

Detailed experimental and theoretical investigation of jet was started by Prantdl in 1920s. Among the numerous researchers of jets, Albertson et al. (1950) carried out extensive quantitative experimental measurements on both slot jets (two-dimensional jet) and round jets (three-dimensional jet or axisymmetrical jet, i.e. Fig. 2.1) in the zone of flow establishment (ZFE) and the zone of established flow (ZEF). Based on

the experimental data, a series of theoretical relationships regarding the decrease of velocity with the axial distance from the jet outlet, velocity distributions in both the lateral (radial) and axial directions and the jet width spreading rate (increase in the jet half-width with the axial distance), were derived. Since dimensional analysis has also been performed, the derived non-dimensional equations can be applied to all jets discharged into the stagnant ambience. A couple of years later, Abramovich (1963) summarized the previous theoretical and experimental studies of turbulent jets. This is possibly the first reference book in the topic on the theory and use of turbulent jets.

Afterwards, studies on turbulent jet characteristics, such as the mean velocity, turbulence intensity, intermittency, jet half-width, were still carried on over the next few decades. Most of the experimental data and results were summarized by Fischer et al. (1979) and List (1982) for both academic and engineering application purposes. The latest findings of jet behaviour investigated with improved experimental tools were summarized by Lee and Chu (2003).

An important concept, the jet entrainment hypothesis, in the study of jets was proposed by Morton, Taylor and Turner (1956). They used Eq. 2.1 to describe the increase in jet flow with the axial distance due to the entrainment of the ambient fluid into the jet.

$$\frac{\partial Q}{\partial x} = 2\pi b \alpha u_c \tag{2.1}$$

where Q = flow rate, b = jet half-width, defined as the distance from the jet centerline to the velocity ratio of $1/e$ where the Gaussian velocity profiles is formed, α = entrainment coefficient, u_c = jet centerline velocity and x = jet axial distance. Many researchers (e.g. Albertson et al. 1950; Ricous and Spalding 1961; Papanicolaou and List; 1988) observed that the jet width varies linearly with the axial distance which support the entrainment assumption as stated in Eq. 2.1.

Normally, a jet with a Reynolds number above 2000 is recognized as a turbulent jet. In the middle of the 20th century, ring vortices structure was reported during the observation of the discharge of turbulent jets (i.e. Mollϕ-Christensen 1967; Becker and Massaro 1968). The generated vortices wrap the surrounding fluid into the jet fluid. This violent mixing between the jet fluid and the surrounding fluid shows the generation of turbulence and the jet itself grows thicker. As the jet region along the jet axis becomes larger, the ambient fluid is then induced to rotate by the generated vortices around the jet region. If Q_0 is the initial discharge flow rate and Q is the flow rate at certain sections in the jet body, the ratio Q/Q_0 will be greater than unity. The jet velocity keeps on decreasing along the jet axis, while the flow rate keeps on increasing along every jet section. This means the jet entrains the surrounding fluid by increasing the flow sectional area. According to Lee and Chu (2003), eddies, generated by the discharged fluid to the receiving fluid, entrap the ambient fluid into the jet body,

known as turbulent entrainment. This special feature then provides a good condition for mixing the discharge fluid and the ambient fluid. This is why turbulent (buoyant) jets are often used as mixing devices in environmental discharge, especially for the release of hot gas, thermal water or wastewater.

Most of the investigation on jets characteristics normally refers to a single jet discharge, however, the environmental discharge, especially for the wastewater discharge, always employs multiple port diffusers to speed up the dilution rate. In addition, though all types of fluid own similar characteristics, the receiving fluid body may be subject to a different condition (i.e. currents, waves) which influences jet discharge and fluid mixing mechanisms. The presence of currents is believed to transport the discharge fluid during mixing while the presence of waves or unsteady currents induces the fluid oscillation which influences the entrainment process.

2.3 Jets in moving fluid

When a jet is discharged into a current, additional entrainment mechanism exists due to the shear of the current, leading to the deflection of the jet trajectory. The orientation of the current with respect to the jet can be classified as coflows (e.g. Chu, Lee and Chu 1999; Davidson and Wang 2002), counterflows (Lam and Chan 2002) and crossflows (Davidson and Pun 1999; Li and Lee 1991). Also the current may be bi-directional due to the existence of waves.

2.3.1 *Jets in crossflows*

Keffer and Baines (1963) and Pratte and Baines (1967) examined a round turbulent air jet in a crossflow within a wind tunnel. They distinguished 3 regions in the deflected jet trajectory: the potential core, zone of maximum deflection and vortex zone. According to their experimental data, a two-phase relationship with respect to the jet trajectory was obtained and used to identify the boundary of the zone of maximum deflection and the vortex zone.

This two-phase relationship used to describe the jet trajectory under crossflow was further verified by Wright (1977) for buoyant jet. The jet trajectory was illustrated by adding dye into the discharge fluid. The developed jet trajectory with a dye tracer was then photographed for subsequent analyses. The jet trajectory can be satisfactorily described by two straight lines at different phases using the length scale of l_m (Eq. 2.2). Wright (1977) classified the two phases for pure momentum jets as momentum dominated near field (MDNF) and momentum dominated far field (MDFF) and presented equations (Eqs. 2.3) with suggested coefficients in predicting the jet trajectory in a crossflow.

$$l_m = \frac{M^{1/2}}{U_a} \quad \text{(momentum dominated)} \tag{2.2}$$

where M = kinematic momentum flux, and U_a = ambient crossflow velocity.

$$\begin{cases} \dfrac{z}{l_m} = C_1 \left(\dfrac{x}{l_m} \right)^{1/2} & z < l_m \quad \text{(MDNF)} \\ \dfrac{z}{l_m} = C_2 \left(\dfrac{x}{l_m} \right)^{1/3} & z > l_m \quad \text{(MDFF)} \end{cases} \tag{2.3}$$

where C_i = constant , x = longitudinal distance and z = vertical distance. This length scale system was later used to distinguish the jet region by Davidson and Pun (1999).

Andreopoulos (1982) and Andreopoulos and Rodi (1984) conducted jet-in-crossflow (JICF) experiments in a wind tunnel to examine the deflected jet behaviour. The experiments were conducted for a range of values of the jet-to-crossflow velocity ratio ($R = \dfrac{U_0}{U_a}$, where U_0 is the jet discharge velocity). Andreopoulos (1982) found that the discharge jet body, within the potential core, separates the ambient current which causes the formation of a horse-shoe vortex in the exit plane. Andreopoulos and Rodi (1984) used DISA anemometers and DISA hot-wire probe, to collect data of the 3 dimensional jet velocity and turbulence. They presented detailed figures to describe the turbulence intensity distribution and the change of mean velocity profiles along the flow direction. Experiments were conducted based on R = 0.5, 1 & 2. The measured velocity vectors showed the generation and existence of counter-rotating vortex pairs (CVP). Most literature elaborating the generation and the formation of CVP theoretically were gathered by Morton and Ibbetson (1996). In the same year, Kelso et al. (1996) conducted a visual analysis of the jet discharge into the cross current in the medium of water and air in

which *R* ranged from 2 – 6. They employed dye tracers to give clear images on the jet trajectory and the vortex establishment, which demonstrates how the ambient fluid is entrapped into the jet fluid. They found that there was a separation zone inside the jet pipe which is important in the initial generation of the CVP. The ring vortex within the shear layer and the vortex generated by the wake were also components contributing, throughout the whole process, to the development of the CVP.

2.3.2 *Jets in wave environments*

Ocean outfall is an efficient system for wastewater disposal. Ocean provides abundant water for diluting the treated effluent. For the discharge device diffuser is normally used on which holes or nozzles are installed to generate jet flow which enhances the initial dilution and improve the overall mixing rate. But discharge in ocean is somewhat different from discharge into the stagnant ambient, i.e. lakes, because waves will exist in the former water body. Wave induced fluid motion is similar to tidal flow but with a much shorter period.

The first study of jet-wave interaction was carried out by Shuto and Ti (1974). They compared the results of a vertical jet discharged into a standing wave environment and a vertical jet discharged into a stagnant ambient environment. The results showed the time-averaged surface dilution was higher when the jet was under the influence of wave movement.

Sharp (1986) investigated the physical phenomenon of a submerged buoyant jet discharged into shallow water or deep water regular waves and investigated the formation of dye clouds due to wave induced oscillation of fluid particles. The cloud formation under the wave effect led to the increase in dilution rate. Similar results were also achieved by Ger (1979) and Chin (1987) who investigated horizontal jets discharge into regular surface wave environments.

The measurement of jet characteristics such as jet centerline velocity and the velocity distribution for submerged jets in regular waves were made in the last decade. Koole and Swan (1994) conducted an experimental study of a 2-D non-buoyant jet discharged horizontally in the direction counter to the propagation of surface waves. They showed that the volume flux of the jet in regular wave conditions was greater than that in stagnant ambience, showing evidence that the waves provided a positive effect on entrainment. Their results suggested that the presence of waves reduce the length of the potential core which implies that waves can speed up the formation of the zone of flow establishment (ZFE). They also found that certain cross-sectional velocity profiles are non-Gaussian, which is resulted from the periodic advection effect by regular waves.

Similar study was conducted with the use of a submerged vertical jet discharge into regular waves by Chyan and Hwung (1993). Laser equipment was employed in

their study. They discharged the dye as wastewater through the jet nozzle to observe the difference in the jet area between the pure jet condition and the regular wave environment. Since the regular horizontal wave motion is a constant periodic motion, the velocity induced by the wave motion consistently changes periodically. Twin peaks velocity profiles were noticed when the jet discharge in strong wave environments. This presence of twin peaks profiles was later explained by the wave induced jet lateral displacement by Koole and Swan (1995) who demonstrated the formation of the twin peak velocity profile graphically. They also presented a reference length ratio as a criterion for the formation of the twin peaks velocity profile.

According to the experimental observation, Chyan and Hwung (1993) observed that horseshoe vortex was generated when the cross-wave was passing through the jet area. The formation of vortex was related to the wave-induced current which was similar to that in crossflow environment. Chyan and Hwung also subdivided the jet-wave flow into three regions, deflection, transition and developed. Deflection region is the region where the general jet discharge behaviour is still under-controlled by the jet momentum. While the jet discharge fluid is discharged up to a certain distance away from the jet orifice, the wave momentum is comparatively stronger than the jet momentum. The jet flow pattern is governed by the propagated surface waves.

This region is recognized as the developed region. A buffer region is located between the developed region and the deflection region and is denoted as the transition region. The experimental results obtained from Mossa (2004a) strongly supported the existence of these three different regions. However, no rigorous mathematical definition of the three regions was given. Similarly, Mori and Chang (2003) classified the jet motions into three categories: symmetric, asymmetric and discontinuous. The symmetric motion is the one with symmetrical jet flow pattern. Asymmetric motion refers to the jet with trajectory deflected into an asymmetric shape and a continuous jet trajectory is still maintained. Discontinuous motion refers to jet motion with axially asymmetric but discontinuous jet trajectory. They interpreted the formation of different form of jet trajectory with a suggested value of the momentum flux ratio of wave to jet. Nevertheless, the suggested ratio is only valid for submerged horizontal jets.

Related study has been carried out by Lam and Xia (2001) who simulated the wave-current condition with two different methods: 1. by discharging the jet fluid into the uniform crossflow together with the use of a stepper motor to generate an oscillating motion of the jet discharge port, and 2. by applying surface regular waves to the current. Similar jet discharge patterns were observed based on the two simulation methods. With the use of the LIF technique, Lam and Xia (2001) revealed

that the dual peak cross-sectional concentration profiles were formed in the wave-current environment. The LIF images showed that the jet widths obtained in unsteady crossflows were enlarged by two to three times of that in steady crossflows. Xia and Lam (2004) also concluded that the increase of jet width was controlled by the unsteady crossflow, $U(t) = U_a + a_p \sin(\omega t)$, particularly the ratio of the unsteadiness parameter, a_p / U_a, where a_p = amplitude of the oscillating velocity component and U_a = crossflow velocity.

2.4 Jets modeling

Numerical model is always useful for carrying out the preliminary design in engineering works. Chin (1988) formulated a Lagrangian model to estimate the behaviour of the jet discharged in regular wave conditions. The model is validated by Koole and Swan (1994a) with satisfactory results. Kwan and Swan (1997) also proposed a similar Lagrangian integral model by the modification of the original model formulated by Chu and Lee (1996). Numerical simulations of jet discharge in wave-current conditions using the computation fluid dynamics code (FLUENT) have also been performed (Xia and Lam 1997; Kwan and Swan 1999). However, these works are limited to the situation of jet discharge in regular waves only.

The phenomenon of jet discharged under arbitrary ambient flow condition (including random waves) can be investigated numerically through the direct

solution of the Navier Stokes (NS) equations, leading to direct numerical simulation (DNS), or the solution of the spatially filtered NS equations, leading to Large Eddy Simulation (LES), as well as the solution of the Reynolds Averaged Navier Stokes equations (RANS). Literature on this topic is very extensive and a thorough review is difficult. In particular, Chen, Li and Zhang (2004) developed a numerical model using the LES technique to simulate jet discharged into a stagnant fluid with free surface. Their model will be extended to study jet under random wave environment.

2.5 Random waves – JONSWAP

Natural surface waves are usually generated by winds. They are usually irregular in shape and with a range of frequency. The peak wave period and the significant wave height are usually used to characterize the wave properties. The peak wave period is the most frequently occurred wave period and the significant wave height *(H_s)* is the mean height of the highest one-third of all waves H (i.e. $H_s = \frac{1}{N/3}\sum_{i=1}^{N/3} H_i$, where N = total number of waves). The concept of the significant wave height was first introduced by Sverdrup and Munk (1947). It was found that the value of significant wave height is very close to the estimated visual height by an experienced observer (Kinsman 1965). Thus, peak wave period and the significant wave height are commonly used in random wave conditions.

Random sea wave conditions can be described by a series of random signals. These random sea wave signals follow some probability laws and can be investigated statistically. Energy density spectrum is an important random sea wave property. Among the available energy density spectra, the spectrum obtained from the Joint North Sea Wave Project (JONSWAP) by Hasselmann et al. (1973) is general and commonly used. The JONSWAP spectrum is an extension of the wave spectrum by Pierson-Moskowitz (PM) (1946). Since the PM spectrum is only valid when wind blows over sea at constant speed with a single direction for a very long duration, the random waves simulated by the PM spectrum may not perfectly reflect the real sea wave situation. The JONSWAP study was carried out in the field and it was discovered that the nonlinear energy transfer due to resonant wave-wave interactions, which is not considered in PM spectrum, is critical for the growth of random waves. Hasselmann et al (1973) then proposed a spectrum with sharp spectral peak (the equation for the spectrum equation is given in Chapter 3) to represent the properties of wind generated random sea waves. The spectrum can be tuned to fit the wave conditions in field easily. In this study, random waves follow the typical JONSWAP spectrum will be employed.

3 EXPERIMENTS

3.1 Introduction

An experimental investigation on jets in random waves was carried out in the hydraulics laboratory of the Department of Civil and Structural Engineering, the Hong Kong Polytechnic University. The apparatus used in this study, including the random wave flume and the acoustic Doppler velocimeter (ADV), are described. The experimental methodologies, including the velocity measurement and flow visualization techniques, are also outlined in this chapter. A table of summary, listing all the experimental conditions, is also presented in this chapter.

3.2 Apparatus

3.2.1 *Random wave flume*

The laboratory experiment was conducted in the 27m long, 1.5m wide and 1.5m deep random wave flume in the hydraulic laboratory at the Department of Civil and Structural Engineering, the Hong Kong Polytechnic University. The wave flume is mainly composed of structural steel while one of the long side walls is made of glass. This allows flow visualization to be carried out with the use of any kind of visual tracer. A wave paddle and a wave absorber are placed at the two ends of the

wave flume. A multi-purpose net is also placed close to the wave absorber to dissipate the generated wave energy and to diminish the magnitude of the reflected waves.

3.2.2 *DHI random wave maker*

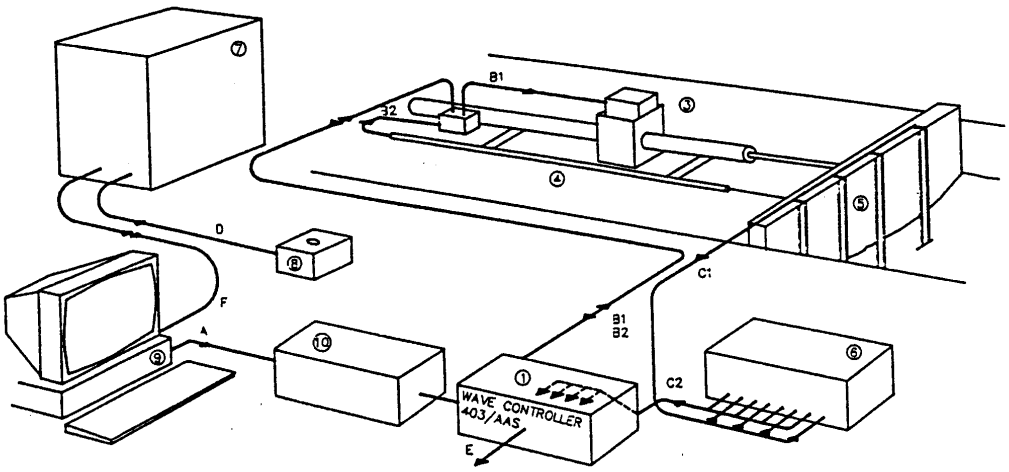

Figure 3.1. The Danish Hydraulic Institute Active Wave Generating System (Source: DHI Wave Controller Type 403 User Manual).

Water waves are generated by the Danish Hydraulic Institute (DHI) Active Wave Generating System. The whole system as shown in Fig. 3.1 consists of 10 different components: 1. DHI Wave Controller, 2. Hydraulic servo actuator, 3. Servo valve, 4. Position feedback transducer, 5. Wave feedback gauges, 6. Wave meter, 7. DHI Hydraulic Power Pack, 8. Power pack remote control box/ Emergency stop, 9. Dos-mode personal computer with 3 ISA slot and, 10. DHI input/ Filter Cabinet (type 153/IF). The 4 wave feedback gauges on a 1.5m x 1.5m flat wave paddle (Photo 3.1) connected to the DHI wave meter are used to control the wave paddle in order to

absorb part of the reflected waves. The DHI Filter Cabinet is part of the DHI data acquisition setup. This is designed for collecting the conditioned signals from a number of probes used in the same model tests.

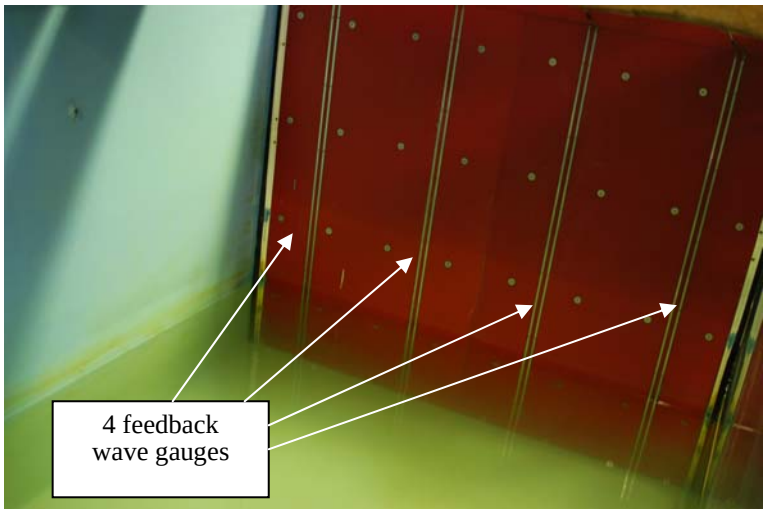

Photo 3.1. 4 wave feedback gauges on a 1.5m x 1.5m flat red wave paddle.

In this study, the paddle signals were fully controlled by the DHI Wave Synthesizer. This software is a set of menu-driven programs which allows user to control the wavemaker and to log data during experiments. The software package contains programs for the synthesis of regular and irregular waves. The basic time series analysis and the spectrum analysis of the wave data are included. The complete time-series data can also be output as an ASCII file for further checking of the output significant wave height, root mean squares wave height and the peak wave period. Irregular waves in the form of JONSWAP, Pierson-Moskowitz (PM), Bretschneider, ISSC, Darbyshire or Neumann spectrum can be implemented by the DHI Wave Generating System together with the DHI Wave Synthesizer.

3.2.3 *Seasim wave height gauge*

The Seasim auto-compensating wave height gauge by Seasim Controls Limited was used. Wave probes, each of 400mm length stainless steel, are connected to the processor module for water elevation measurement. The processor module can accommodate up to 8 wave probes to measure surface fluctuation simultaneously. The received voltage signals from the processor module are transmitted to the DHI Filter Cabinet of the DHI wave generating system and stored in the computer system. The obtained data can be reviewed and analyzed by the DHI Wave Synthesizer software. Wave gauge calibration is carried out before experiments. The calibration allows the DHI Wave Synthesizer software to compute the surface fluctuation from voltage into the corrected physical unit, i.e. millimeter.

3.2.4 *Acoustic Doppler velocimeter (ADV)*

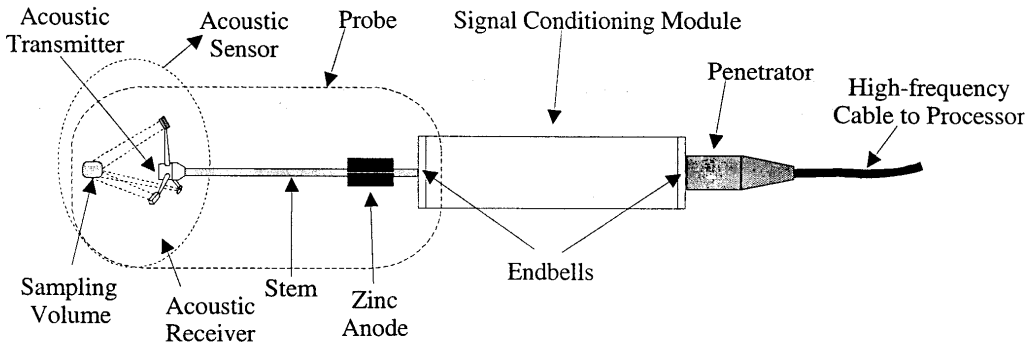

Figure 3.2. Standard 10 MHz ADV Probe (Source: ADV Operation Manual).

The velocity profile and the associated turbulence profile across the jet orifice were measured by a 10 MHz ADV by SonTek (Fig. 3.2). This is a velocity measurement

device using the sound speed to compute the velocity based on the acoustic Doppler shift velocity measurement principle. The transmitter of the ADV probe transmits the acoustic pulses in the fluid medium. The pulses are reflected by the suspended particle inside the fluid medium and then received by the 3 receivers slanted 30° relative to the transmitter. The 10 MHz ADV sampling frequency can be set between 0.1 Hz to 25Hz. Five different standard velocity ranges (i.e. ± 3, ± 10, ± 30, ± 100cm/s and ± 2.5m/s) can be selected. Since the instrument generated noise in the velocity data is proportional to the velocity range, the lowest velocity range which can cover the expected velocity should be chosen in order to minimize the uncertainty of the measurement. According to the specifications, the uncertainty of the ADV measured velocity can be up to ± 0.25cm/s, however, this may only occur in very low flow conditions. In this study the turbulent jet is discharged in waves. The jet Reynolds number is usually above 2000. The high Reynolds number eliminates the occurrence of very low flow conditions. Referring to the SonTek ADV technical document, the accuracy of the factory calibrated ADV probe is ± 1% of the measured velocity.

The 3D ADV sensor is connected to the signal conditioning module by a 100cm flexible cable which enables the acoustic sensor to be oriented in a down looking or side looking configuration. This flexible cable allows the sensor to be

mounted easily within the fluid without strong influence of the vertical jet flow pattern. In addition, the sampling point is 5cm away from the sensor. Thus the influence to the jet motion can be minimized even though the probe is mounted inside the fluid medium during experiments. The sampling volume by the 10MHz ADV is about $0.25cm^3$ according to the performance specifications, which is sufficiently small as a 13.5mm diameter jet is used in the present study.

The ADV probe is connect to a desktop computer via an ADVLab processor PC card and is controlled by the factory provided software. The SonTek ADV includes the real time data acquisition software, the hardware diagnostic software and the recorder data extraction software. The ADV Data Acquisition software, version 4.4, developed by Sontek, is used in this study. This software allows the user to adjust the acquisition settings such as the water temperature, salinity, expected velocity range, sampling frequency, sampling mode and sampling time. The data acquisition screen displayed is divided into four sections: 1. the status of data acquisition, 2. the velocity and diagnostic data in numerical format, 3. the real-time plots of SNR, correlation and velocity data, and 4. the key menu to control the system during data acquisition.

3.2.5 *Jet discharge system*

A stainless steel tube with an inner diameter (*d*) of 13.5mm was chosen as the jet nozzle. The tube was plugged vertically into a PVC pipe mounted at the bottom of the wave flume. The jet nozzle, including the riser length, was 125mm vertically above the channel bed. A water pump placed under the wave absorber from one end of the wave flume was used to transfer water to a constant head tank located above the random wave flume. This can ensure the discharge fluid and the receiving fluid body are from the same source. Hence, the buoyancy effect owing to the difference in fluid temperature and density can be minimized.

Photo 3.2. The constant head tank locates above the wave flume used in this study.

The vertical jet was fed by the constant head tank as displayed in Photo 3.2. The jet was then discharged constantly into the receiving water body in the flume. A flow adjustment valve and an in-line flow meter were connected between the constant head

tank and the vertical jet in order to adjust and measure the jet flow rate. A schematic diagram of the jet experimental setup of this study is shown in Fig. 3.3.

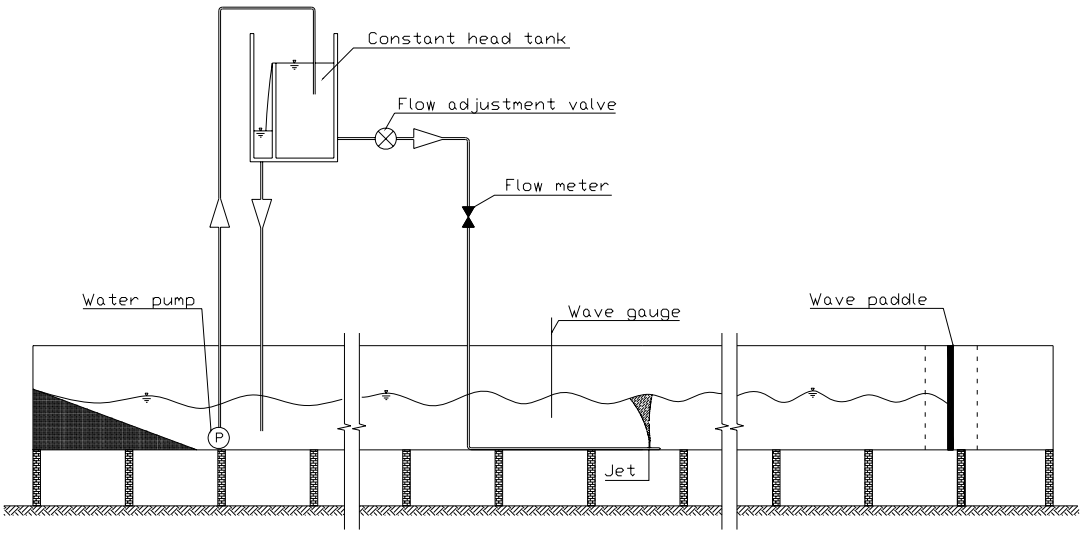

Figure 3.3. A schematic diagram of the experimental setup used in this study.

3.3 Experimental arrangement

3.3.1 *Experimental conditions*

A total of 42 experimental runs with 5 different jet discharge velocities, i.e. 0.137, 0.53, 0.75, 0.8, 1.038m/s, and 2 different water depths, i.e. 0.5 and 0.8m, were conducted. The key parameters of the 42 sets of experiment including the experiments for jet discharges in stagnant environments and in JONSWAP random wave environments are listed in Table 3.1.

Table 3.1. Experimental conditions.

Run	Case	Jet discharge velocity W_0 (m/s)	Jet Reynolds number Re	Water depth h (m)	Peak wave period T_p (sec)	Significant wave height H_s (mm)	Root mean square wave height H_{rms} (mm)
1	A0	0.8	10800	0.5	-	-	-
2	A1-1	0.8	10800	0.5	1	7.601	5.368
3	A1-2	0.8	10800	0.5	1	14.167	10.005
4	A1-3	0.8	10800	0.5	1	25.905	18.294
5	A1-4	0.8	10800	0.5	1	36.465	25.752
6	A2-1	0.8	10800	0.5	2	17.716	12.511
7	A2-2	0.8	10800	0.5	2	34.805	24.580
8	A2-3	0.8	10800	0.5	2	65.577	46.311
9	A2-4	0.8	10800	0.5	2	93.707	66.177
10	B0	0.53	7155	0.5	-	-	-
11	B1-1	0.53	7155	0.5	0.5	5.702	4.027
12	B1-2	0.53	7155	0.5	0.5	11.72	8.277
13	B1-3	0.53	7155	0.5	0.5	21.484	15.172
14	B2-1	0.53	7155	0.5	1	11.602	8.194
15	B2-2	0.53	7155	0.5	1	20.984	14.819
16	B2-3	0.53	7155	0.5	1	38.242	27.007
17	B3-1	0.53	7155	0.5	2	15.519	10.960
18	B3-2	0.53	7155	0.5	2	28.736	20.294
19	B3-3	0.53	7155	0.5	2	50.657	35.775
20	C0	1.038	14013	0.5	-	-	-
21	C1-1	1.038	14013	0.5	1	11.602	8.194
22	C1-2	1.038	14013	0.5	1	20.984	14.819
23	C1-3	1.038	14013	0.5	1	38.242	27.007
24	C2-1	1.038	14013	0.5	2	15.519	10.960
25	C2-2	1.038	14013	0.5	2	28.736	20.294
26	C2-3	1.038	14013	0.5	2	50.657	35.775
27	C3-1	1.038	14013	0.5	3	15.745	11.119
28	C3-2	1.038	14013	0.5	3	29.212	20.630
29	D0	0.75	10125	0.8	-	-	-
30	D1-1	0.75	10125	0.8	1.5	32.93	23.256
31	D1-2	0.75	10125	0.8	1.5	60.343	42.615
32	D1-3	0.75	10125	0.8	1.5	85.048	60.062
33	D2-1	0.75	10125	0.8	2	32.416	22.893
34	D2-2	0.75	10125	0.8	2	60.728	42.887

35	D2-3	0.75	10125	0.8	2	88.35	62.394
36	E0	0.137	1850	0.5	-	-	-
37	E1-1	0.137	1850	0.5	1	11.602	8.194
38	E1-2	0.137	1850	0.5	1	20.984	14.819
39	E1-3	0.137	1850	0.5	1	38.242	27.007
40	E2-1	0.137	1850	0.5	2	15.519	10.960
41	E2-2	0.137	1850	0.5	2	28.736	20.294
42	E2-3	0.137	1850	0.5	2	50.657	35.775

3.3.2 *Wave conditions and measurements*

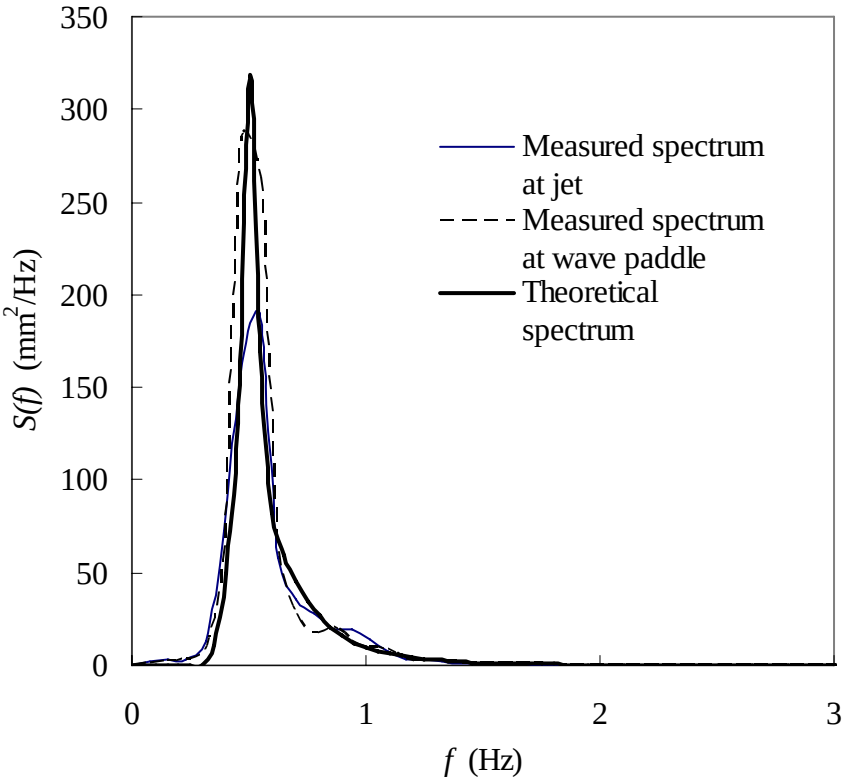

Figure 3.4. Measured JONSWAP wave spectrum (located at jet and wave paddle) for case C2-2.

The propagation of the surface random waves in the form of JONSWAP spectrum (Fig. 3.4) was selected in this study. This is because wind generated random waves in coastal area are usually conformed to JONSWAP spectrum. The random wave conditions were generated by the Danish Hydraulic Institute (DHI) Active Wave Generation System. According to Hasselmann et al. (1973), the JONSWAP random wave spectrum is characterized by the shape factors σ, peak enhancement factor γ_j, peak frequency f_p and the scaling parameter κ as described in Eq. 3.1.

$$S(f) = \frac{\kappa g^2}{(2\pi)^4 f^5} \exp\left[-1.25\left(\frac{f}{f_p}\right)^{-4}\right] \gamma_j^{\exp\frac{-(f-f_p)^2}{2\sigma^2 f_p^2}} \tag{3.1a}$$

$$\sigma = \begin{cases} \sigma_- \text{ for } f \le f_p \\ \sigma_+ \text{ for } f > f_p \end{cases} \tag{3.1b}$$

where S = spectral density [L^2T], f = the wave frequency, g = the acceleration due to gravity, κ = the scaling parameter, and σ_- and σ_+ are the shape factors corresponding to different frequency range.

This study adopted the mean values of the JONSWAP parameters, i.e. $\gamma_j = 3.3$, $\sigma_- = 0.07$ & $\sigma_+ = 0.09$ (Hasselmann et al. 1973), in order to investigate the interaction between the most frequent random sea waves and the jet discharge. The scaling parameter, κ, is a parameter dependent on the wind speed and the fetch length which actually depends on the input significant wave height, H_s.

Many studies (Andreopoulos 1982; Andrepoulos and Rodi 1983; Andrepoulos 1983; Andrepoulos 1985; Hodgson et al. 1999; Kelso et al. 1995; Pratte and Baines 1967) of jet in crossflow conclude that the jet trajectory, the flow path and the generation of many internal mixing mechanisms such as the formation of vortex ring are dependent on the ratio of the jet discharge velocity (W_0) to the ambient crossflow velocity (U_a), $R = W_0 / U_a$. Hence, it is reasonable to postulate that the wave induced fluid motion would be the key factor to alter the jet flow pattern as well as the mixing mechanism in the presence of wave conditions. The wave induced

velocity is a function of wave parameters. Random waves with different significant wave heights and peak periods result in different degree of wave induced fluid motion. In this study, random surface waves with T_p of 0.5, 1, 2 and 3s and H_s ranges from 7.6mm to 88mm were generated. They were used to set the ambient condition for the jet discharge. The wave conditions for each of the experiments are listed in Table 3.1. The wave density spectrum obtained in each case is shown in the Appendix. The fitted mean JONSWAP spectrum has also been shown.

Two wave probes, located at 2 meters away from the wave paddle and 1 meter after the jet nozzle, respectively, were used to monitor the water surface fluctuations. The jet orifice was located in between the two wave probes. The deformation of waveform in the testing region is expected. This is because wave energy may dissipate when waves are propagating from the wave paddle to the jet discharge area. In addition, reflected waves may influence the wave amplitude and wave length. The two-probe setting helps to monitor the change of the wave spectrum within the two wave probes locations. As shown in Fig. 3.4, the spectral peaks for the measured wave spectra were not as sharp as those of the input spectra. However, the energy distribution of the waves within the jet region can still be fitted by the JONSWAP spectrum. This shows that energy loss and wave deformation occurred while spectral shape of the random wave was preserved.

Wave probe calibration was done before any data acquisition to ensure the data accuracy. The surface elevation data were acquired at a sampling rate of 20Hz. The acquired data were stored in the DHI Wave Synthesizer. This can be used for spectral analysis. The complete time-series results can also be output as an ASCII file for further examining wave heights and the wave periods. In this study, significant wave height, i.e. the mean height of the highest one-third of all waves (H_s), the root mean square wave height (H_{rms}) and the peak wave period (T_p) are used in the data analysis. The mathematical definitions of H_s and H_{rms} are described in Eqs. 3.2 and 3.3.

$$H_s = \frac{1}{N/3}\sum_{i=1}^{N/3} H_i \tag{3.2}$$

$$H_{rms} = \sqrt{\frac{1}{N}\sum_{i=1}^{N} H_i^2} \tag{3.3}$$

where H_i = the wave height of the i^{th} wave and N = the total number of waves.

The significant wave height, H_s, and the root mean square wave height, H_{rms}, can be obtained based on Eqs. 3.2 and 3.3, respectively. However, this study used a simplified approach to obtain the two wave heights mentioned above. The output of the total wave spectrum energy, $E_{spectrum,}$ through spectral analysis, is available in the DHI Wave Synthesizer. The spectrum energy is indeed the total area of the wave spectrum. The root mean square wave height and the significant wave height can be

derived from the total wave energy based on statistical analysis of the Rayleigh distribution. The related equation is described below in Eqs. 3.4 and 3.5:

$$H_s = 4\sqrt{E_{spectrum}} \tag{3.4}$$

$$H_{rms} = 2\sqrt{2E_{spectrum}} \tag{3.5}$$

The two methods for calculating the wave heights have been compared by analyzing the raw data. The values of H_s obtained in Eq. 3.2 are 1.0155 times of those obtained in Eq. 3.4 as shown in Fig. 3.5. This small difference ensures the statistical analysis of the Rayleigh distribution is appropriate in computing the significant wave height and the root mean square wave height in the current experimental setup.

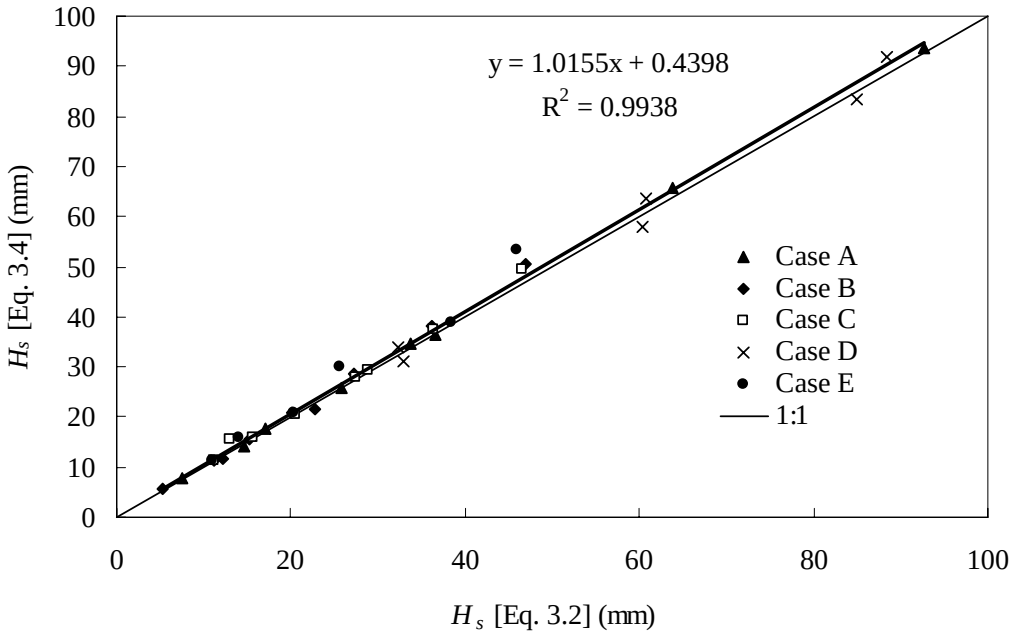

Figure 3.5 The H_s obtained in Eq. 3.4 is plotted against the H_s obtained in Eq. 3.2.

3.3.3 *Velocity measurements*

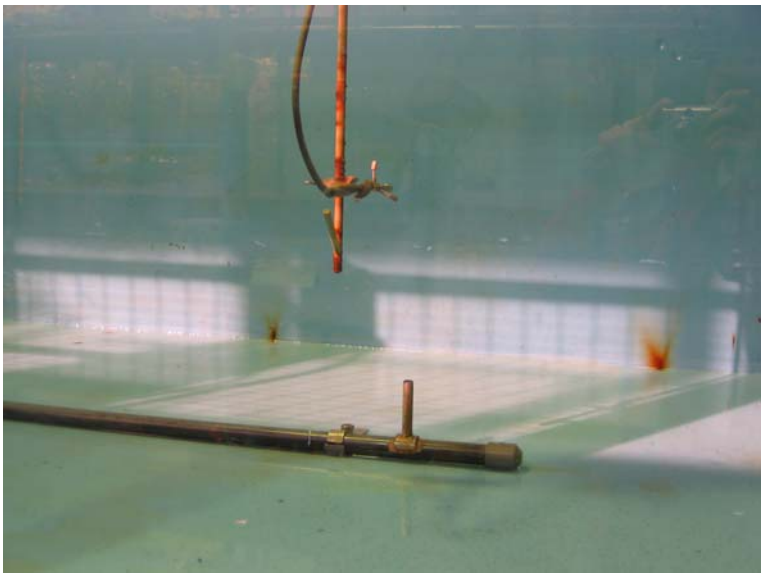

Photo 3.3. The 100cm flexible cable connected ADV sensor oriented looking to the side.

The 10MHz 3D ADV probe was employed in this study. The ADV with the flexible connected sensor was used. The sensor was oriented looking to the side as displayed in Photo. 3.3. This ADV sensor was positioned selectively at different points in order to measure the jet velocity and the velocity fluctuation component within the jet body. The sampling positions for cases A, B & C, D and E are presented in Figs. 3.6, 3.7, 3.8 and 3.9, respectively. The ADV was set at a sampling rate of 20Hz. The sampling time for the jet in stagnant ambient water was 120s while the sampling times for T_p=0.5, 1, 2 and 3s waves were set to 90, 150, 280 and 430 seconds, respectively. The sampling time was set to be at least 120 times of the selected peak wave period to ensure more than 100 complete cycles of waves have interacted with the jet

discharge. The collected velocity data were then used to calculate the time-averaged velocity as well as the associated turbulent intensity.

As mentioned above, the ADV generated noise is proportional to the velocity range used during measurement. The velocity range was chosen to be the smallest one which can cover the maximum velocity occurred in the experiments. The ADV correlation coefficient is a data quality parameter that is an output of the Doppler velocity calculation. The ideal correlation factor is 100%. The ADV technical manual stated that for highly turbulent situation, the correlation values should be ranged from 70 to 100%. During the experiment, the correlation coefficient was kept at 85% or above in order to ensure the data quality.

The measured data were transferred to Microsoft Excel for further analysis. Velocity data were also used for contour plotting with the freeware, MayaVi version 1.3.

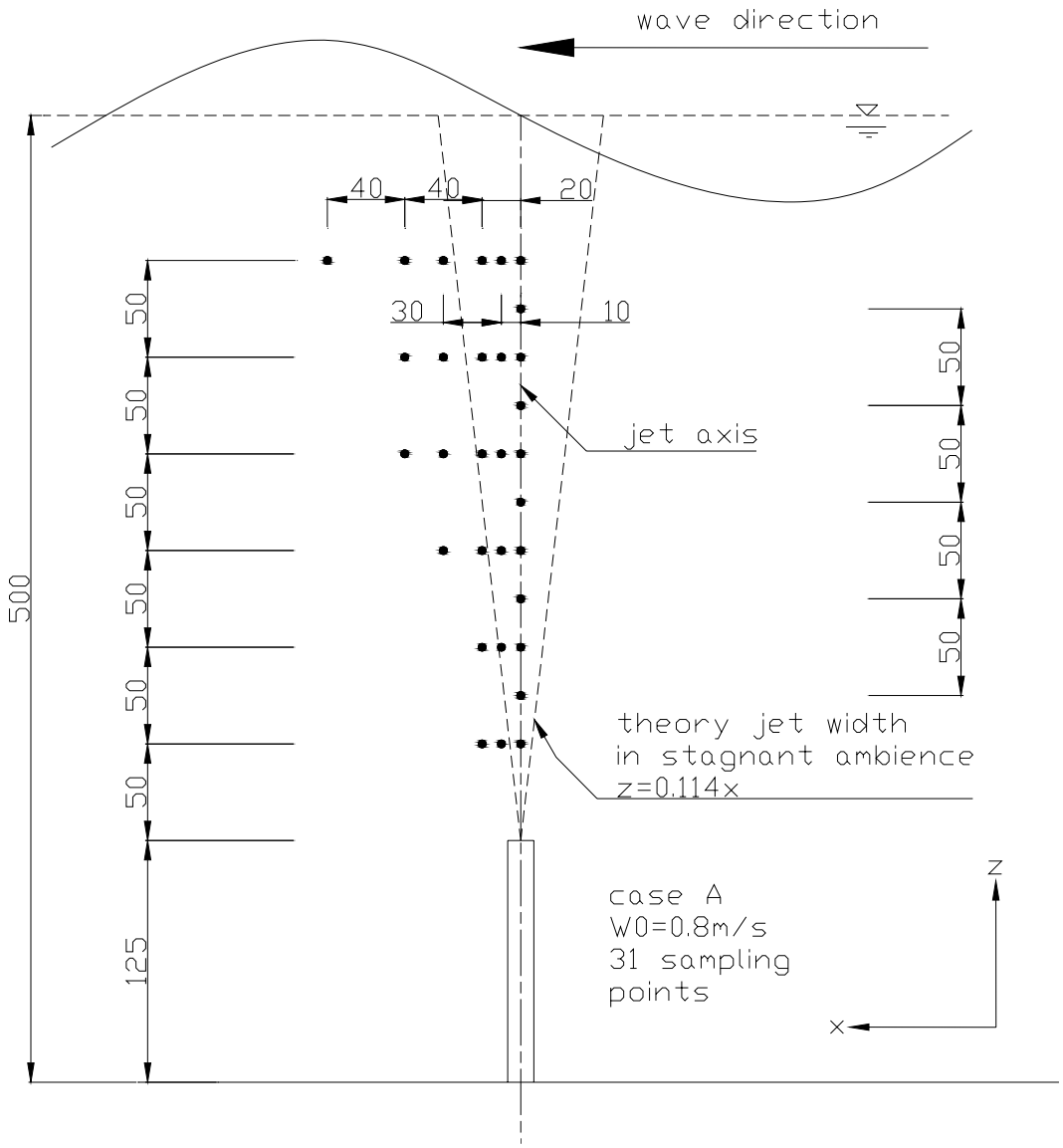

Figure 3.6. The selected ADV sampling points for case A experiments.

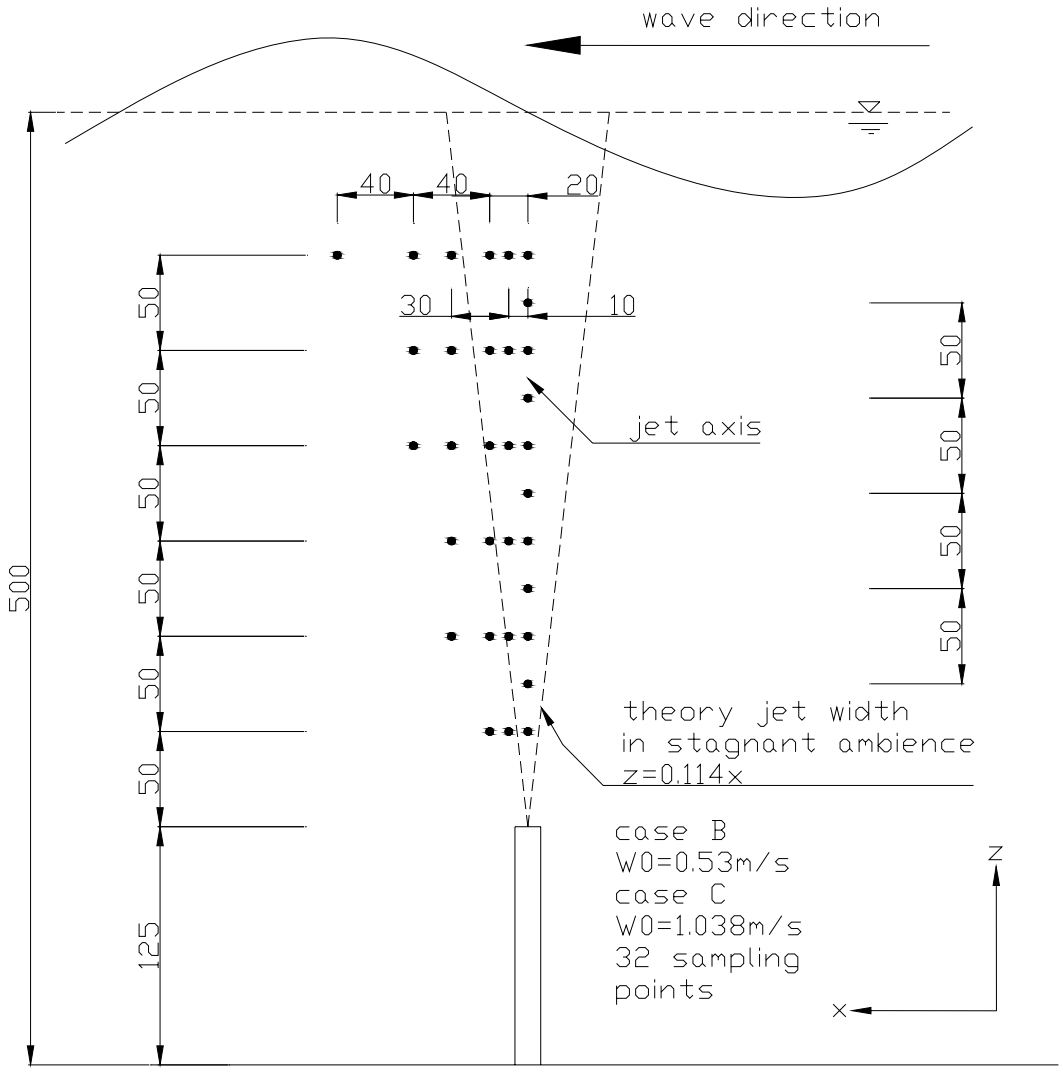

Figure 3.7. The selected ADV sampling points for case B & C experiments.

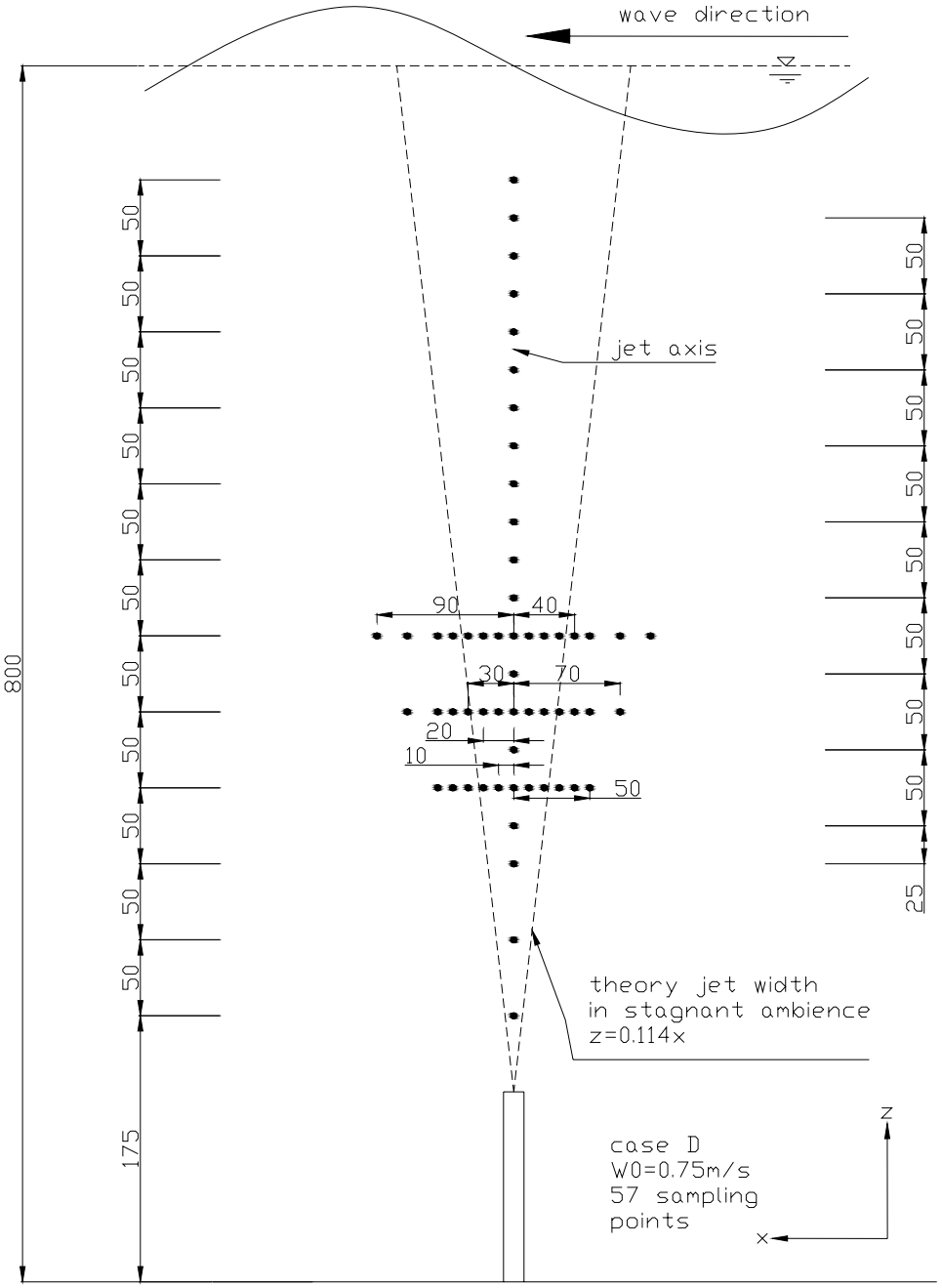

Figure 3.8. The selected ADV sampling points for case D experiments.

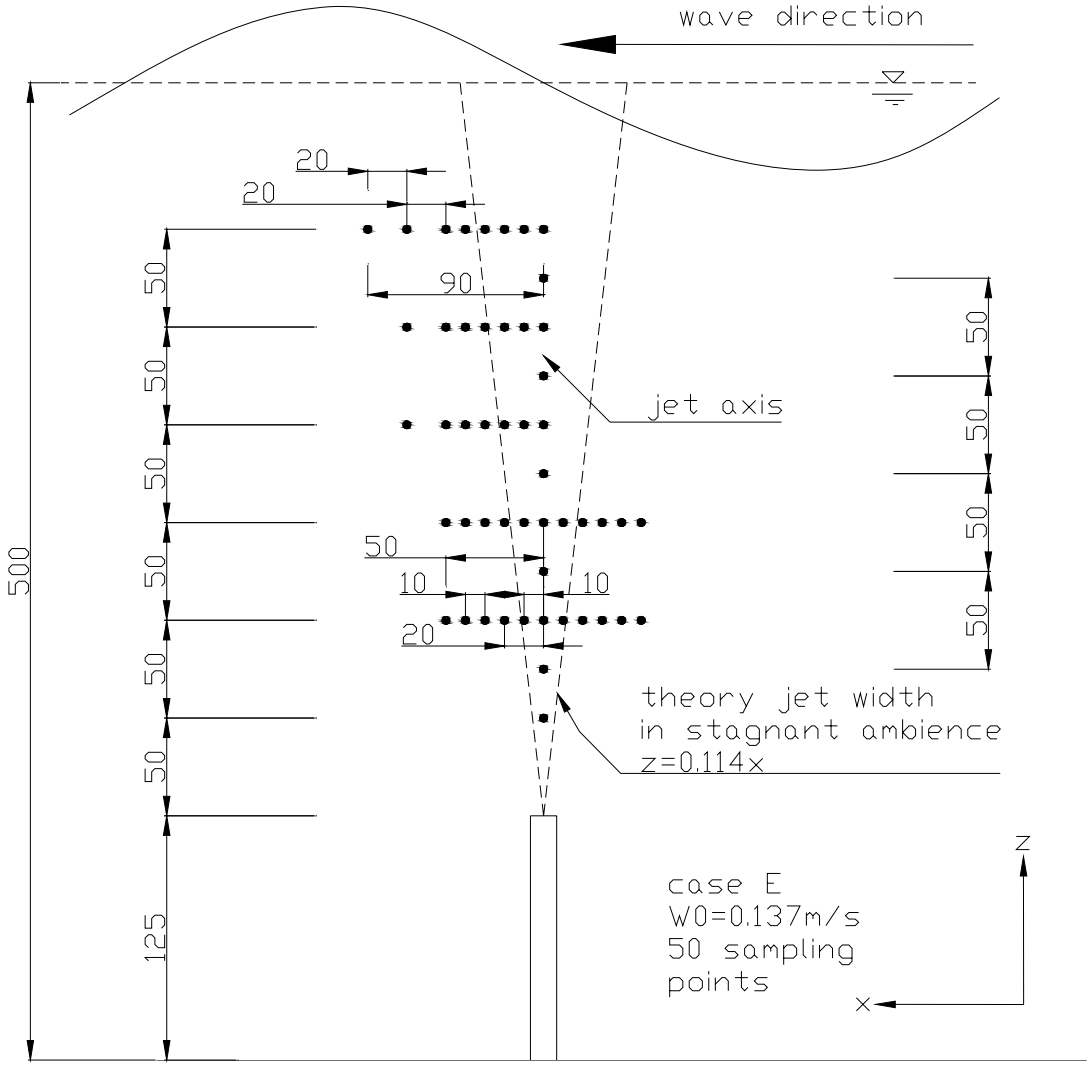

Figure 3.9. The selected ADV sampling points for case E experiments.

3.3.4 *Flow visualization*

Flow visualization was conducted at the end of each set of experiments. A common fluorescent dye, Rhodamine B ($C_{28}H_{31}N_2O_3Cl$) was used. Rhodamine B is highly soluble in water and has density very close to that of water when it is fully mixed with water. Hence, the jet discharge fluid density and the ambient fluid density were almost the same.

The water jet was then fed by the dye tracer and discharged into the receiving water body. A 3-CCD digital video camera was placed at one side of the wave flume. The jet discharge process was then captured by the video camera through the glass wall of the wave flume as shown in Photo 3.4.

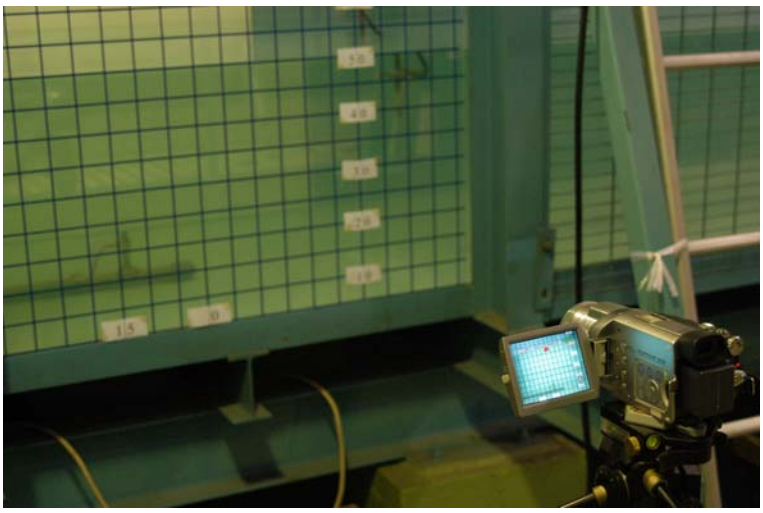

Photo 3.4. The 3-CCD digital video camera focuses on the jet discharge setup.

Each experimental condition listed in Table 3.1 was repeated while the jet discharged fluid was mixed by the colour tracer. The jet flow pattern in a given period of time was recorded. This was used to analyse the jet discharge behaviour in random wave environments and in stagnant ambience.

4 THEORETICAL ANALYSIS

4.1 Introduction

The mechanism of the jet-wave interaction is briefly discussed in this chapter. The technique of dimensional analysis is used to simplify the analysis of the experimental data and to obtain physical insight of the phenomenon. The selection of the characteristic velocity for the random wave-induced fluid motion is described. In the analysis, the concept of crossflow momentum length scale proposed by Wright (1977) is adopted. Wave characteristic velocities calculated by the wave energy spectrum are introduced to construct the wave-induced momentum characteristic length, which is similar to the crossflow momentum length scale.

4.2 Mixing mechanism

The jet discharge in stagnant ambience usually generates the turbulent entrainment process. Turbulent entrainment occurs when jet discharges with high Reynolds number, i.e. Re > 2000. The turbulent eddies, generated at the boundary of the jet body, entrain the surrounding fluid into the jet. This mechanism enhances the jet width and reduces the concentration of the tracer in the jet body along the jet discharge direction.

The jet discharge in the presence of surface wave is expected to have an additional mechanism of mixing which will speed up the mixing process and to enhance the rate of dilution. The jet discharge into a crossflow ambient usually experiences a counter-rotating vortex pair (CVP) as display in Fig. 4.1. The formation of the CVP is possibly initiated by the shear layer at the potential core (Kelso et al. 1996; Lim et al. 2001). A vortex street is generated behind the potential core. The vortex street is then emerged to the jet body. After that, the CVP begins to form. The counter-rotating vortex pair entraps the ambient fluid to the jet body resulting in an extra mixing mechanism in the jet in crossflows. Because additional fluid mass is enrolled into the jet body, the jet velocity is increasingly dissipated due to the additional fluid entrainment mechanism. Consequently, the jet centerline half-width will have a larger spreading rate (i.e. $b = \beta z$, $\beta = 0.297$, Lee and Chu 2003) in crossflows than that in stagnant condition (i.e. $\beta = 0.114$, Albertson et al. 1950). Similar concept is applied to the jet in wave conditions as the propagation of surface waves is indeed a periodical forward and backward fluid motion. As long as the jet trajectory is kept on oscillating by the wave motion, the ambient fluid is entrapped to the center of the jet body. This was confirmed by the flow visualization by Chyan and Hwung (1993). They used the laser induced fluorescence (LIF) technique to lighten the jet body cross-section. A horseshoe shape jet body boundary

in the presence of regular surface wave was clearly presented by their image analysis. This horseshoe shape vortex mechanism confirmed the ambient water was entrapped into the jet body. Although the wave induced current is an unsteady current, the oscillating wave property allows the jet to entrap the surrounding fluid to the jet main body based on the generated vortex mechanism. Consequently, the jet body in the transverse direction is greatly expanded and the rate of dilution is improved in the presence of wave motion.

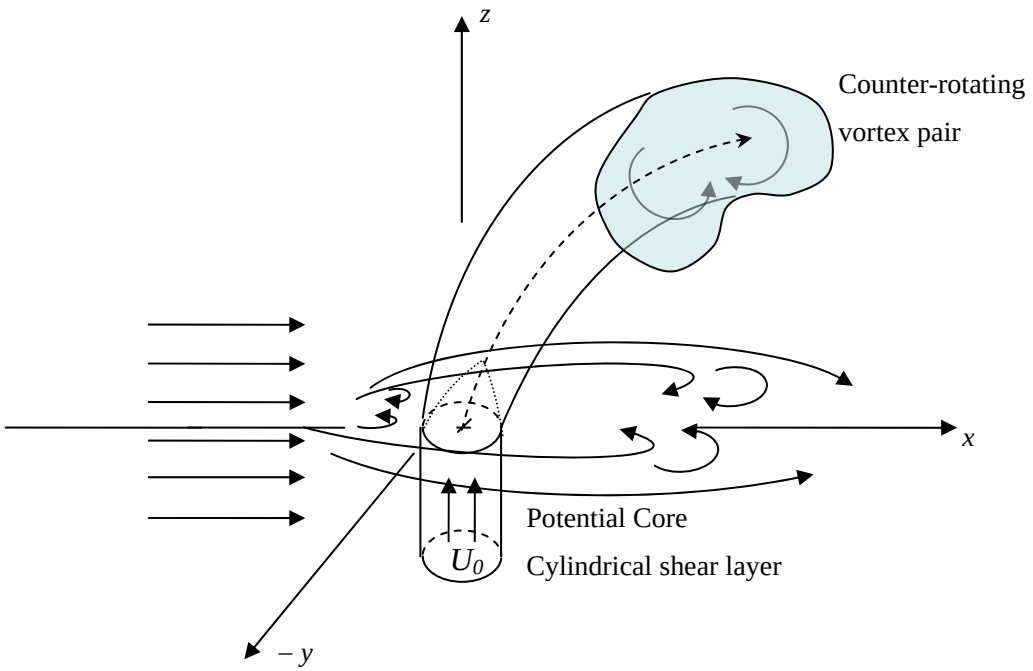

Figure 4.1. Schematic diagram showing the generation of counter-rotating vortex pair.

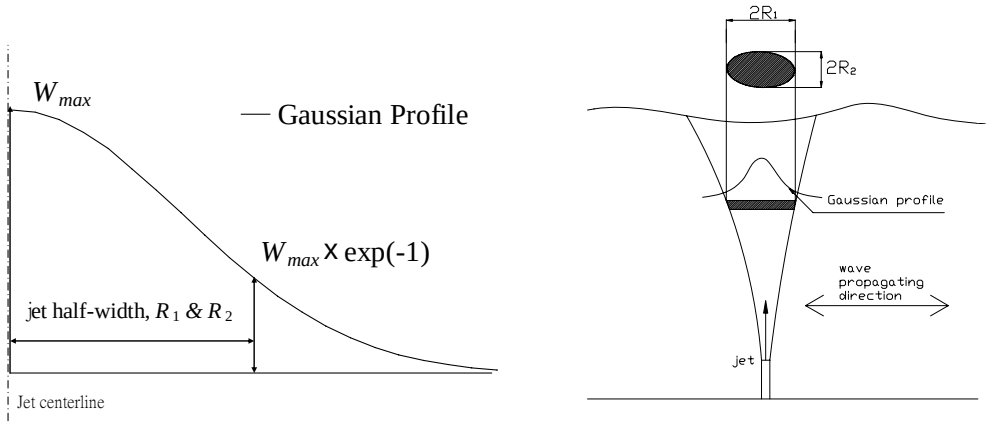

Figure 4.2. Definition sketch of jet half-width in the wave environment.

Fig. 4.2 shows the definition of the jet half-width which is defined as the distance measure from the jet centerline to the point at which the velocity is equal to 1/*e* of the centerline velocity (W_{max}). For the round jet discharges into a two-dimensional wave environment, the time-averaged jet width is expected to be widened in the direction of wave propagation. An elliptical jet cross-sectional flow area is then formed. As the jet width is the parameter to define the flow cross-sectional area, this study suggests the jet half-width should be determined by Eq. 4.1:

$$b = \sqrt{R_1 R_2} \tag{4.1}$$

4.3 Dimensional analysis

The method of dimensional analysis is usually adopted for the analysis of jet characteristics. Most dimensional analyses of turbulent jets in stagnant ambience consider only the independent variables in Eq. 4.2:

$$\phi = f(d, M_0 = Q_0 W_0, Q_0 = \frac{W_0 \pi d^2}{4}, W_0, z) \tag{4.2}$$

where d = jet nozzle diameter, M_0 = initial momentum flux, Q_0 = initial jet flow rate, W_0 = jet discharge velocity and z = distance along jet axis. The variables are combined to form two non-dimensional terms (Eq. 4.3), in which l_Q is a characteristic length. The relationship between this dimensionless velocity and dimensionless jet distance was obtained by Albertson et al. (1950) expressed explicitly by Eq. 4.4 and shown in Fig. 4.3.

$$\phi\left(\frac{z}{l_Q}, \frac{w_c}{W_0}\right) = 0 \tag{4.3}$$

$$\frac{w_c}{W_0} = 7\left(\frac{z}{\sqrt{A}}\right)^{-1} \tag{4.4}$$

where $l_Q = \frac{Q_0}{\sqrt{M_0}} = \sqrt{A}$, w_c = centerline velocity and A = jet area.

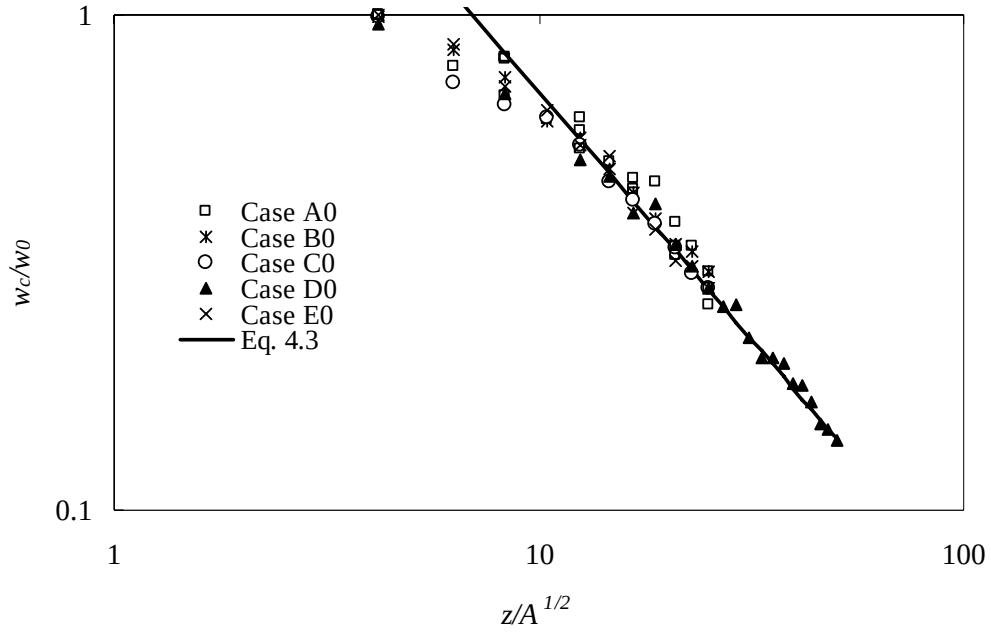

Figure 4.3. Jets discharge in stagnant ambience fluid.

The experimental results obtained in no wave condition in this study are also introduced to Fig. 4.3. All the data agree with Eq. 4.4 for $z/\sqrt{A} > 10$. This shows the experimental setup as described in Chapter 3 is proper and suitable for carrying out the jet-wave experiments.

In an attempt to determine the relevant parameters in the jet discharge in wave environment, a dimensional analysis for jet motion is performed. The following variables are considered significant for jet in wave environment:

$$\phi = f(d, g, h, H, T, W_0, w_c, z) \tag{4.5}$$

where d = jet nozzle diameter, g = acceleration due to gravity, h = water depth, H = wave height, T = wave period, W_0 = jet discharge velocity, w_c = centerline velocity and

z = distance along jet axis. As the acceleration due to gravity is a constant equal to 9.81m/s^2, Eq. 4.5 can be reduced to Eq. 4.6.

$$\phi = f(d, h, H_i, T_i, W_0, w_c, z) \tag{4.6}$$

4.3.1 *Crossflow length scale*

Considering a buoyant jet discharge in crossflows, any dependent variable ϕ can be expressed as a function of various independent variables as shown in Eq. 4.7 :

$$\phi = f\left(Q_0 = \frac{W_0 d^2}{4}, M_0 = Q_0 W_0, B, U_a, z\right) \tag{4.7}$$

where B = buoyancy flux, M_0 = initial momentum flux, Q_0 = initial jet flow rate, U_a = ambient crossflow velocity. Wright (1977) combined those variables in Eq. 4.7 and proposed the momentum length scale (l_m, Eq. 4.8) and the buoyancy length scale (l_b, Eq. 4.9) for the analysis of buoyant jet in crossflow.

$$l_m = \frac{\sqrt{M_0}}{U_a} \tag{4.8}$$

$$l_b = \frac{B}{U_a^3} \tag{4.9}$$

The momentum length scale is used when the jet body is momentum dominated while the buoyancy length scale is used when the jet body is buoyancy dominated. These length scales are then used to distinguish the flow properties at different region measured by the relative distance from the jet origin (z). For

instance, the jet momentum, *M*, is dominant when the dimensionless jet distance, *z*, is smaller than the momentum length scale, l_m. And U_a is dominant when $z >> l_m$. The region of $z << l_m$, is denoted by the momentum dominated near field (MDNF) while the region of $z >> l_m$ is denoted by the momentum dominated far field (MDFF).

Using those crossflow length scales mentioned above, the velocity along the deflected jet axis, u_j, can be characterized in the form of Eq. 4.10.

$$\phi\left(\frac{z}{l_m}, \frac{l_b}{l_m}, \frac{u_j}{U_a}\right) = 0 \tag{4.10}$$

For a non-buoyant jet discharge into a cross current, Eq. 4.10 is further simplified to Eq. 4.11,

$$\phi\left(\frac{z}{l_m}, \frac{u_j}{U_a}\right) = 0 \tag{4.11}$$

If the crossflow velocity is relatively small compared with the jet discharge velocity then $z/l_m \le 1$, and the region is jet momentum dominated. This region is also known as the strong jet region. The crossflow momentum only slightly affects the jet momentum. Davidson and Pun (1998) derived a set of relationships for the strong jet region as shown in Eq. 4.12

$$\frac{u_j}{U_a}\frac{\Delta_0}{\Delta} = C\left(\frac{s}{M_{e0}^{1/2}/U_a}\right)^{-1} \tag{4.12}$$

where C is a constant composed of a shape constant and a Gaussian spread constant, M_{e0} = initial jet momentum, s = distance along the jet trajectory, Δ = centerline density deficit and Δ_0 = initial density deficit. Regarding the submerged vertical non-buoyant jet discharge to the crossflow, if the jet velocity to crossflow velocity ratio tends to zero, $R = W_0 / U_a \to 0$, the jet trajectory, in general, is roughly the same as the jet discharge in the stagnant ambient fluid. Davidson and Pun (1999) then rewrote Eq. 4.12 to Eq. 4.13.

$$\frac{w_c}{U_a} = C\left(\frac{z}{l_m}\right)^{-1} \tag{4.13}$$

Wave motion is periodic with the fluid particles moving to and fro. The degree of wave-induced fluid movement is dependent on the level. Considering a submerged vertical jet discharge into the wave environment, the wave induced horizontal velocity should be relatively small in the jet orifice except in the presence of shallow water waves. A formation of strong jet region is expected. For small amplitude waves, the net fluid particle displacement is zero based on linear wave theory. The time-average jet trajectory obtained in wave environment should be the same as that obtained in stagnant ambience. The lateral entrainment of water into the jet body due to wave motion will be similar to that due to crossflow. However, a

proper selection of the characteristic velocity to represent the wave effect is required to replace the ambient velocity, U_a in the case of crossflow.

4.3.2 *Characteristic wave velocity*

The wave induced fluid motion is the key factor causing the deflection of the jet trajectory and the change of the jet characteristics. Wave characteristics are dependent on the wave period and the wave height. Chyan and Hwung (1993) used the depth-averaged time-averaged wave induced horizontal velocity, u_{avg} (Eq. 4.14), as the characteristic velocity for regular surface waves.

$$u_{avg} = \frac{gHT}{2h\pi^2}\tanh kh \tag{4.14}$$

where g = acceleration due to gravity, h = water depth, H = wave height, k = wave number and T = wave period.

However, this characteristic velocity may underestimate the influence of the wave motion on jets. The maximum jet deflection is due to the maximum wave induced velocity. In addition, Eq. 4.14 may further underestimate the degree of influence by the presence of waves. Therefore, Chin (1987) suggested to use the maximum wave induced velocity located at the bottom boundary, u_{bottom} (Eq. 4.15), based on the linear wave theory as the wave characteristic velocity.

$$u_{bottom} = \frac{agk}{\sigma\cosh kh} = \frac{\pi H}{T\sinh kh} \tag{4.15}$$

where a = wave amplitude and σ = angular wave frequency.

Irregular waves do not have a constant wave height and wave period. Although the jet discharges under a chain of irregular waves under narrow-banded spectrum may by subjected to a similar impact as that of jet discharge in regular waves, the flow behaviour due to random waves and that due to regular waves are fundamentally different. In addition, the choice of the appropriate key wave parameters may be crucial to the selection of the characteristic velocity.

$$E_{wave} = \frac{1}{8}\rho g H^2 \tag{4.16}$$

$$E_{wave} = \rho g E_{spectrum} = \frac{\rho g H_s^2}{16} = \frac{\rho g H_{rms}^2}{8} \tag{4.17}$$

where $E_{spectrum}$ = total area of the wave energy spectrum and ρ = fluid density.

The significant wave height, H_s, and the peak wave period, T_p, are usually used in random sea waves for coastal engineering design purposes. The significant wave height obtained in irregular waves cannot be directly compared with the constant wave height obtained in regular waves. This is because the total wave energy calculated with the use of H_s is indeed half of the total energy achieved in the corresponding constant wave height as reflected in Eqs. 4.16 and 4.17. This suggests that it may not be a right approach to determine the random wave characteristic velocity by adopting either Eq. 4.14 or Eq. 4.15 with the use of H_s and T_p instead of H and T.

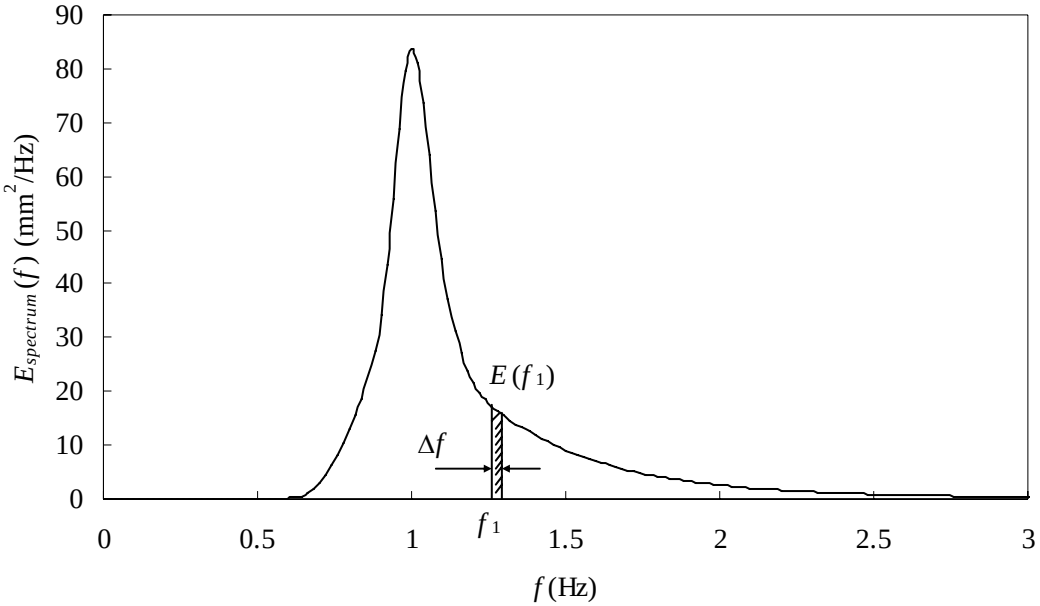

Figure 4.4. Wave energy density spectrum obtained in Case E1-2 experiment.

Fig. 4.4 shows a wave energy density spectrum obtained in Case E1-2 experiment. Wave periods and wave heights in association with the known energy spectrum can be calculated by Eqs. 4.18 and 4.19. The phase angle associated with each pair of wave height and wave period is given by Eq. 4.20.

$$H(f_1) = 2\sqrt{2E_{spectum}(f_1)\Delta f} \tag{4.18}$$

$$T(f_1) = 1/f_1 \tag{4.19}$$

$$\varepsilon(f_1) = 2\pi R_N \tag{4.20}$$

where the R_N is the random number generator and Δf is the frequency interval. The free surface wave or the surface elevation fluctuation (η) regarding the change of time, *t*, can then be simulated numerically by using of Eq. 4.21:

$$\eta(t) = \sum_{n=1}^{N} \frac{H(n)}{2} \cos\left[\frac{2\pi}{T(n)} t - \varepsilon(n)\right] \tag{4.21}$$

The random waves induced fluid particle velocities for horizontal component (u_{wave}) and vertical component (w_{wave}) are then given by Eq. 4.22 and 4.23, respectively.

$$u_{wave}(t) = \sum_{n=1}^{N} \frac{\pi H(n)}{T(n)} \frac{\cosh[k(n)Z]}{\sinh[k(n)h]} \cos\left[\frac{2\pi}{T(n)} t - \varepsilon(n)\right] \tag{4.22}$$

$$w_{wave}(t) = \sum_{n=1}^{N} \frac{\pi H(n)}{T(n)} \frac{\sinh[k(n)Z]}{\sinh[k(n)h]} \sin\left[\frac{2\pi}{T(n)} t - \varepsilon(n)\right] \tag{4.23}$$

where h = water depth, k = wave number corresponding to the n^{th} wave and Z is the flow depth measure from the bottom to the free surface.

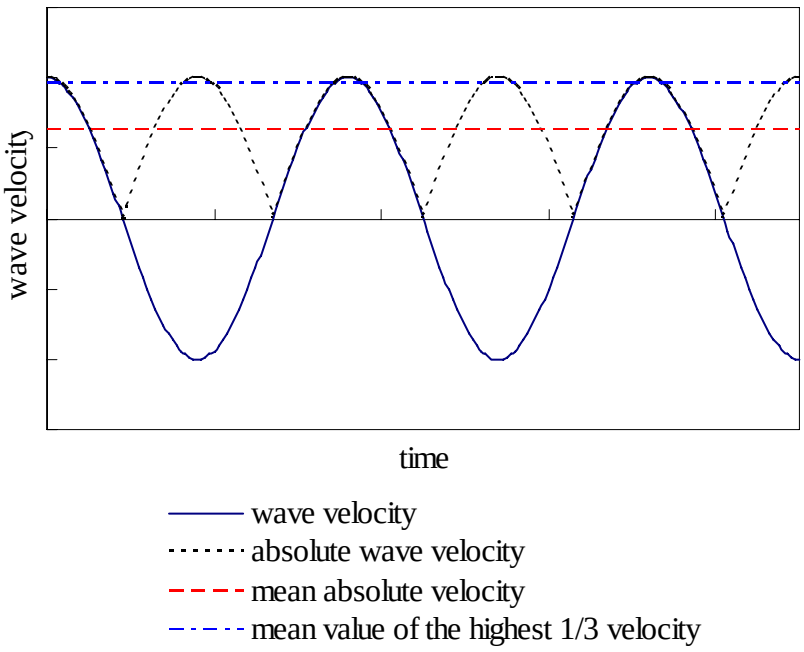

Figure 4.5. Definition sketch of absolute wave-induced horizontal velocity.

With regard to the chain of waves, the wave-induced horizontal velocity is in the form of an oscillating current as displayed in Fig. 4.5 (solid line). Because the

horizontal wave-induced velocity is normal to the jet discharge direction, the velocity pushing and pulling the jet should also be considered as the characteristic velocity. The wave characteristic velocity should be the mean value of the absolute horizontal wave-induced velocity. In the presence of random wave motion, the wave characteristic velocity (u_w) is, therefore,

$$u_w = \frac{1}{T_{total}} \int_0^T \left| \sum_{n=1}^{N} \frac{\pi H(n)}{T(n)} \frac{\cosh(kZ)}{\sinh(kh)} \cos\left[\frac{2\pi}{T(n)} t - \varepsilon(n) \right] \right| dt \qquad (4.24)$$

where T is the total sampling time. Because the wave-induced velocity is a depth-dependent variable, the degree of wave-induced horizontal velocity should be dependent on the level.

As described in the analysis of jet in regular waves, the maximum horizontal wave-induced velocity (i.e. Eq. 4.15) is usually used as the velocity scale. Because the maximum state is difficult to be defined in the random wave condition, the mean value from the greatest one-third of the waves is commonly used to represent the significant value for engineering design purposes. Based on Eq. 4.22, the time series of the wave-induced velocity can be re-generated. By ranking all the absolute velocity data from the highest to the lowest, the wave-induced significant velocity (u_{sig}), which is the mean absolute values of the highest one-third of wave-induced horizontal velocity in the given sampling period, can be defined by Eq. 4.25.

$$u_{sig} = u_{1/3} = \frac{1}{N/3}\sum_{i=1}^{N/3}\left|u_{wave}(i)\right| \tag{4.25}$$

where N = number of velocity data $\left|u_{wave}(i)\right|$ in a record ranked highest to lowest in the given sampling time T_{total}.

4.3.3 *Characteristic wave velocity – choice of flow depth*

As mentioned, in previous studies regarding the jet-regular-wave interaction the wave-induced velocity at the bottom boundary was used. Because this velocity is depth dependent and decreases from the free water surface, it should reach the minimum at the bottom based on the linear wave theory.

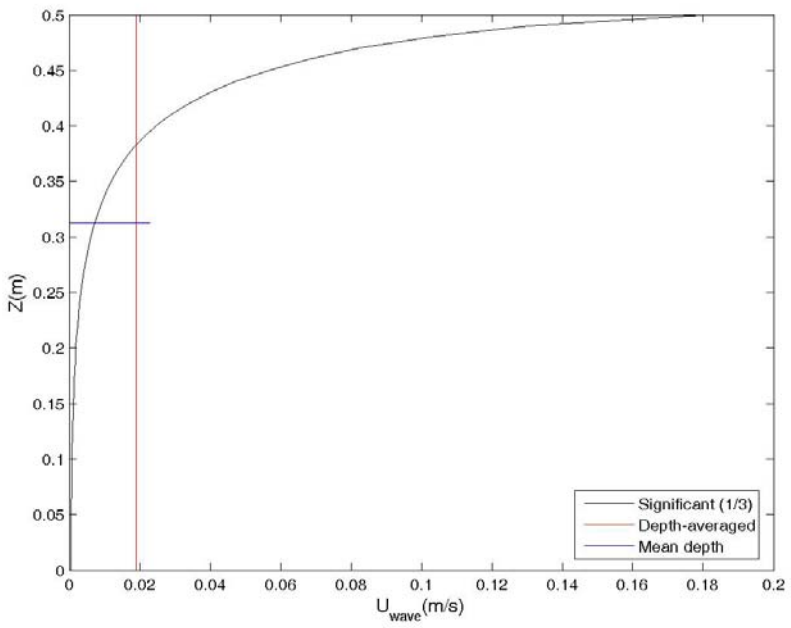

(a)

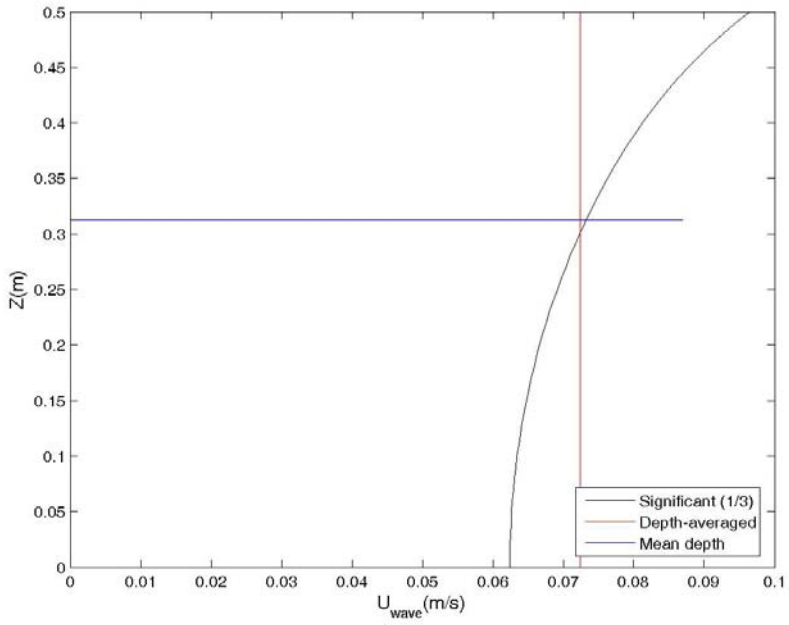

(b)

Figure 4.6. Wave-induced horizontal velocity at various depth obtained in random waves with (a) T_p=0.5s; and (b) T_p=2s.

Figs 4.6 (a) & (b) show the vertical variation of the wave-induced horizontal velocity of the random waves with peak period of 0.5s (deep water waves) and 2s (transitional water waves). The depth-averaged velocity for these two wave conditions are also shown in the figures. It is expected that the interaction between the jet and the wave-induced motion should be the most significant at the jet near field for submarine outfall. Using the minimum wave-induced velocity (at bottom boundary) may underestimate the degree of influence on jet contributed by the deep water waves. On the contrary, the maximum wave velocity as well as the depth-average velocity may overestimate the wave effect on jet. Hence, it is difficult to determine the appropriate water depth at which the wave-induced velocity reflects

the correct jet-random-wave interaction effect. For engineering design purpose, it is common to avoid complicated calculation. The wave-induced velocity which can be easily calculated and reflects appropriately the wave effect is at the mid-depth (the mid-point between the free surface and the jet orifice, i.e. Z_a = water depth (h) at half of the distance from jet orifice to the free water surface). This mid-depth velocity will be used in the subsequent analysis.

4.3.4 *Wave-induced momentum characteristic length*

The above wave-induced characteristic velocities using the mean value and the significant value of the absolute velocity (Eqs. 4.24 and 4.25) are used to replace the ambient velocity, U_a, in Eq. 4.8. The crossflow length scales are modified and expressed as the wave momentum length scales in the form of Eqs. 4.26 and 4.27.

$$l_w = \frac{\sqrt{M_0}}{u_w} = \frac{\sqrt{\pi d^2 W_0^2}}{2u_w} \tag{4.26}$$

$$l_{sig} = \frac{\sqrt{M_0}}{u_{sig}} \tag{4.27}$$

Using the wave-induced momentum length scale and the wave characteristic velocity, the group of variables mentioned in Eq. 4.7 can be expressed in the non-dimensional form of Eqs. 4.28 and 4.29 and can be used to describe the variation of the jet centerline velocity.

$$\phi\left(\frac{z}{l_w},\frac{w_c}{u_w}\right)=0 \tag{4.28}$$

$$\phi\left(\frac{z}{l_{sig}},\frac{w_c}{u_{sig}}\right)=0 \tag{4.29}$$

Based on the crossflow length scale for jets in crossflows, the jet momentum dominates the flow characteristics within the region for $z << l_w$, the wave momentum dominates the flow characteristics within the region for $z >> l_w$, and there is a transition region at $z \sim l_w$. This possibly suggests that the jet characteristics obtained within the region of $z << l_w$ would be similar to those obtained in stagnant ambience while the jet behaviour is mainly controlled by the wave-induced to and fro motion when $z >> l_w$. (similar interpretation can be obtained with the use of l_{sig}).

The length and velocity scales proposed in this chapter is then used to analyze the jet characteristics such as the declining rate of centerline velocity (hereafter referred as the velocity decay rate) and jet width spreading rate for jet in waves. The results are presented in the next chapter.

5 RESULTS AND DISCUSSION

5.1 Introduction

The results of the experiments outlined in Chapter 3 are presented in this chapter. Flow visualization concerning the jet-wave interaction and the jet motion are shown in this chapter together with the DV captured images. The velocity measurements such as the declining rate of jet centerline velocity, radial profiles of axial velocity and the turbulence intensity conducted with the use of acoustic Doppler velocimeter (ADV) are presented. The jet characteristics such as the jet width spread rate, the length of the potential core are discussed.

5.2 Flow visualization

Flow visualization was conducted with the use of a 3-CCD digital camera. Rhodamine B ($C_{28}H_{31}N_2O_3Cl$) was used as the colour tracer to show the interaction of the jet discharge in wave environment. The three types of jet motions: symmetric, asymmetric and discontinuous jet motions, suggested by Mori and Chang (2003) were also observed and are discussed in this section.

5.2.1 *Jet-wave interaction*

Regarding the flow patterns for experiment A2-3 at different instants, Fig. 5.1 (a) – (d) show the interaction between the jet body and the wave motion. At the very beginning, when the surface wave has not reached the jet region, the jet flow pattern is the same as that in stagnant ambient as shown in Fig. 5.1(a). Once the wave reaches the jet region from right to left, the jet trajectory begins to bend to the left side as indicated in Fig. 5.1(b). The jet trajectory is deflected from left to the middle and then to the right once the wave trough has passed through the jet region from right to left [Figs. 5.1(c) & (d)]. Because the jet trajectory kept on oscillating, more ambient water is entrained into the jet body, resulting in a larger jet volume under the presence of waves. The ambient fluid is effectively entrapped into the jet center area and dilutes the dye tracer. The mechanism observed in this study, should be “the

wave tractive mechanism" proposed by Chyan and Hwung (1993). This mechanism repeated frequently in the continuous propagated horizontal random waves to enhance the rate of dilution.

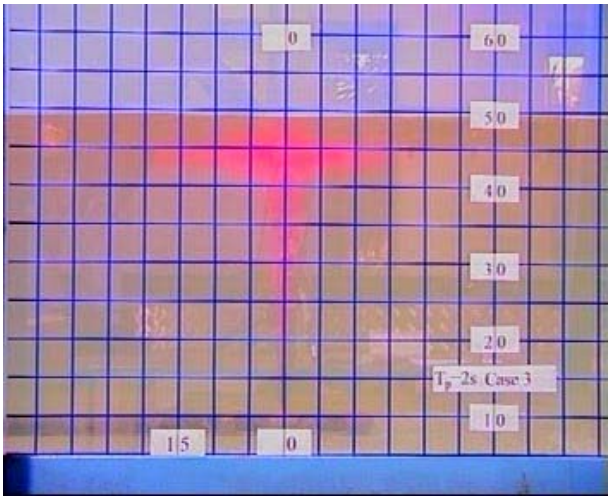

(a) $t/T_p = 0$

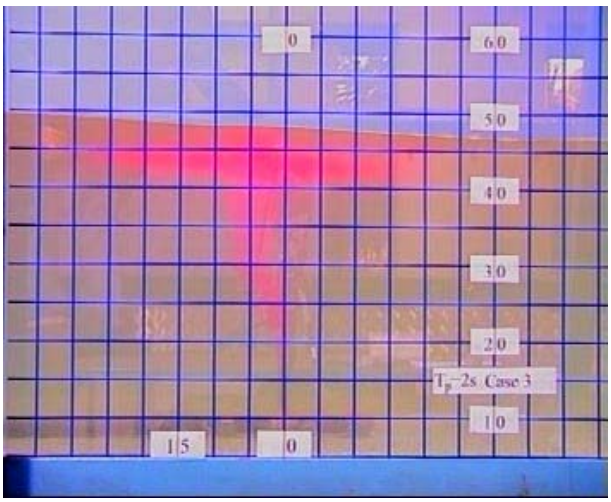

(b) $t/T_p = 1/2$

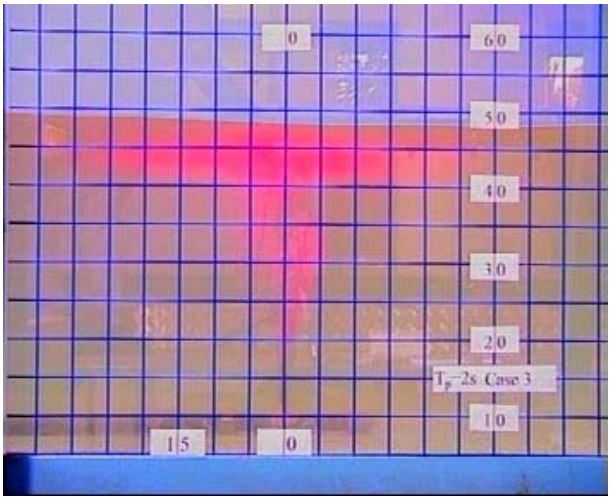

(c) $t/T_p = 3/4$

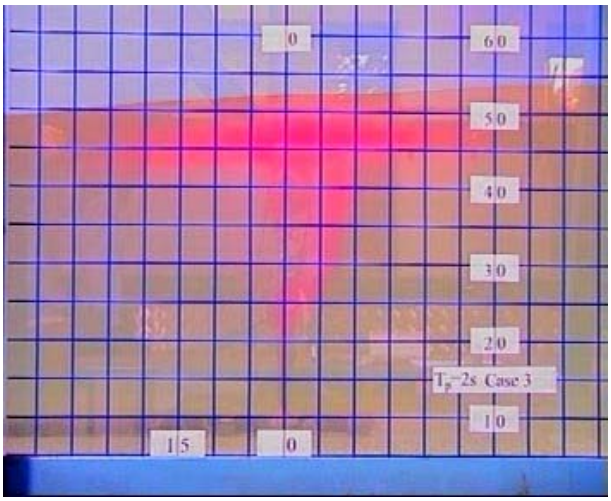

(d) $t/T_p = 1$

Figure 5.1. Jet flow patterns on different wave phases (Case A2-3): t/T_p= (a) 0; (b) 1/2; (c) 3/4; (d) 1.

Recently, a similar image analysis using Rhodamine B colored dye, a video camera and a video recorder to investigate the jet flow pattern in regular wave environment was performed by Mossa (2004a). The analysis confirmed the existence of three different regions which are deflection, transition and developed regions as defined by Chyan and Hwung (1993). A similar experimental phenomenon has been reproduced in this study. As shown in Fig. 5.2, the colored tracer shows a new bud of

the jet trajectory during a surface wave pass through the jet region. The deflection and developed regions can roughly be identified while the transition region is not apparent based on the captured images in this study. Although the transition region cannot be clearly reflected in the images, the length of the deflection region is noticed to be dependent on the discharge velocity as shown in Figs. 5.2, 5.3(a) and (b) (as denoted by the white line) under the same wave condition. The stronger the jet discharge was imposed, the longer the deflection region obtained.

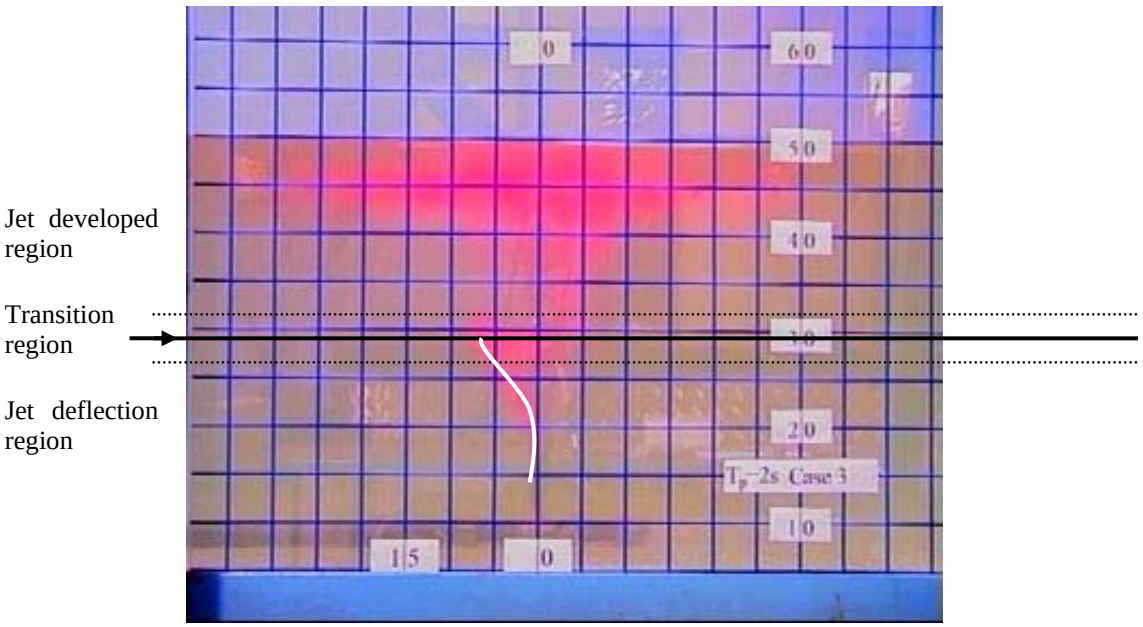

Figure 5.2. Schematic description of the jet deflection, transition and developed regions (Case B3-3).

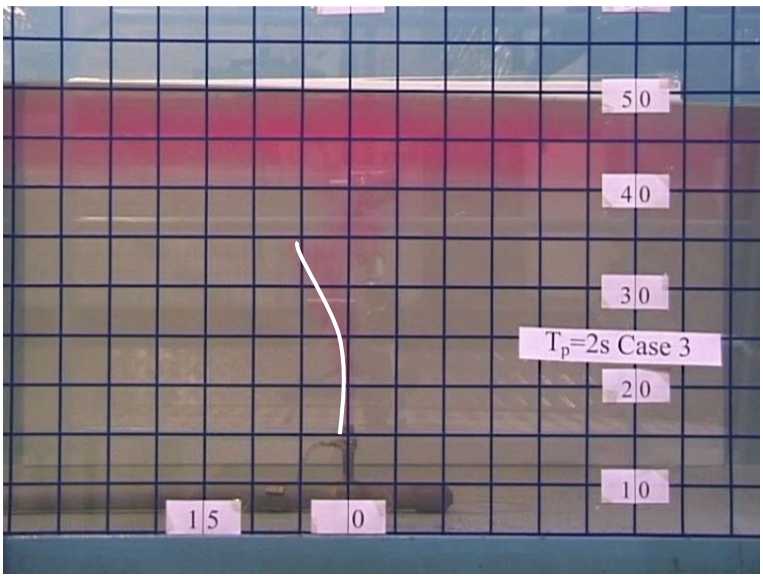

(a)

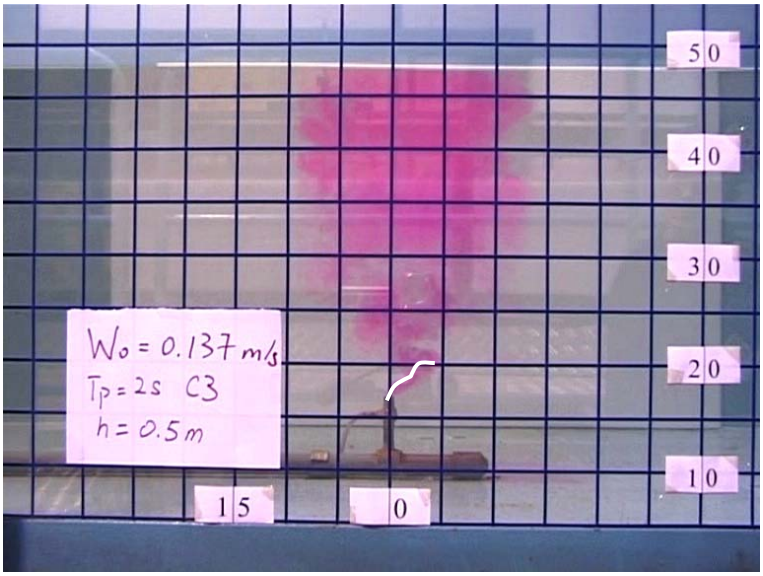

(b)

Figure 5.3. Deflection region obtained at (a) Case C2-3; and (b) Case E2-3.

5.2.2 *Jet motions*

The discharge of a momentum jet interacts with the cross-current resulting in a deflected jet trajectory. Many studies for jet in crossflows have used the velocity ratio, $R = W_0/U_a$, to identify the degree of influence due to the ambient velocity (U_a) to the jet discharge velocity (W_0). This study also uses the velocity ratio to quantify

how jet discharge is influenced by the wave induced fluid motion. The ambient velocity here is replaced by the wave-induced horizontal velocity, u_w, which was described in Chapter 4. The relationship between u_w and other wave parameters is described by Eq. 4.24. As the wave length is comparatively short for peak wave period of 0.5s (i.e. T_p=0.5s), the induced velocity is slow resulting in small jet deflection. This explains why the photo taken for case B1-2 [Fig. 5.4(b)] shows a symmetrical pattern which is very similar to the pattern obtained in stagnant ambience [Fig. 5.4(a)].

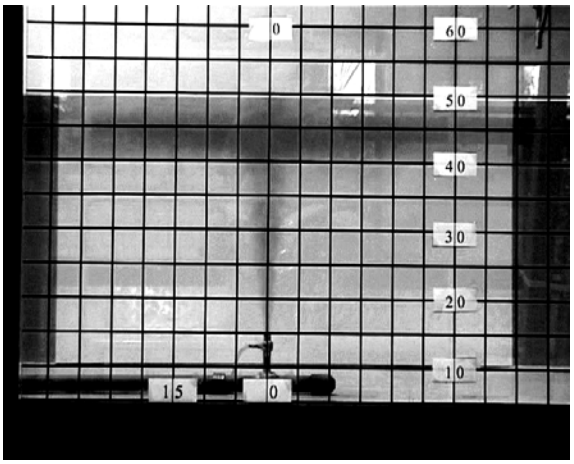

(a)

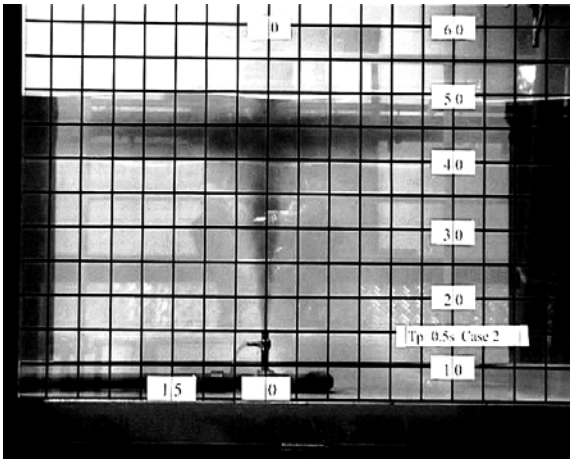

(b)

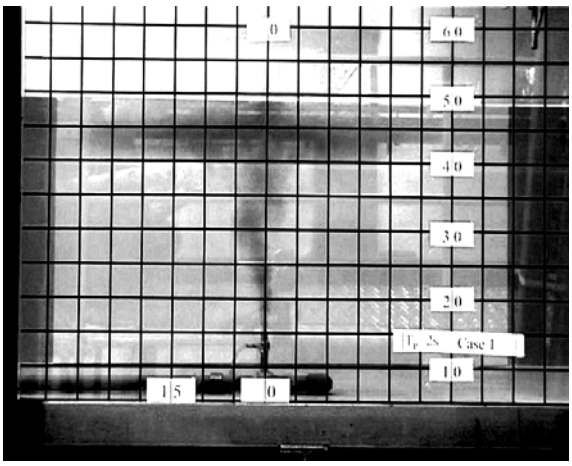

(c)

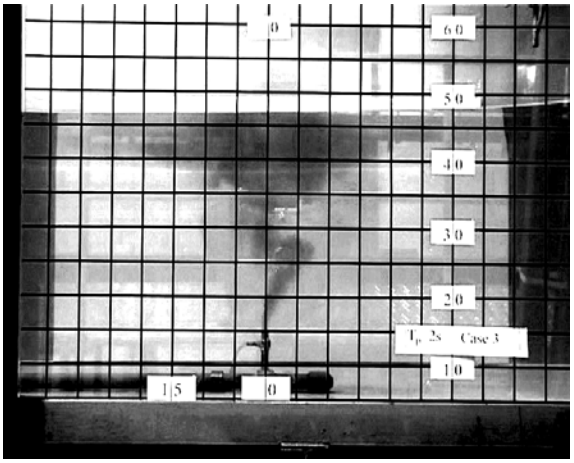

(d)

Figure 5.4. Jet flow visualization obtained in: (a) stagnant ambient at W_0=0.53m/s; (b) Jet in Case B1-2; (c) Jet in Case B3-1; and (d) Jet in Case B3-3 at W_0=0.53m/s.

Jet trajectory deflects and oscillates in the presence of waves. Once waves with long wave periods or great amplitudes are applied, asymmetric jet trajectory or discontinuous jet trajectory are expected. Symmetric, asymmetric and discontinuous motions were reported by Mori and Chang (2003). These 3 types of motions were also noticed in this study with the use of random waves. The symmetric motion is the one with a very symmetrical jet trajectory as shown in Figs. 5.4(a) & (b). Asymmetric

motion refers to the jet with trajectory deflected into an asymmetric shape and a continuous jet trajectory is still maintained as shown in Fig. 5.4(c). Discontinuous motion refers to the jet with trajectory deflected into an asymmetric shape while the continuous jet trajectory is no longer formed. The discontinuous jet trajectory is presented as shown in Fig. 5.4(d). The discontinuous motion is formed because of the presence of strong wave field which induces a relatively fast ambient fluid oscillation and the jet body cannot be sustained. The submerged vertical jet is utilized in this study. The condition of the formation of each type of fluid motion may be different from that of the horizontal jet utilized by Mori and Chang (2003). Nevertheless, the condition should be dependent on the water depth (h) and the velocity ratio of jet discharge to the wave-induced fluid flow, $R = W_0 / u_w$.

5.3 Velocity field

The 10MHz acoustic Doppler velocimeter (ADV) is employed in this study to measure the discharge velocity within the jet body at pre-selected points. The locations of the pre-selected points for each experiment have been listed in Chapter 3. The experimental results for jet centerline velocity decay rate and the cross-sectional velocity profile (in radial direction) for jet in stagnant ambient condition with different jet outlet velocities were conducted and the results are presented in Figs. 5.5 and 5.5.

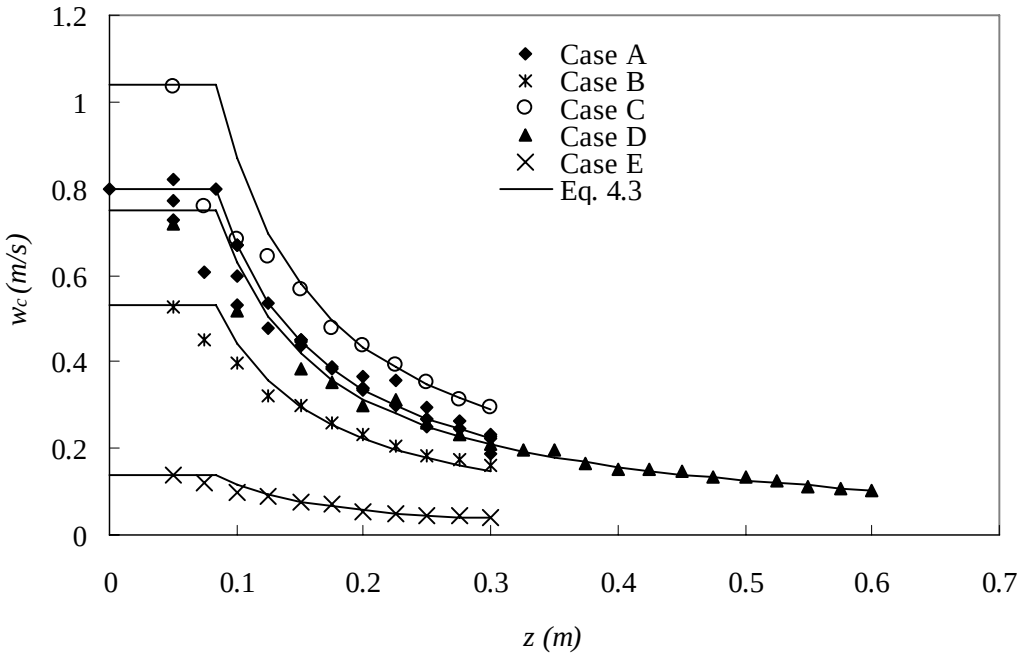

Figure 5.5. Downstream variation of jet centerline velocities under different discharge velocities.

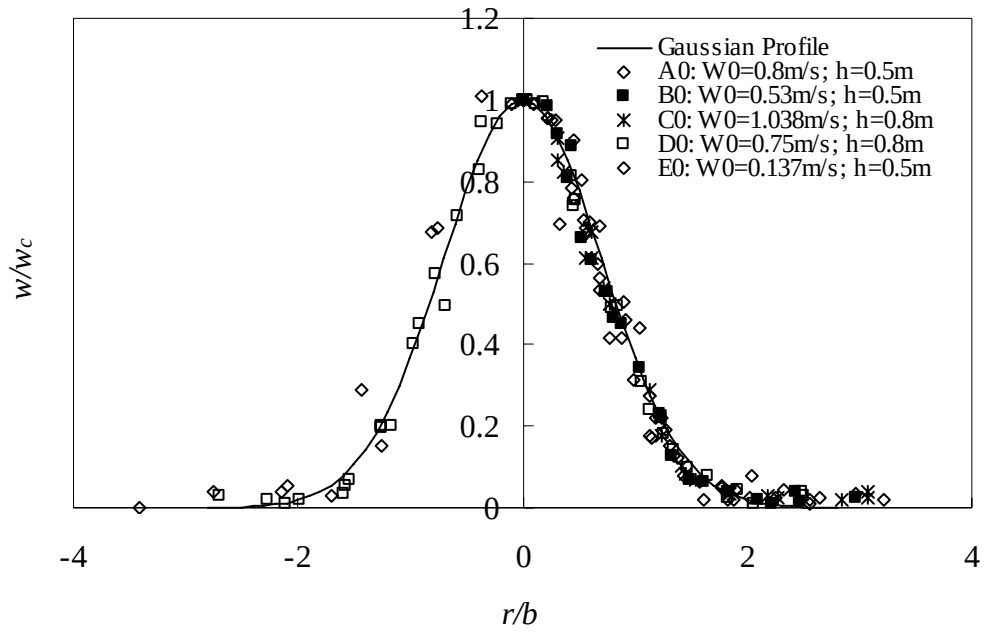

Figure 5.6. Cross-sectional velocity profile measure at stagnant condition.

The velocity decay rates obtained experimentally conform with the well accepted empirical results (Eq. 4.4) while the cross-section velocity distributions follow the Gaussian curve. The agreement in the experimental results of jets in stagnant ambient condition with those reported by others shows that the experimental setup is appropriate for the implementation of further experiments on jets in random wave conditions. The results displayed in Figs. 5.5 and 5.6 can be used as basis for comparison with the corresponding results obtained in a wave environment. In this section, the results of jet centerline velocities and the cross-sectional velocity distribution are addressed.

5.3.1 *Cross-sectional velocity profiles*

Many experimental studies reported that in the zone of established flow (ZEF, $z > 6.2d$), the radial profiles of velocity and concentration generated by submerged turbulent round jet follow a Gaussian distribution curve. Eqs. 5.1a & 5.1b are usually used to estimate the radial velocity and concentration profiles, respectively.

$$\frac{w}{w_c} = e^{\left[-\left(\frac{r}{R_1}\right)\right]^2} \tag{5.1a}$$

$$\frac{c}{c_c} = e^{\left[-\left(\frac{r}{\lambda R_1}\right)\right]^2} \tag{5.1b}$$

where R_1 = jet half-width measured in the direction of wave propagation, defined as the distance from the jet centerline to the point at which the velocity is equal to 1/*e* of the centerline velocity of the same cross section, c = concentration, r = radial distance from jet center, w = vertical velocity, λ = ratio of concentration width to velocity width and subscript "*c*" refers to the jet centerline value.

In this study, the velocity distribution in the direction of wave propagation was examined by positioning a 3D probe of an acoustic Doppler velocimeter (ADV) across the jet flow area. The time-averaged velocity contours of Case B0 (W_0=0.53ms/, stagnant condition) and Case B3-2 (W_0=0.53ms/, random waves of T_p=2s, H_s=28.736mm) were plotted with the freeware, MayaVi, and are presented in

Figs. 5.7(a) – (b). These figures apparently show the jet area is dramatically increased in the presence of random waves.

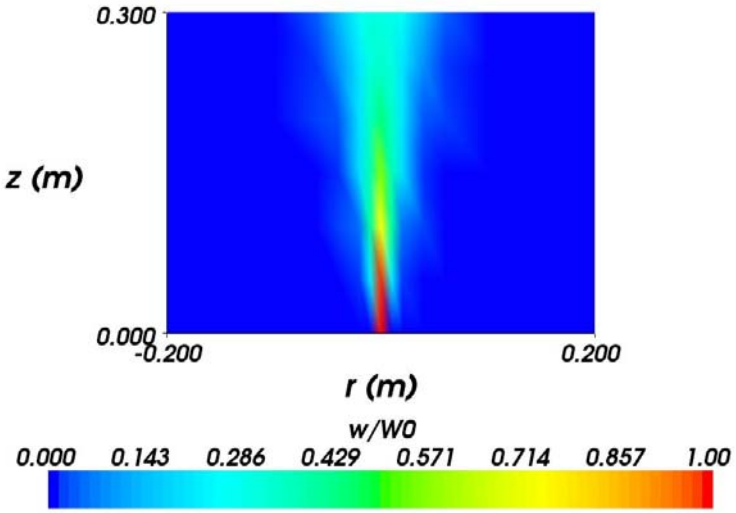

(a) W_0=0.53m/s; no wave

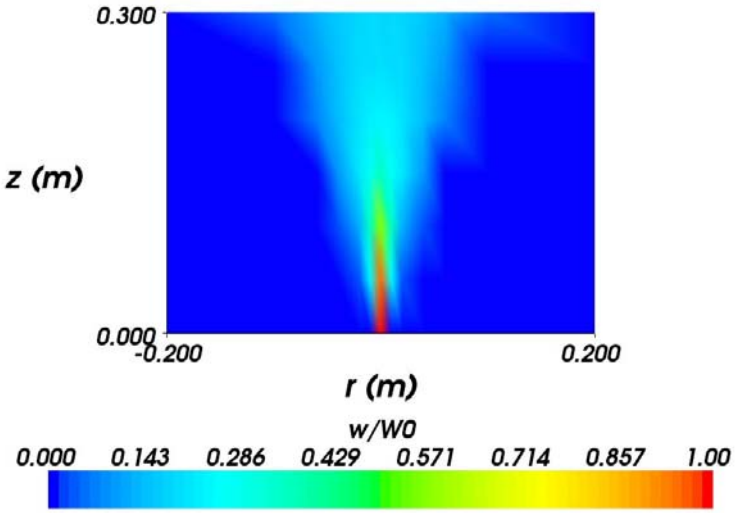

(b) W_0=0.53m/s; B3-2

Figure 5.7 Velocity contour for (a) Case B0; and (b) Case B3-2 experiments.

The time-averaged profiles of vertical velocity in cases of stagnant ambience and in cases with waves are scaled and plotted in Figs. 5.8(a) – (e). The radial distance and the velocity are scaled with the corresponding jet width and the jet center velocity. Although the velocity contour plotting in Fig. 5.7(b) shows a larger jet area in random waves than that in stagnant water, the radial profiles of velocity obtained in this study in general follow the Gaussian distribution.

The data obtained in Case E were much more scattered than the others. It is possibly due to the high value of the velocity ratio R (where $R = W_0 / u_w$, W_0 = jet discharge velocity and u_w = wave-induced velocity based on Eq. 4.24). A high value of R means that the jet flow behaviour is significantly affected by wave induced momentum. It is possibly to have discontinuous jet motion in the jet upstream region. This may alter the jet flow pattern and cause the radial profiles of the velocity departing from the Gaussian distribution. In addition, the low Reynolds number obtained in Case E (Re < 2000) may also affect the shape of the distribution.

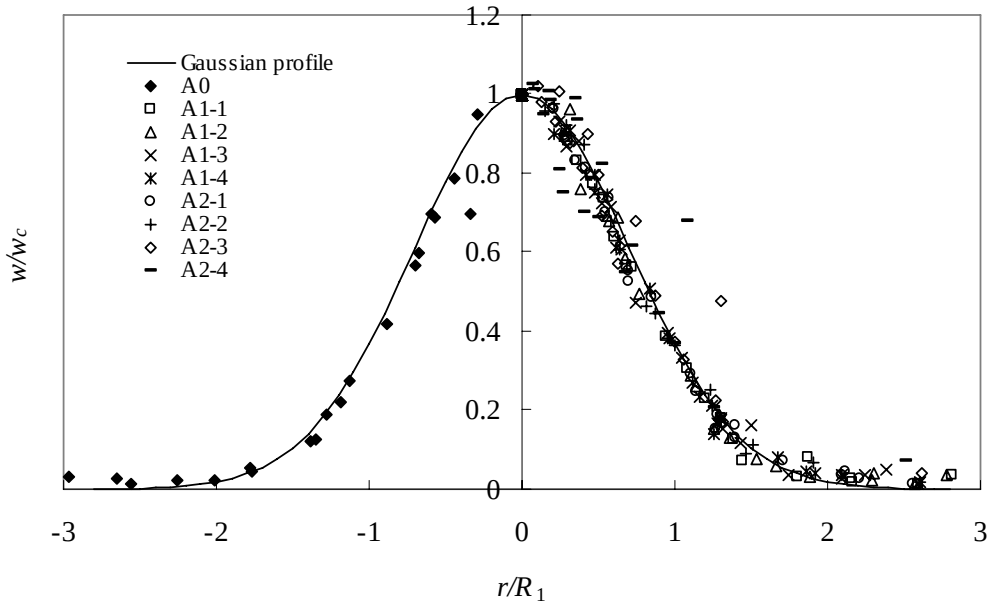
Gaussian profile
A0
A1-1
A1-2
A1-3
A1-4
A2-1
A2-2
A2-3
A2-4
w/w_c
r/R_1
1.2
1
0.8
0.6
0.4
0.2
0
-3
-2
-1
0
1
2
3

(a)

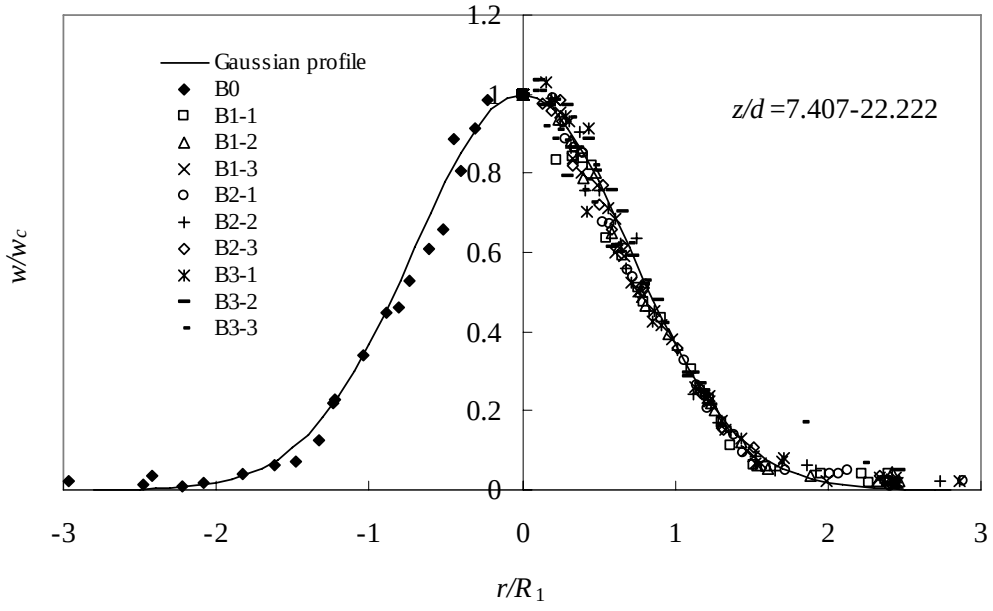
Gaussian profile
B0
B1-1
B1-2
B1-3
B2-1
B2-2
B2-3
B3-1
B3-2
B3-3
z/d =7.407-22.222
w/w_c
r/R_1
1.2
1
0.8
0.6
0.4
0.2
0
-3
-2
-1
0
1
2
3

(b)

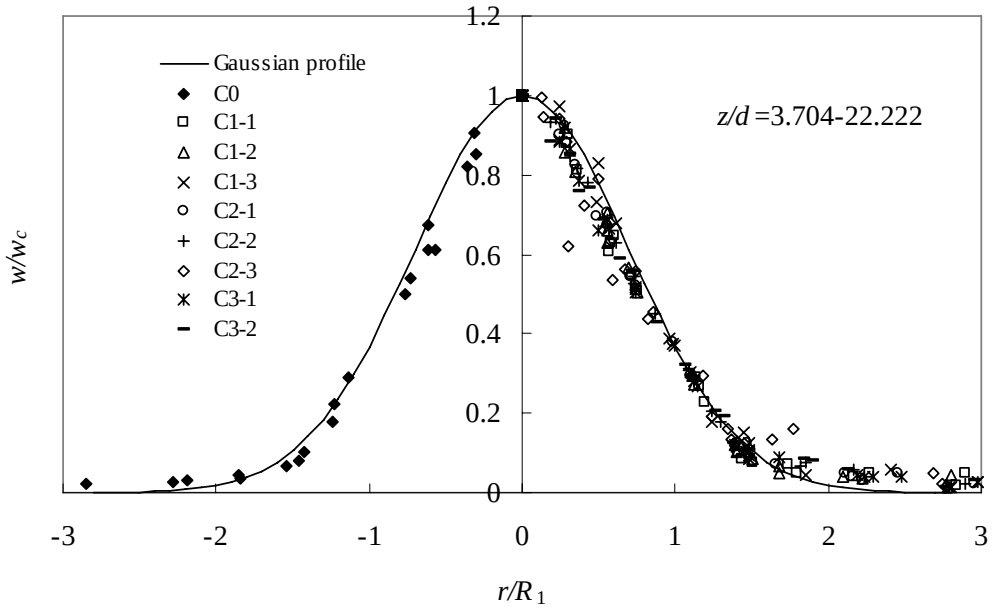
Gaussian profile
C0
C1-1
C1-2
C1-3
C2-1
C2-2
C2-3
C3-1
C3-2
z/d =3.704-22.222
w/w_c
r/R_1
1.2
1
0.8
0.6
0.4
0.2
0
-3
-2
-1
0
1
2
3

(c)

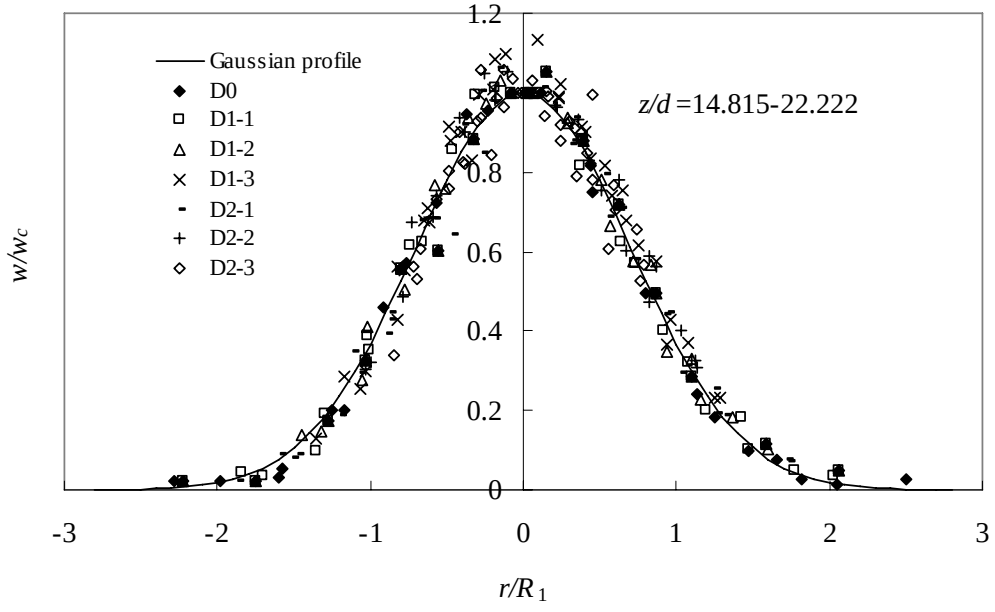
Gaussian profile
D0
D1-1
D1-2
D1-3
D2-1
D2-2
D2-3
z/d =14.815-22.222
w/w_c
r/R_1
1.2
1
0.8
0.6
0.4
0.2
0
-3
-2
-1
0
1
2
3

(d)

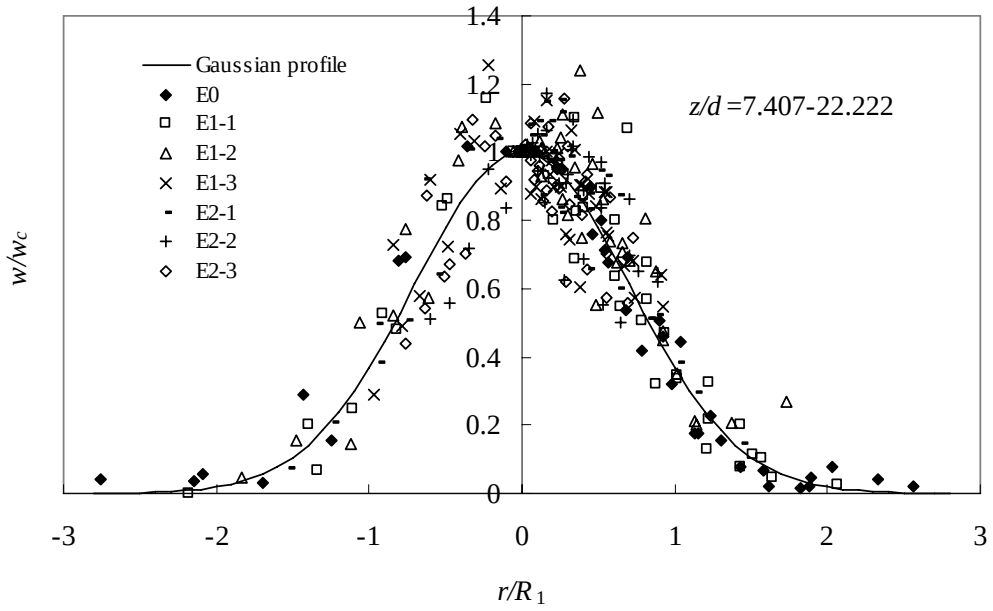

(e)

Figure 5.8. Cross-sectional (along wave direction) velocity profiles for (a) Case A; (b) Case B; (c) Case C; (d) Case D; and (e) Case E.

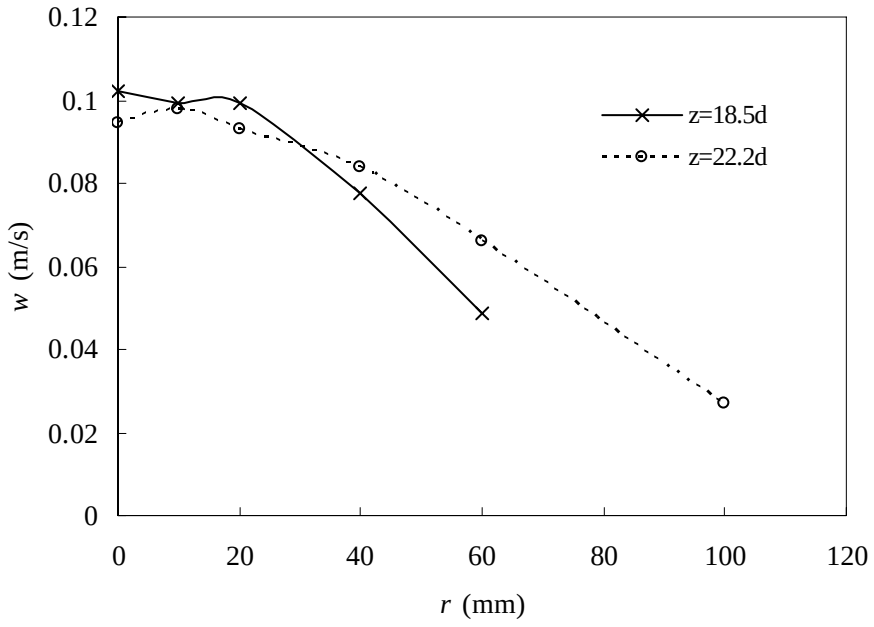

Figure 5.9. Twin peak radial velocity profiles observed in Case B3-2

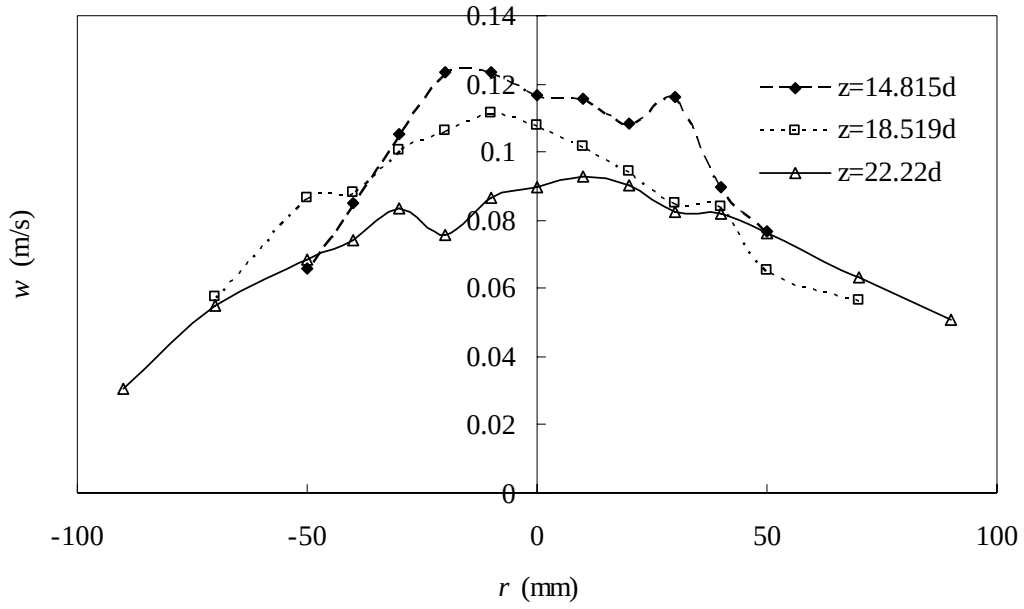

Figure 5.10. Multiple-peak radial velocity profiles observed in Case D2-3

Chyan and Hwung (1993) discovered the occurrence of twin peak radial profiles of velocity for cases with longer period waves. This phenomenon was occasionally observed in some of our experiments, i.e. Case B3-2 (Fig. 5.9) and D2-3 (Fig. 5.10). The formation of a twin peak or multiple-peak radial profile of velocity is possibly due to the wave induced motion that alters the jet trajectory. Detailed explanation has been given by Koole and Swan (1994b). The normal distribution profile is shifted periodically in the presence of regular waves as illustrated in Fig. 5.11. Consequently, the twin peak velocity profile as shown in Fig. 5.12 is formed based on the time-averaged analysis. As the profiles may not be advected regularly and periodically in random wave environment, multiple-peak profiles as observed in Fig. 5.10 may possibly be formed.

It was observed that the twin peak radial profiles of velocity are formed easily when the wave field is relatively strong or the jet momentum is relatively weak. It can be explained by that strong waves usually have longer wavelengths (L) and higher particle velocity u_w. The wave induced non-dimensional jet displacement, L/R_1, thus will be relatively large and lead to a higher probability for the formation of twin peak (or multiple-peak) velocity profiles after time-averaging.

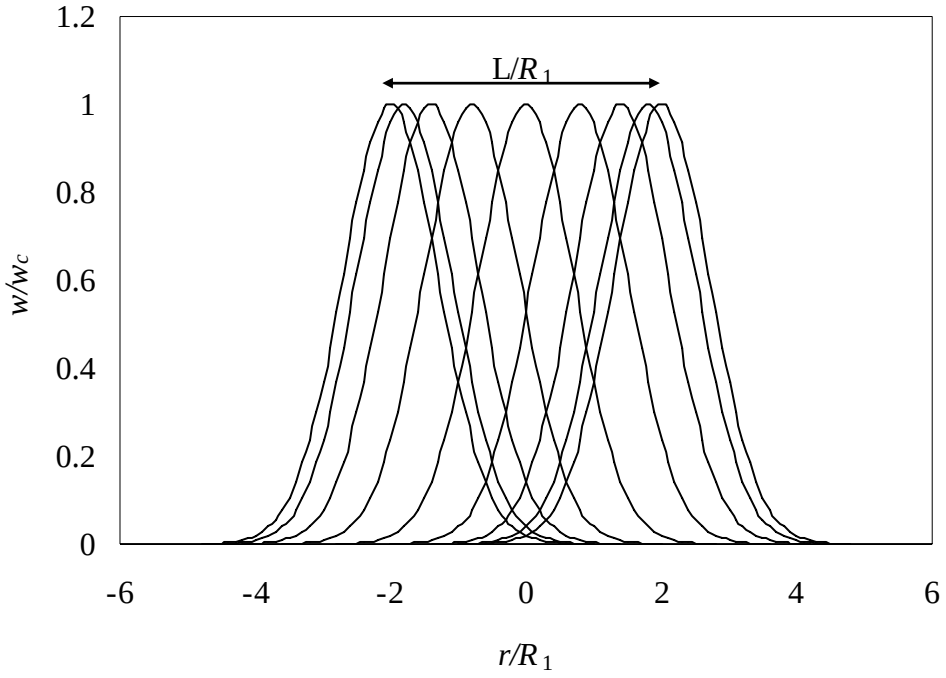

Figure 5.11. The lateral displacement of velocity distribution owing to the wave motion.

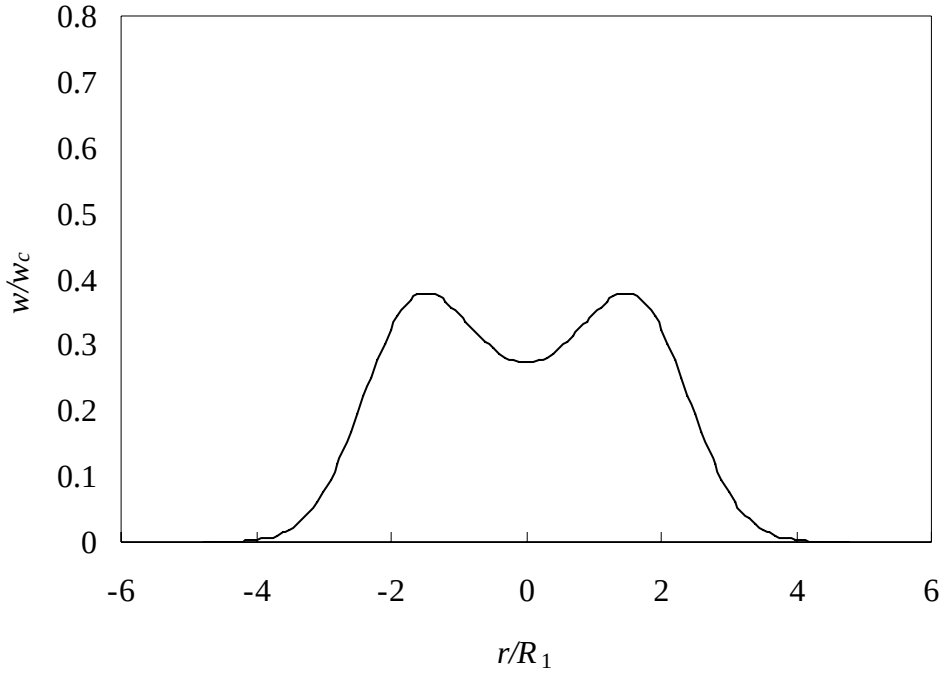

Figure 5.12. The formation of the twin peak profile based on time-averaging the velocity profiles as described in Fig. 5.11.

5.3.2 *Jet centerline velocity*

The variation of the vertical component of the jet centerline velocity (w_c) with distance z is shown in Figs. 5.13(a) – (e). The presence of random wave motion causes the deflection of the jet trajectory as indicated in Fig. 5.11. The spreading rate for the jet fluid under a wave environment is significantly larger than that occurs in stagnant ambience. The increase in jet spreading rate is reflected in the captured images as displayed in Figs. 5.14 (a) – (c), i.e. Case A. The cross-current also enhances the turbulent entrainment by enrolling ambient water into the jet body. The jet velocity is further dissipated by the additional entrainment process. Thus, the measured time-averaged jet centerline velocity under wave conditions is less than that in stagnant ambience.

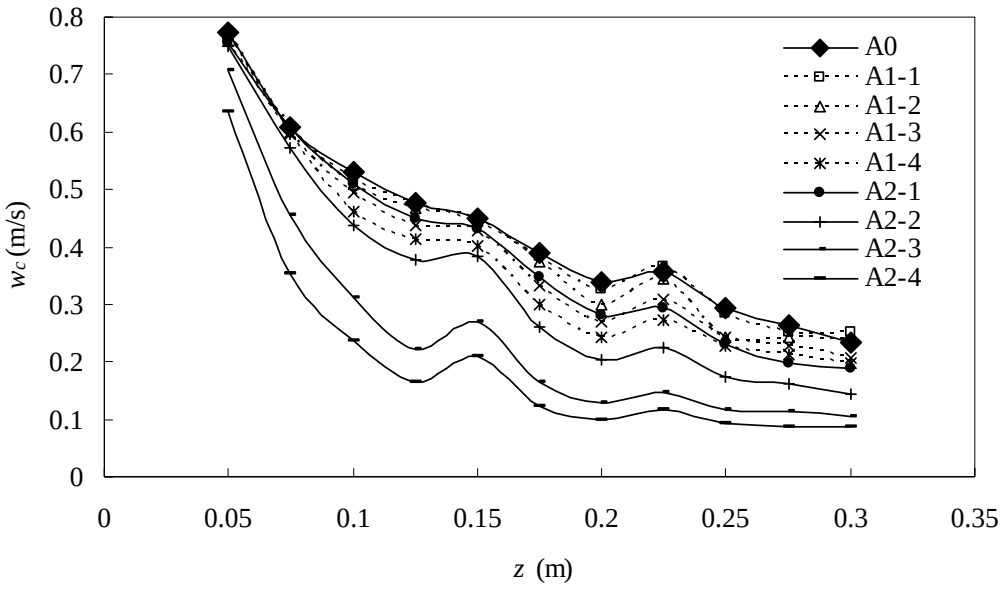

(a)

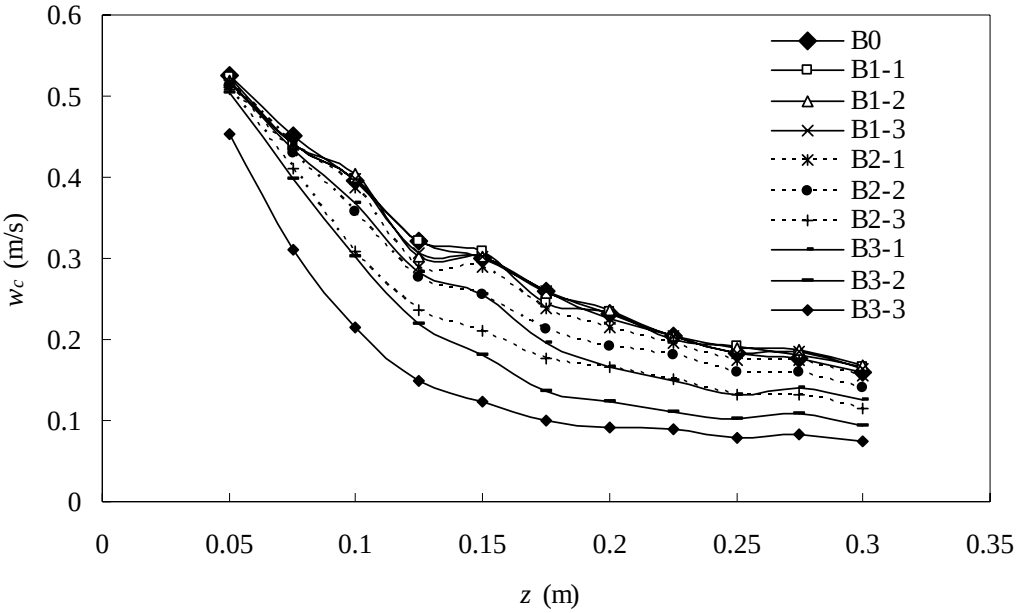
0.6
0.5
0.4
0.3
0.2
0.1
0
w_c (m/s)
0
0.05
0.1
0.15
0.2
0.25
0.3
0.35
z (m)
B0
B1-1
B1-2
B1-3
B2-1
B2-2
B2-3
B3-1
B3-2
B3-3

(b)

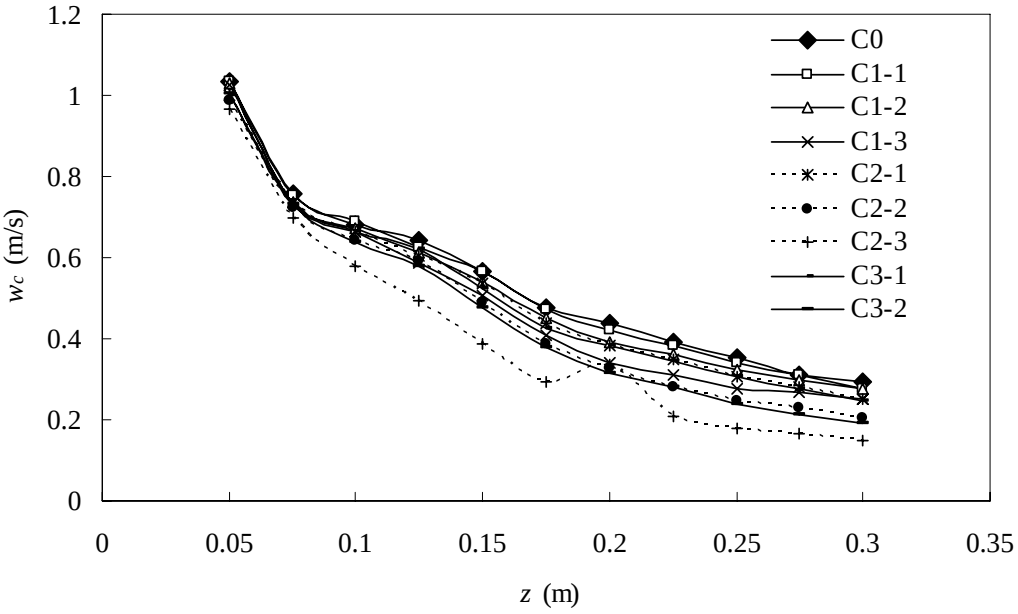
1.2
1
0.8
0.6
0.4
0.2
0
w_c (m/s)
0
0.05
0.1
0.15
0.2
0.25
0.3
0.35
z (m)
C0
C1-1
C1-2
C1-3
C2-1
C2-2
C2-3
C3-1
C3-2

(c)

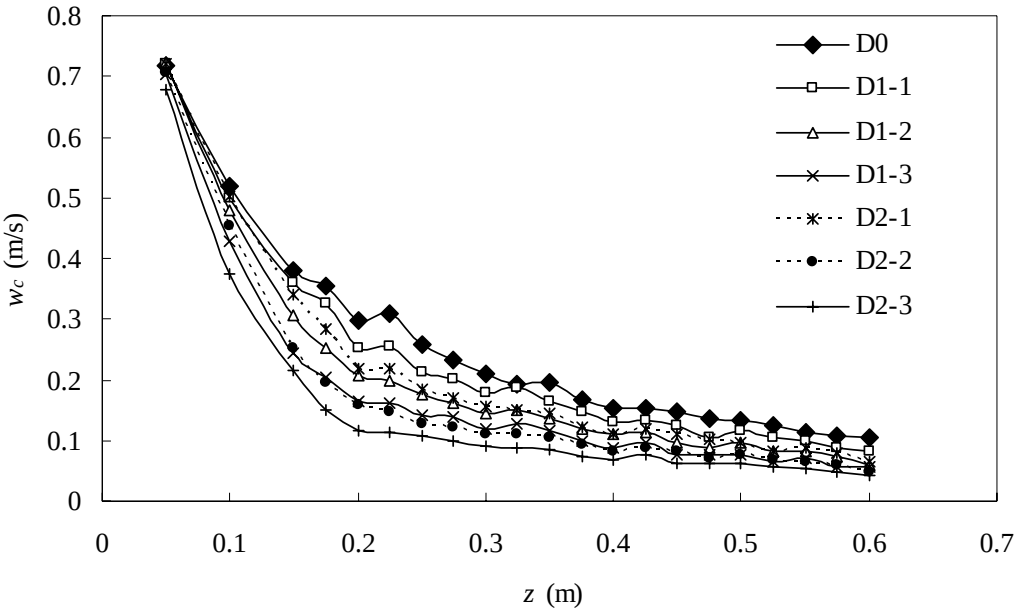

(d)

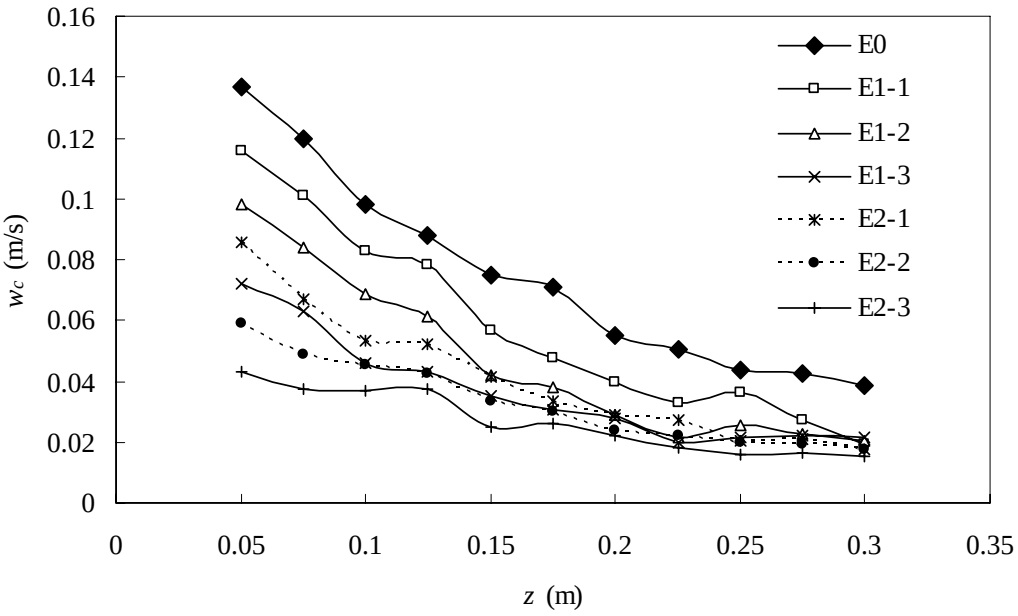

(e)

Figure 5.13. Centerline velocity profiles for (a) Case A; (b) Case B; (c) Case C; (d) Case D and; (e) Case E experiments.

Note: The zigzag trend of time-averaged data in Case A may be related to imprecise measurement employed in that particular experimental case.

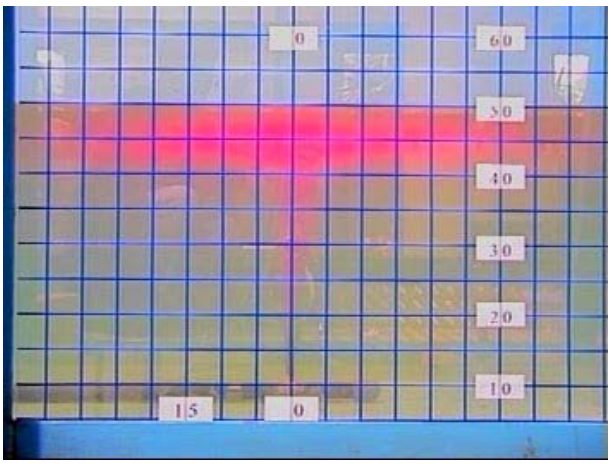

(a) Case A0 (Pure jet)

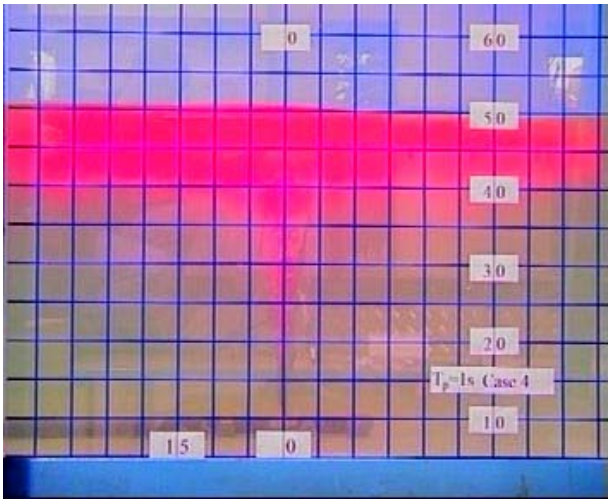

(b) Case A1-4

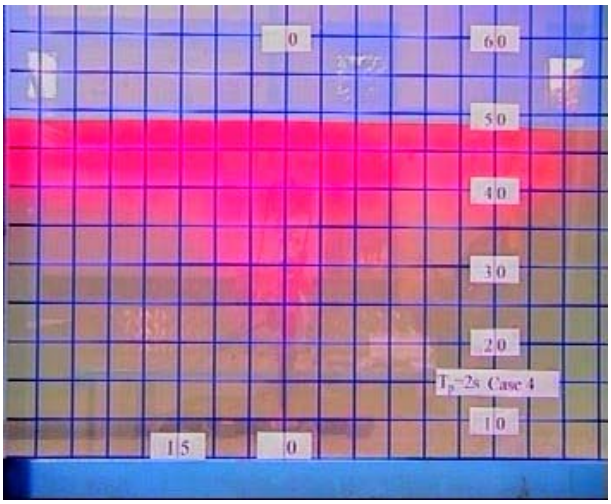

(c) Case A2-4

Figure 5.14. The developed jet body in (a) Case A0; (b) Case A1-4; (c) Case A2-4.

Figs. 5.13 (a) – (e) also show that the centerline velocity decreases with the increase in wave height and wave period. This suggests that the centerline velocity and its declining rate against the jet distance from the jet orifice (velocity decay rate) should be functions of the wave properties. As the wave parameters in Case B, C and E experiments (T_p=1s and T_p=2s) were almost the same, the net effect due to the change of discharge velocity can be observed. Apparently, the reduction of discharge velocity greatly decreases the velocity gradient in the jet upstream region. The jet velocity gradient decreases significantly while the significant wave height and the peak wave period increase. However, the centerline velocities along the jet distance obtained in T_p=3s (Cases C3-1 and C3-2) were just slightly greater than that obtained in T_p=2s (Cases C2-1 and C2-2) for similar significant wave heights. This indicates that the effect of waves on jet due to the increase in wave period is not as significant as that due to the increase in wave height.

5.3.3 *Variation of non-dimensional centerline velocity (scaled with u_w)*

The experimental data are then scaled with the wave characteristic velocity and the wave-induced momentum characteristic length as described in Chapter 4. The scaled data of the centerline velocities of all experiments are then plotted in Fig. 5.15 based on the non-dimensional form of Eq. 4.26: $\phi\left(\frac{z}{l_w}, \frac{w_c}{u_w}\right) = 0$ where $u_w = \frac{1}{T}\int_0^T \left| \sum_{n=1}^{N} \frac{\pi H(n)}{T(n)} \frac{\cosh(kZ)}{\sinh(kh)} \cos\left[\frac{2\pi}{T(n)} t - \varepsilon(n)\right] \right| dt$ and $l_w = \frac{\sqrt{M_0}}{u_w} = \frac{\sqrt{\pi d^2 W_0^2}}{2u_w}$. It is worth noting that the wave characteristic velocity varies with the vertical distance. Hence, the centerline velocity measured at different jet distances would have to scale with a pair of corresponding wave characteristic velocity and the wave-induced momentum characteristic length.

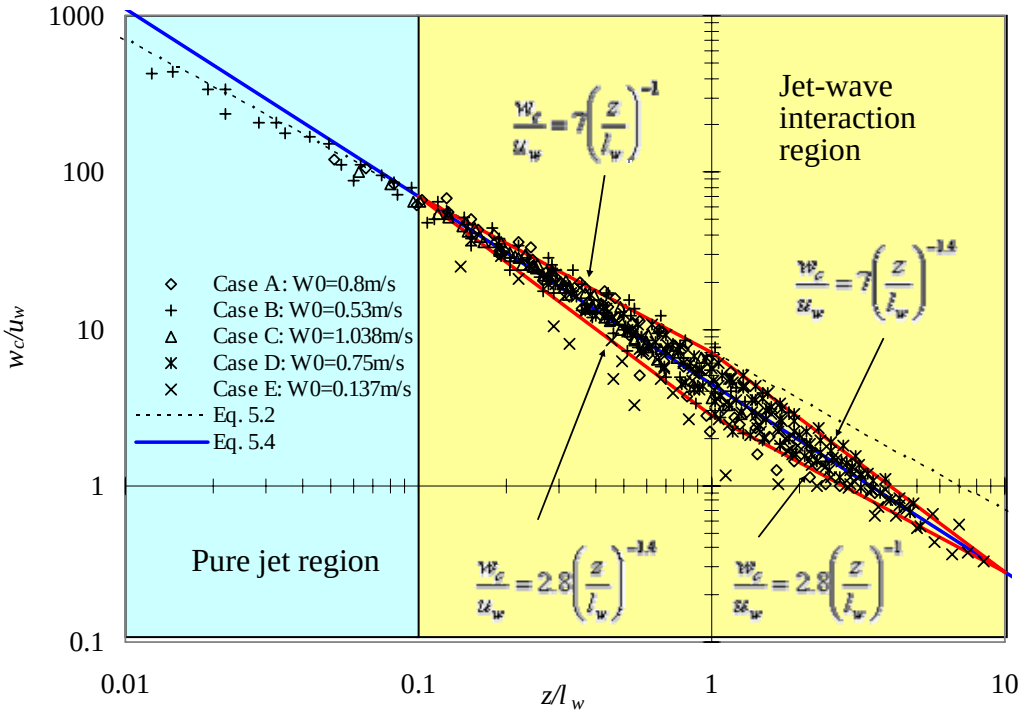

Figure. 5.15. Centerline velocity decay rate using the non-dimensional form as displayed in Eq. 4.26.

Since the centerline velocity obtained in wave condition are shown to have a lesser value than that obtained in stagnant condition, all the experimental data are located below the line corresponding to Eq. 5.2, which is an alternative form of Eq. 4.4 used to describe the velocity decay rate in stagnant environment. The jet discharge behaviour in wave conditions is similar to that in stagnant ambience at the region $\frac{z}{l_w} < 0.1$. This study suggests the region of $\frac{z}{l_w} < 0.1$ can be called the pure jet region, which is formed under the condition that the wave period is short and the wave-induced velocity tends to zero. The jet-induced velocity thus is much larger than the wave-induced velocity and consequently the jet is only slightly affected by the propagation of surface waves. In addition, the small wave characteristic velocity

leads to a very large wave characteristic length. Thus, this is not surprising the velocity decay rate of Case B1: T_p=0.5s is very close to that stated in Eq. 5.2 (jets in stagnant ambience). At that pure jet region, the jet properties will be the same as those in the case of stagnant ambience, which, therefore, can be described by the empirical formulas obtained for jet in stagnant ambience.

$$\frac{w_c}{u_w} = 7\left(\frac{z}{l_w}\right)^{-1} \tag{5.2}$$

Except for the results obtained at Case B, most of the experimental results are located within the range of $0.1 < z/l_w < 10$ as shown in Fig. 5.15. The degree of data scattering increases at $z/l_w > 0.01$. Those data were bounded by an envelope with a set of suggested equations as shown below:

$$\begin{cases} \dfrac{w_c}{u_w} = 7\left(\dfrac{z}{l_w}\right)^{-1} & (0.1 < z/l_w \le 1) \\ \dfrac{w_c}{u_w} = 7\left(\dfrac{z}{l_w}\right)^{-1.4} & (1 < z/l_w \le 10) \end{cases} \quad \text{(upper boundary)} \tag{5.3a}$$

$$\begin{cases} \dfrac{w_c}{u_w} = 2.8\left(\dfrac{z}{l_w}\right)^{-1.4} & (0.1 < z/l_w \le 1) \\ \dfrac{w_c}{u_w} = 2.8\left(\dfrac{z}{l_w}\right)^{-1} & (1 < z/l_w \le 10) \end{cases} \quad \text{(lower boundary)} \tag{5.3b}$$

The definition of wave-induced momentum characteristic length suggests that the jet flow characteristics should be dominated by the jet momentum at $z << l_w$ and by the wave momentum at $z >> l_w$. The degree of scattering increases from

$z/l_w = 0.1$ and reaches the highest at $z/l_w \sim 1$. The degree of data scattering is then reduced when $z > l_w$. This phenomenon shows that a transition region (hereafter, renamed as the jet-wave interaction region) between the jet-momentum dominant region (or pure jet region) and the wave-momentum dominated region should exist. Within that jet-wave interaction region, the jet flow characteristics can be sensitive to the jet initial momentum and wave momentum. The presence of random surface waves causes the large amplitude jet trajectory oscillation, the increased dissipation of turbulent energy, and the forced entrainment with the ambient water. The mechanism involved in the jet-wave interaction becomes more complicated in the jet-wave interaction region than that in the pure jet region. As a result, the effect of random surface waves on jet can vary significantly and the velocity decay rate within the region of $0.1 < z/l_w < 10$ cannot be simply represented by a linear function.

Some data obtained in Case E experiments are located out of the suggested envelope. This is possibly because the jet Reynolds number ($\mathrm{Re} = \frac{\rho W_0 d}{\mu}$, where ρ = fluid density, μ = dynamic viscosity) for Case E (W_0=0.137m/s) experiments is around Re ~ 1800 which is smaller than the definition of turbulent jet of Re > 2000. The length of the potential core for jet with low Reynolds number is greatly reduced when the wave motion is relatively strong to govern the jet flow characteristics. The velocity gradient, $\frac{\partial w}{\partial z}$, particularly for the region of $z \to 0$, increases

tremendously, resulting that some non-dimensional data for case E locates outside the proposed envelope (Eq. 5.3) as shown in Fig. 5.15.

$$\begin{cases} \dfrac{w_c}{u_w} = 4.4\left(\dfrac{z}{l_w}\right)^{-1.2} & (0.1 < z/l_w \le 10) \quad \text{(mean value)} \end{cases} \tag{5.4}$$

Eq. 5.4 is proposed to represent the mean velocity decay rate within the jet-wave interaction region ($0.1 < z/l_w < 10$). The power index linked between $(w_c/u_w)$and (z/l_w) reduces from 1 (pure jet, Eq.5.2) to 1.2 (Eq. 5.4). The coefficient linked between the velocity and the jet centerline distance is also reduced from 7 to 4.4. The decrease in coefficient suggested that the jet spreading rate is improved while the greater power index of the equation indicates a faster period-averaged velocity decay rate. Hence, the presence of random wave effects is shown to exert a more significant effect in the jet centerline dilution.

5.3.4 *Variation of non-dimensional centerline velocity (scaled with u_{sig})*

The wave-induced velocity varies with the depth of flow resulting in a variation of wave-induced momentum characteristic length with depth. To simplify the calculation, the flow depth used to compute the wave-induced significant velocity is suggested to be the flow depth corresponded to the mid-point between the free surface and the jet orifice (i.e. Z_a = water depth (h) at half of the distance from jet orifice to the free water surface) as shown in Fig. 5.16. Thus, the random wave-induced velocity corresponding to all flow depths is modified by Eq. 5.5.

$$u_{wave}(t) = \sum_{n=1}^{N} \frac{\pi H(n)}{T(n)} \frac{\cosh[k(n)Z_a]}{\sinh[k(n)h]} \cos\left[\frac{2\pi}{T(n)} t - \varepsilon(n)\right] \tag{5.5}$$

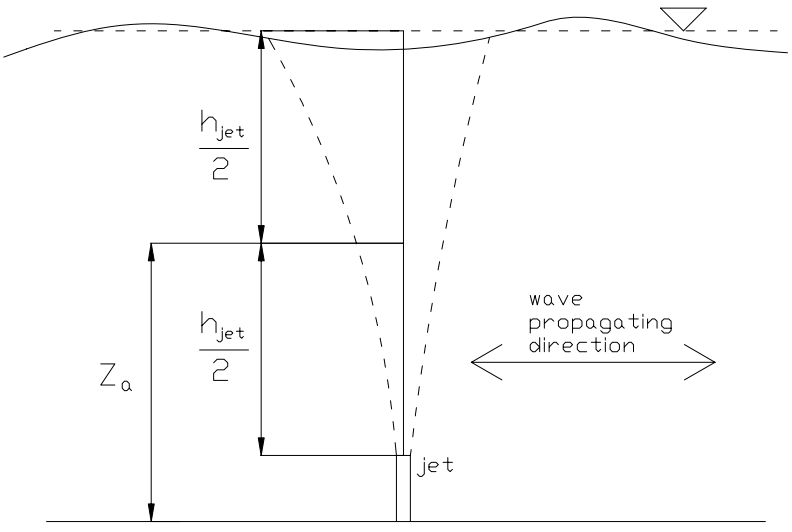

Figure 5.16. Definition sketch of Z_a.

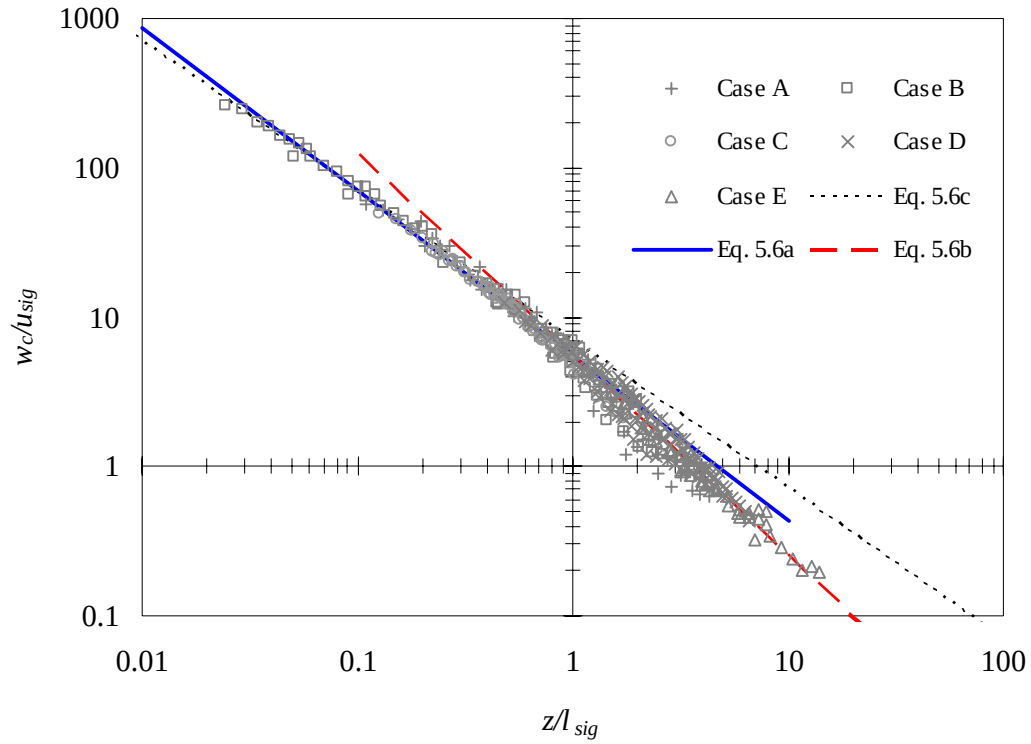

Figure 5.17. The centerline velocity decay rate displays in the form of Eq. 4.29.

The wave-induced significant velocity and the corresponding characteristic length are shown in Eqs. 4.25 and 4.27.

$$u_{sig} = u_{1/3} = \frac{1}{N/3}\sum_{i=1}^{N/3}\left|u_{wave}(i)\right| \qquad (4.25)$$

$$l_{sig} = \frac{\sqrt{M_0}}{u_{sig}} \qquad (4.27)$$

where N = number of velocity data $\left|u_{wave}(i)\right|$ in a record ranked highest to lowest in the given sampling time T_{total}. Adopting the non-dimensional group of variables in the form of Eq. 4.29: $\phi\left(\frac{z}{l_{sig}}, \frac{w_c}{u_{sig}}\right) = 0$, the data located within the region of $\frac{z}{l_{sig}} \le 0.1$ follow the decay rate in stagnant condition as shown in Fig. 5.17. This

indicates that the jet general behaviour in the region of $\frac{z}{l_{sig}} \le 0.1$ is remained the same as the pure jet condition even though u_{sig} is used in the analysis. The degree of data scattering increase when $\frac{z}{l_{sig}} > 0.1$. However, the jet centerline velocity, obtained under random wave conditions within the region of $0.1 < \frac{z}{l_{sig}} \le 10$, decays roughly with a piecewise linear trend with the jet distance. The formulas describing the piecewise relationships are suggested below:

$$\frac{w_c}{u_{sig}} = 5.5\left(\frac{z}{l_{sig}}\right)^{-1.1} \qquad (0.1 < \frac{z}{l_{sig}} \le 1) \tag{5.6a}$$

$$\frac{w_c}{u_{sig}} = 5.5\left(\frac{z}{l_{sig}}\right)^{-1.35} \qquad (1 < \frac{z}{l_{sig}} < 10) \tag{5.6b}$$

$$\frac{w_c}{u_{sig}} = 7\left(\frac{z}{l_{sig}}\right)^{-1} \qquad (\frac{z}{l_{sig}} \le 0.1) \tag{5.6c}$$

The power index in between w_c / u_{sig} and l_{sig} / z are shown to be greater than 1 in both Eq. 5.6(a) and (b). The greater velocity decay rate is obtained where the wave-induced momentum is strong enough to influence the jet characteristics. This phenomenon is in agreement with the discussion previously that the jet-wave interaction region is located at $0.1 < \frac{z}{l_{sig}} < 10$. The cause of the piecewise linear variation is to distinguish the relative strength of momentum between that of jet and that of propagated surface waves.

5.3.5 *Prediction of centerline velocity decay rate in random waves*

The sea wave data usually characterized by the significant wave height (H_s) and the peak wave period (T_p). As the previous analysis is based on the known wave energy spectrum, the wave-induced characteristic velocity, which is the key parameter to represent the strength of wave-induced current, involves a rather complicated computation. It should be more convenient to have the scaling parameters mainly depend on H_s and T_p for engineering design purposes. Although the wave-induced velocity can simply be evaluated based on the linear wave theory, this study has mentioned in Chapter 4 that the wave energy contributed by the significant wave height in random waves is only half of the wave energy contributed by the constant wave height in regular waves. Hence, in order to have simplified scaling parameters in the jet-wave analysis, the root mean square wave height ($H_{rms} = H_s / 1.416$) should be more appropriate to be use instead of the H_s.

Based on the linear wave theory, the wave-induced horizontal velocity for regular waves is in the form of Eq. 5.7:

$$u_p = \frac{\pi H}{T} \frac{\cosh(kZ)}{\sinh(kh)} \sin \sigma t \tag{5.7}$$

To extend the usage of Eq. 5.7 in irregular waves, the wave height and the wave period are replaced by the root mean square wave height and the peak wave period, respectively. The flow depth (Z) is replaced by the mid-point between the free

surface and the jet orifice (i.e. Z_a = water depth (h) – half of the distance from jet orifice to the free water surface). The degree of influence is the maximum when the wave-induced velocity is the greatest. Therefore, the time phase is chosen to be 1 (i.e. $\sin\sigma t = 1$). The equation used to estimate the wave-induced velocity is suggesed in Eq. 5.8:

$$u_{w\_simp} = \frac{\pi H_{rms}}{T_p} \frac{\cosh(k_a Z_a)}{\sinh(k_a h)} \tag{5.8}$$

where k_a = wave number corresponding to the peak wave period.

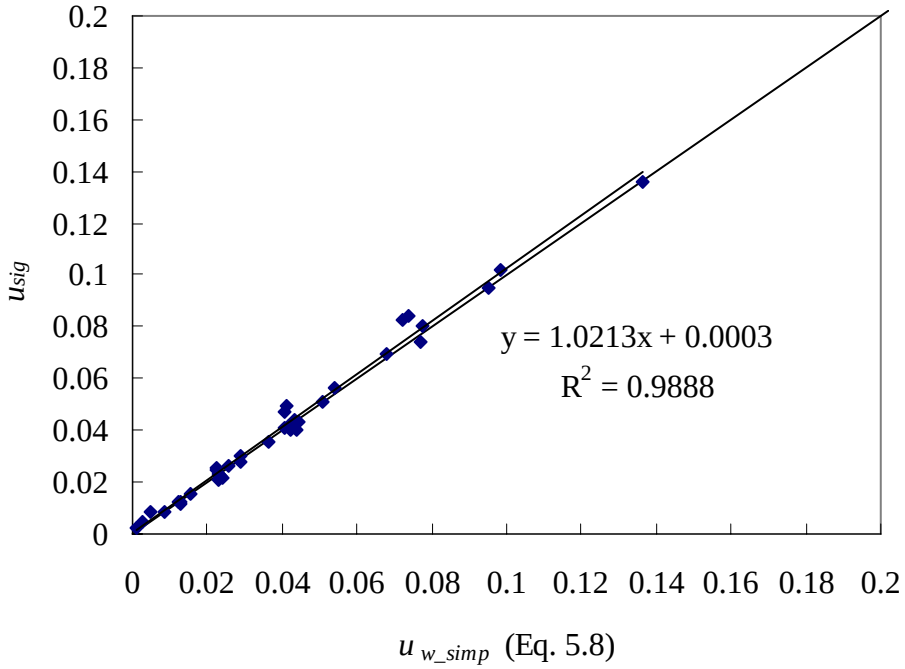

Figure 5.18. The variation of u_{sig} with the u_{w_simp} from Eq. 5.8.

The wave-induced significant velocities (u_{sig}) as defined by Eq. 4.25 are included in the discussion of this section. Fig. 5.18 reveals that, for the irregular waves in the form of typical JONSWAP spectrum, the wave-induced horizontal

velocity defined by Eq. 5.8, based on H_{rms} and T_p in random waves, is roughly equal to the u_{sig}. Assuming $u_{sig} \approx u_{w\_simp}$, Eq. 5.9 is able to determine the mean of the highest one-third wave-induced velocity. Consequently, Fig. 5.17 and the suggested equations of Eqs. 5.6(a), (b) & (c) can be used to determine the jet centerline velocity at various depths.

5.3.6 *Rate of decay of centerline velocity in regular waves*

Based on the analytical approach of jet discharge in cross-current (or cross-wave), the centerline velocity obtained in regular waves should also behave similarly as that in random waves. With the use of linear wave theory, the wave particle velocity (u_p) is given by Eq. 5.7. The time-averaged velocity can be achieved by integrating Eq. 5.7 from t = 0 to t = T/2 as shown in Eq. 5.9. The regular-wave-induced characteristic velocity at each water depth is then given by Eq. 5.9.

$$\overline{u_p} = \frac{1}{T/2}\int_{t=0}^{t=T/2} \frac{\pi H}{T}\frac{\cosh(kZ)}{\sinh(kh)}\sin\sigma t\partial t \tag{5.9}$$

$$\overline{u_p} = \frac{2H}{T}\frac{\cosh(kZ)}{\sinh(kh)} \tag{5.10}$$

where h = water depth, H = wave height, k = wave number, t = time phase, T = wave period, Z = flow depth measured from bottom to free surface, and, σ = angular frequency. The wave-induced characteristic length is then calculated with Eq. 4.26 $\left(l_w = \frac{\sqrt{M_0}}{u_w} = \frac{\sqrt{\pi d^2 W_0^2}}{2u_w} \right)$ by replacing $\overline{u_p}$ instead of u_w. Previous experimental

results (Chyan and Hwung 1993; Mossa 2004a) for jets in regular waves are then scaled with the corresponding pair of scaling parameters and presented in Fig. 5.19 with the same envelope as discussed in Eq. 5.3.

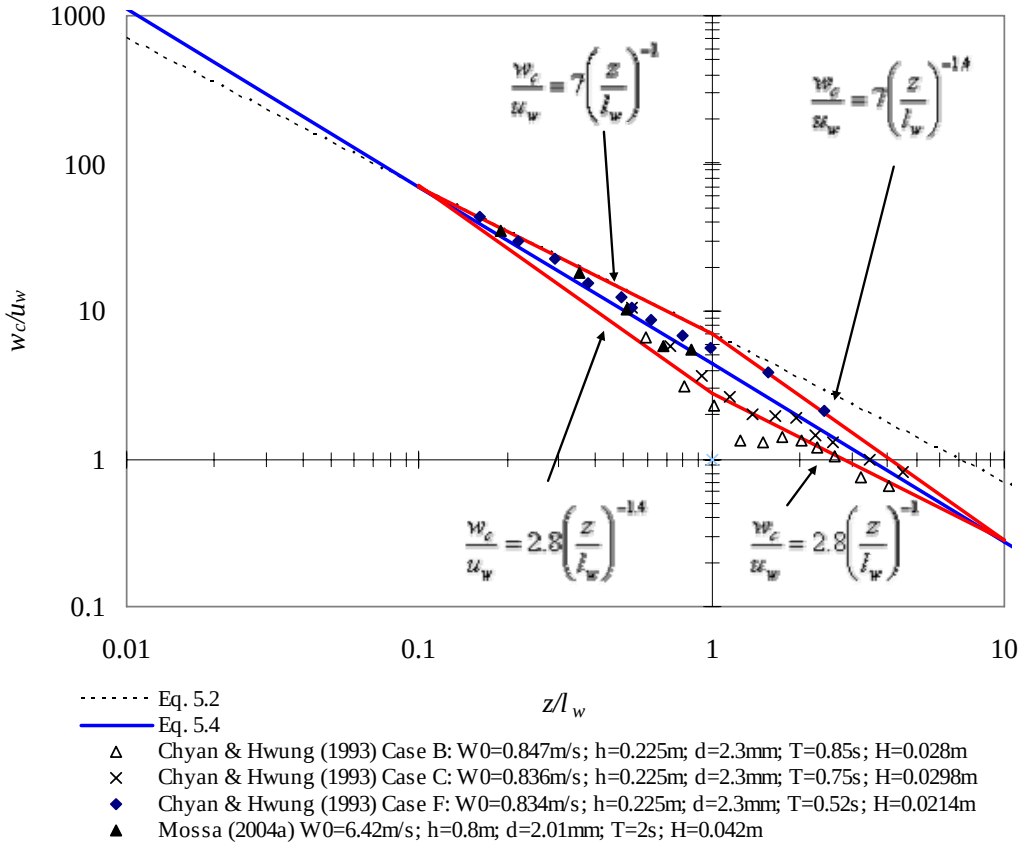

Figure 5.19. Centerline velocity decay rate for regular surface waves.

Most of the experimental data lay inside the envelope except the set of data labelled with open triangle [Case B, Chyan and Hwung (1993)]. Regarding the original data presented by Chyan and Hwung (1993), twin peaks cross-sectional velocity profiles were noticed as the wave period and the wave amplitude were comparatively high resulting in the applied wave field was stronger than the jet

momentum. The occurrence of twin peaks radial profiles for axial velocity will cause a decrease in the jet centerline velocity which in turn causes a lower value of w_c/u_w.

5.4 Potential core and velocity ratio

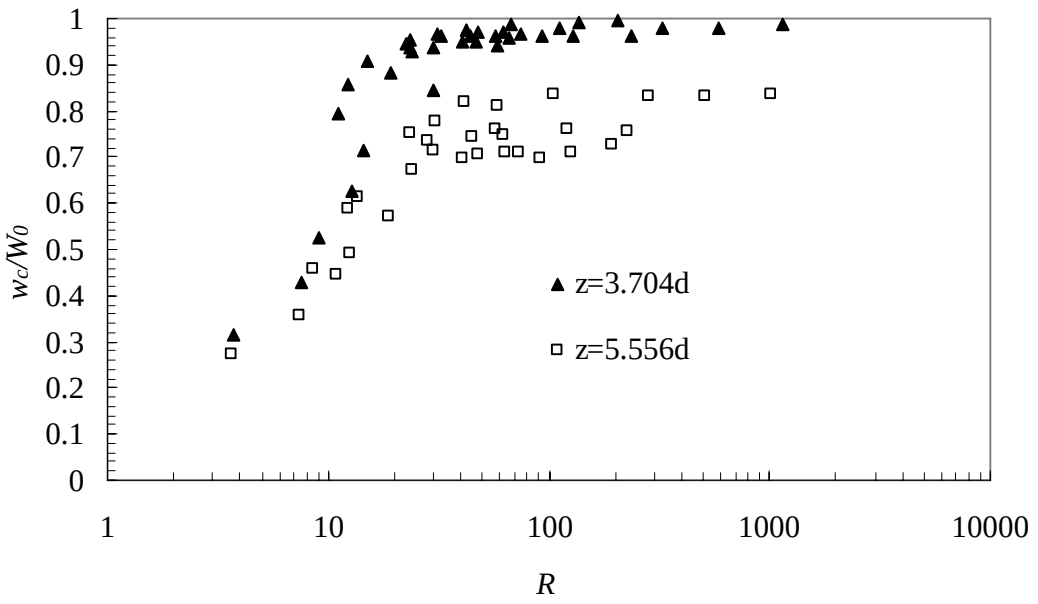

Figure 5.20. Variation of non-dimensional velocity against velocity ratio *R*.

The measured time-averaged velocities under wave conditions are less than that measured at stagnant ambience especially for those obtained in strong wave field. This is expected because the spreading rate for the jet fluid under wave environment is significantly larger than that in stagnant ambience. The wave-induced periodic cross-current shortens the length of zone of flow establishment (ZFE). Fig. 5.20 shows the non-dimensional velocity plotted against the velocity ratio, $R = W_0 / u_w$, for *z=3.704d and z=5.556d*. The figure clearly shows the velocity, measured at the same level, decays much faster when *R* is small. However, the figure also shows the measured velocities within the potential flow core (i.e. *z*=3.704*d* <6.2d) were

roughly constant for $R > 30$. This suggests the turbulent jet potential core may be shortened only when $R < 30$.

It is reasonable to obtain constant values of time-averaged velocity in the same jet distance when the wave field is small (i.e. $R \to \infty$). However, once R is smaller than the critical value (i.e. z=3.704d, $R \sim 30$), the centerline velocity begins to decrease.

5.5 Jet width

Dilution ratio is an important parameter in the engineering design of environmental discharge system. The use of jets in outfall diffusers as described in many books (i.e. Fischer et al. 1979; Metcalf and Eddy 1991) is a proactive approach because the degree of dilution and the amount of mixing have been broadly studied. The dilution of a solute at a particular point is defined as the ratio of the concentration of the solute at the discharge point to the concentration at that point. The average dilution can also be described by the ratio of the flow rate (Q) at a particular level to the discharge flow rate (Q_0). The ratio Q/Q_0 is greater than unity and increases along the jet axis (Rajaratnam 1976, p35). This is because the turbulent eddies in the jet entrain the surrounding stagnant fluid into the main jet body, resulting in the increase of the cross sectional area of the jet. The dilution ratio is, thus, strongly dependent on the jet cross sectional area which is a function of the jet width.

5.5.1 *Jet width in stagnant ambience*

Assuming the lateral distribution of the longitudinal velocity of a jet follows the Gaussian distribution is always held.

$$u(r) = u_c e^{-\left(\frac{r}{b}\right)^2} \qquad \textit{(rewritten form of Eq. 5.1a)}$$

where u is the longitudinal velocity, r is the radial distance from the centerline, u_c is the centerline velocity, and b is defined as the jet half-width where the velocity u is equal to 1/e of the centerline velocity u_c. The present experimental data of the variation of jet width along the centerline for jet in stagnant ambient is plotted together with previous results obtained from Albertson et al. (1950) and Fischer et al. (1979) as shown in Fig. 5.21.

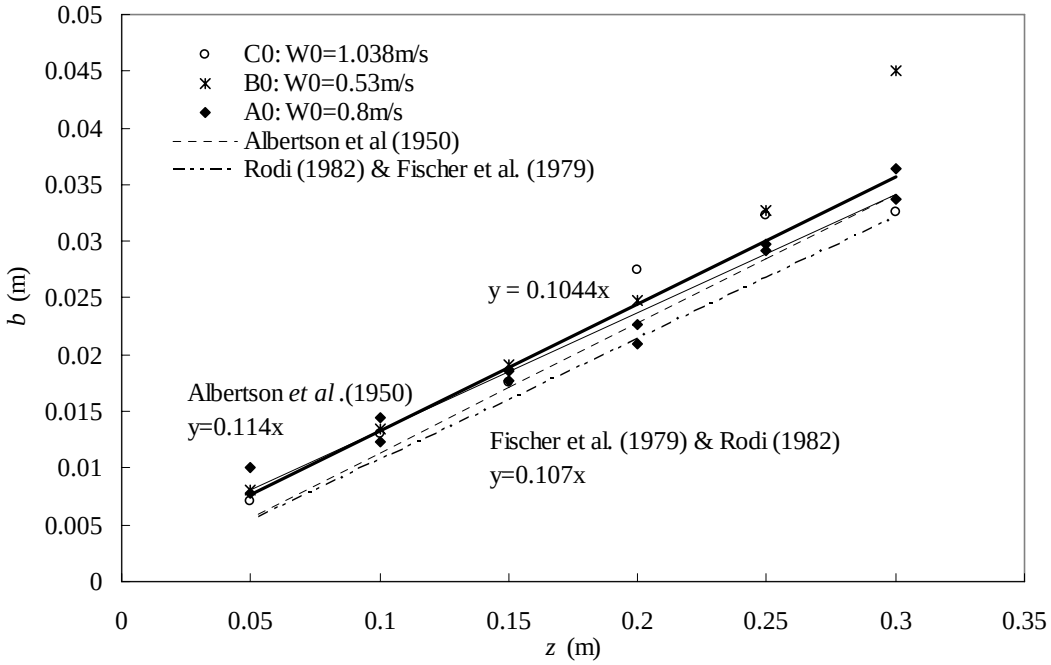

Figure 5.21. Variation of the jet half-width with distance for a single round jet.

The experimental studies on submerged jets discharging into stagnant ambient fluid have been conducted for almost a hundred years. Albertson et al. (1950) found that the variation of the jet half-width (b) with the centerline distance (x) is linear and the coefficient of proportion (jet width spreading rate) $\beta_g = \frac{db}{dx} = 0.114$. Similar results have been obtained in the subsequent studies and summarized by Fischer et al.

(1979). The coefficient β_g falls within the range 0.107 ± 0.03 for a round jet in stagnant ambient. In the present study a 13.5mm diameter jet was used and the coefficient β obtained is of value 0.104 which is at the lower bound of the previous obtained results.

5.5.2 *Jet width in wave environments*

Although the previous section in this study stated the multiple-peak axial velocity profiles in radial direction occasionally occurred for jet discharge in random waves, the shapes of most non-dimensional velocity profiles follow the Gaussian curves as shown in Figs. 5.8 (a) – (e). Assuming the radial profile of the time-averaged axial velocity still follows the Gaussian distribution (i.e. Eq. 5.1), the jet width can be determined using the same definition as that of jet in stagnant ambience. The results are shown in Figs. 5.22 (a) – (d), with the jet half-width and centerline distance scaled by the jet diameter. For reference, the experimental results for jets in regular waves (Mossa, 2004a), are displayed in Fig. 5.22 (e).

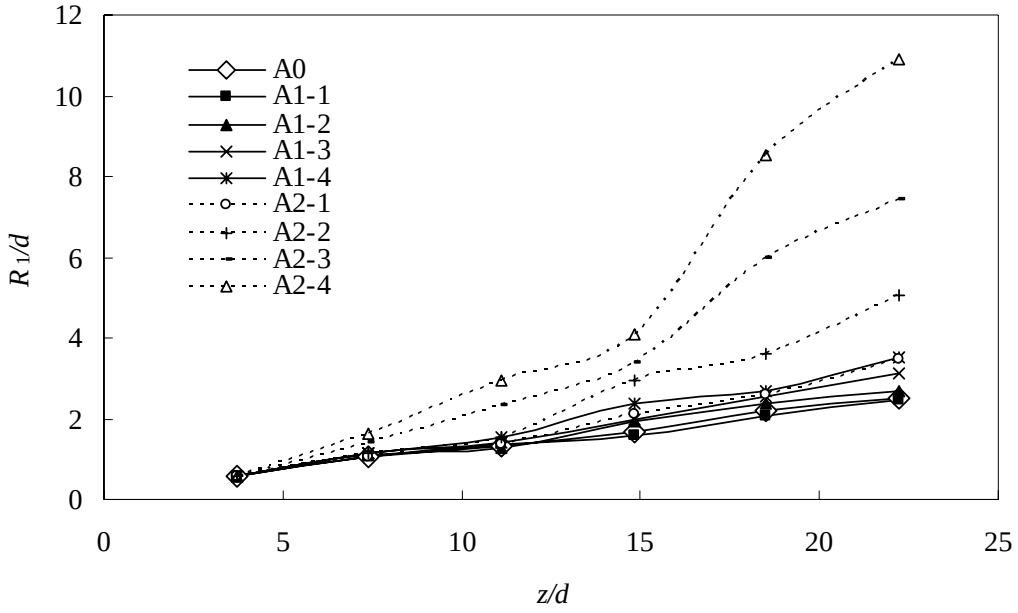
12
10
8
6
4
2
0
0
5
10
15
20
25
R1/d
z/d
A0
A1-1
A1-2
A1-3
A1-4
A2-1
A2-2
A2-3
A2-4

(a)

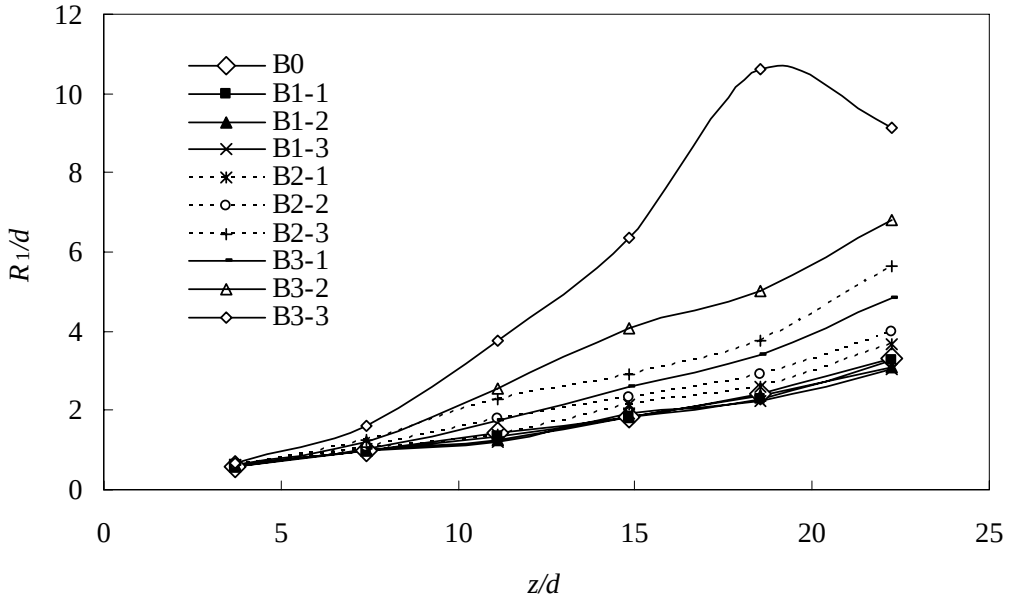
12
10
8
6
4
2
0
0
5
10
15
20
25
R1/d
z/d
B0
B1-1
B1-2
B1-3
B2-1
B2-2
B2-3
B3-1
B3-2
B3-3

(b)

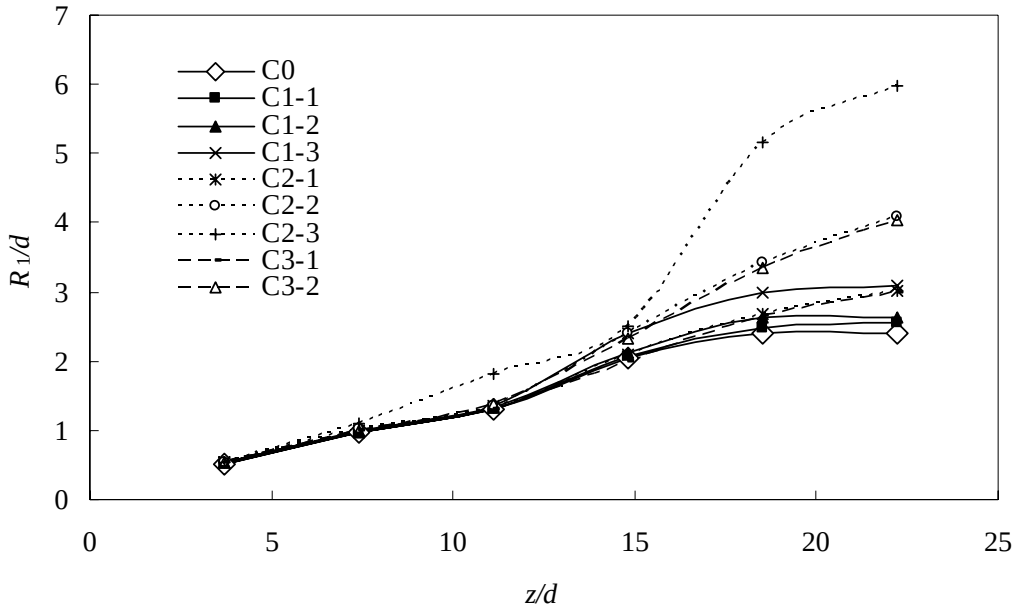
C0
C1-1
C1-2
C1-3
C2-1
C2-2
C2-3
C3-1
C3-2
R1/d
z/d
0
1
2
3
4
5
6
7
0
5
10
15
20
25

(c)

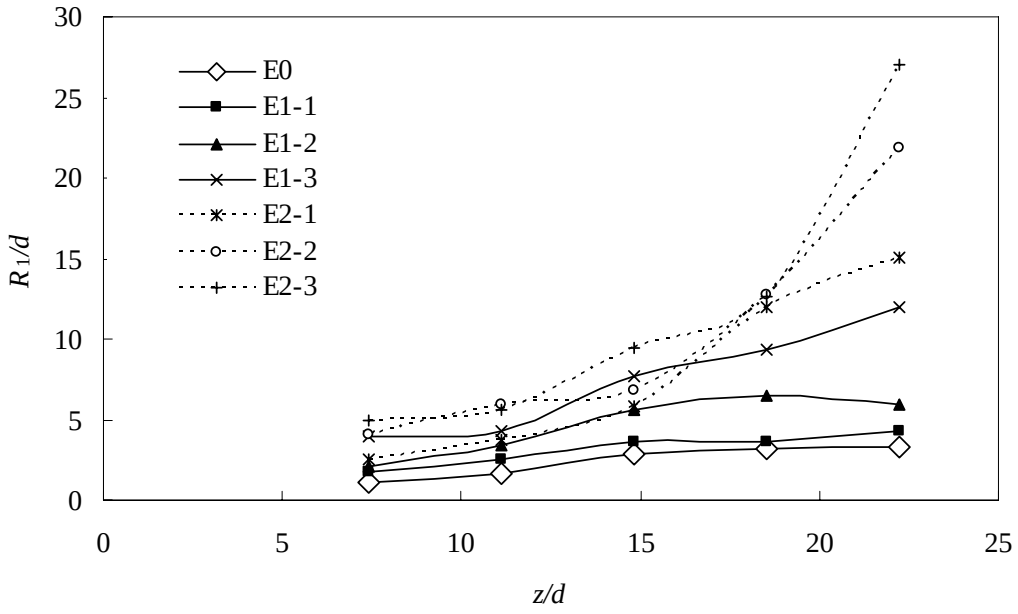
E0
E1-1
E1-2
E1-3
E2-1
E2-2
E2-3
R1/d
z/d
0
5
10
15
20
25
30
0
5
10
15
20
25

(d)

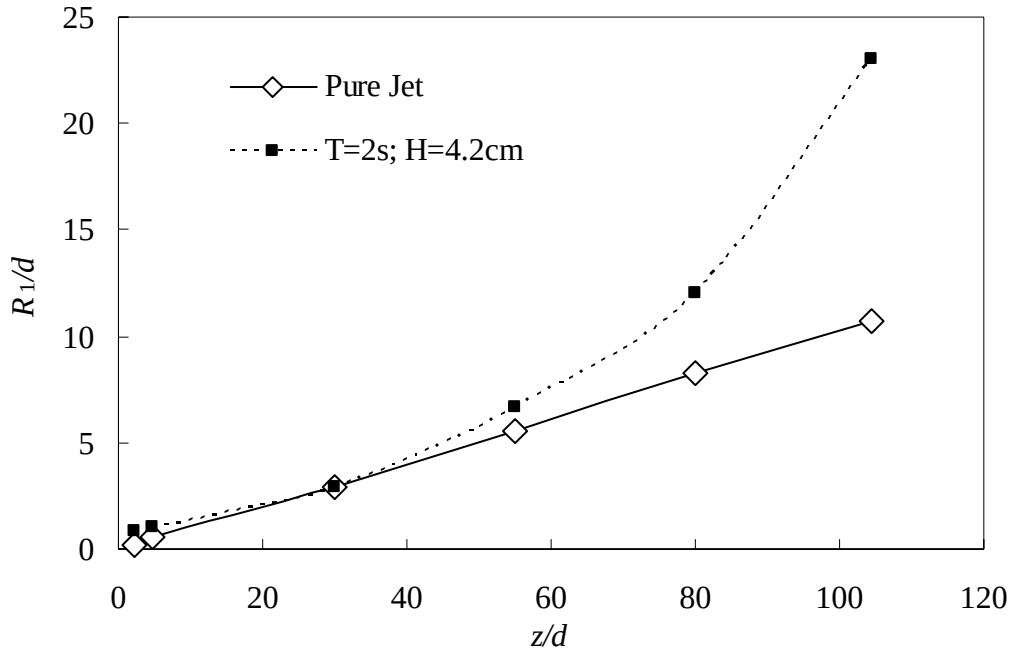

(e)

Figure 5.22. Variation of jet width against centerline distance: (a) Case A; (b) Case B; (c) Case C; (d) Case E and; (e) Regular waves with T=2s; H=4.2cm by Mossa (2004).

The results in both Figs. 5.22 (a) – (e) show that jet half-widths (in the direction of wave propagation) obtained in wave environment are wider than those in stagnant environment. The jet width spreading rate, $\beta_{g\_R1} = \frac{\partial R_1}{\partial z}$, for jet in random waves, is significantly larger in the far field than that in the near field and thus is not a constant. In addition, the jet half-width (R_1) increases with the significant wave height and peak wave period. This can be explained by that stronger wave motion deflects more the jet trajectory which causes more ambient water entrained to the jet body in random wave conditions than in stagnant conditions. Hence, the time-averaged jet half-width in the direction of wave propagation is enhanced. As discussed in Chapter 4, the elliptical jet flow cross-sectional area is formed in the presence of random waves. The jet

width which used to account for the flow area is then described by $b = \sqrt{R_1 R_2}$ (Eq. 4.1) where R_1 and R_2 are the jet half-widths along the wave propagation direction and normal to the wave propagation direction, respectively.

Assuming the jet width spreading rate in the direction normal to the wave propagation is the same as that in stagnant ambience, the jet half-widths ($b = \sqrt{R_1 R_2}$) used to represent the jet cross-sectional flow are included in Fig. 5.23.

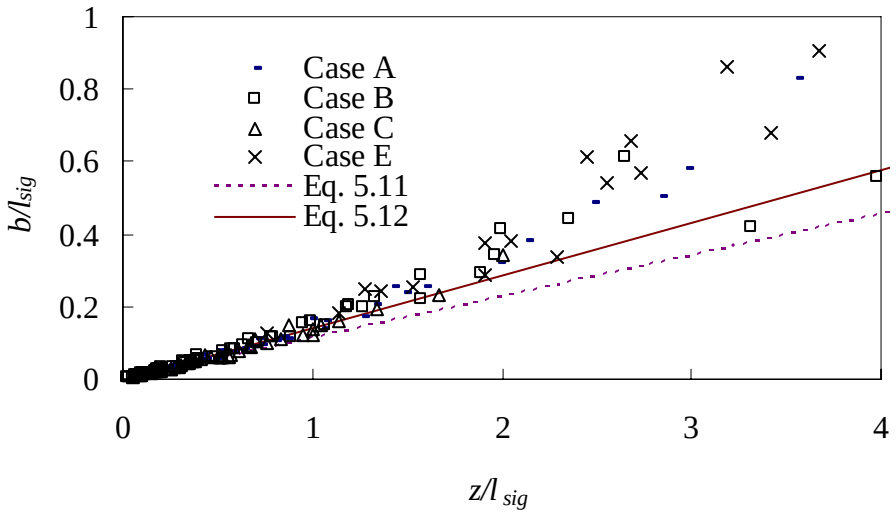

Figure 5.23. Non-dimensional jet width spread rate.

$$\frac{b}{l_{sig}} = 0.114 \frac{z}{l_{sig}} \qquad \left(\frac{z}{l_{sig}} \le 0.1\right) \tag{5.11}$$

$$\frac{b}{l_{sig}} = 0.145 \frac{z}{l_{sig}} \qquad \left(0.1 < \frac{z}{l_{sig}} \le 1\right) \tag{5.12}$$

All the data obtained are scaled the characteristic length of l_{sig} based on the wave-induced significant velocity. The jet width data within the region of $\frac{z}{l_{sig}} \le 0.1$ located closed to the empirical jet width spread rate demonstrated by Eq.

5.11 (the jet spreading coefficient β_g =0.114, by Albertson et al. 1950). The data at $\frac{z}{l_{sig}} \le 0.1$ follow the empirical formula developed in stagnant condition which conforms to the previous section of centerline velocity suggested that the jet discharge in random waves within the region of $\frac{z}{l_{sig}} \le 0.1$ would behave roughly the same as that in pure jet condition (stagnant condition).

As suggested in the previous section, the region of $0.1 < \frac{z}{l_{sig}} \le 10$ should be the jet-wave interaction region where the jet flow behaviour can vary with waves with different wave parameters. The data show a roughly linear relationship (Eq. 5.12) at $0.1 < \frac{z}{l_{sig}} \le 1$ while the degree of scatter increases at $z > l_{sig}$. The data formed linear relationship within the region of $0.1 < \frac{z}{l_{sig}} \le 1$ possibly suggested that the jet is still dominated by jet momentum, otherwise, the jet width should be expanded vigorously owing to the "dump-bell effect" exhibited in the wave momentum dominated far field.

As shown in Fig. 5.23, the degree of data scattering increases at $z > l_w$ and the data lay above Eq. 5.12, which shows the jet width spreading rate, $\beta_g = \frac{\partial b}{\partial z} = \frac{\partial \sqrt{R_1 R_2}}{\partial z} > 0.145$. One of the possible reasons is the wave-induced horizontal movement deflects to jet trajectory laterally. During the jet discharge to the wave-induced cross current, the ambient water is entrapped into the jet body due to turbulent entrainment, i.e. formation of vortex. The amount of water entrained to

the jet increases from the bottom to the water surface as the wave-induced current is the strongest in the free water surface. Consequently, the jet spreading rate, $\frac{\partial b}{\partial z}$, increases with the distance from the jet outlet.

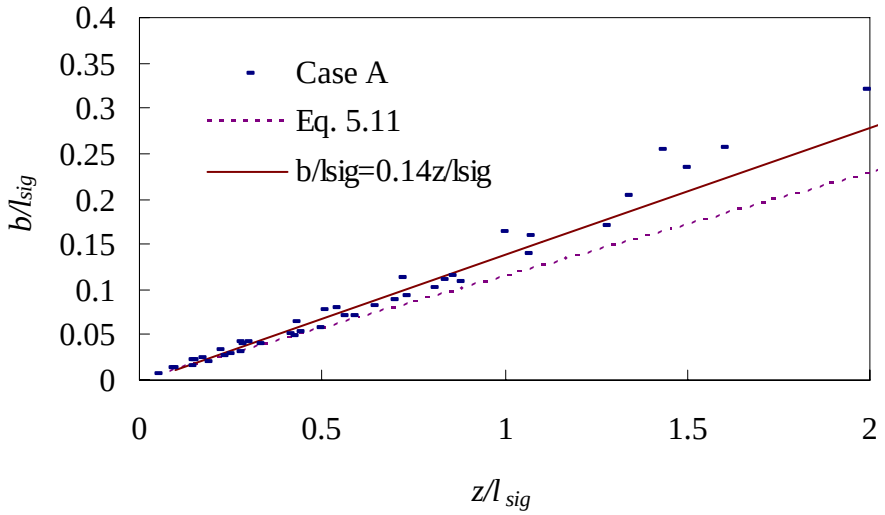

(a)

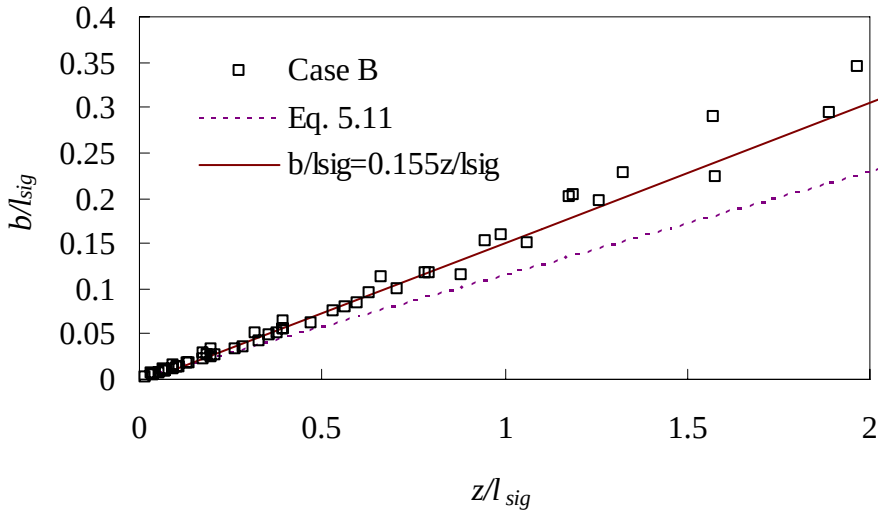

(b)

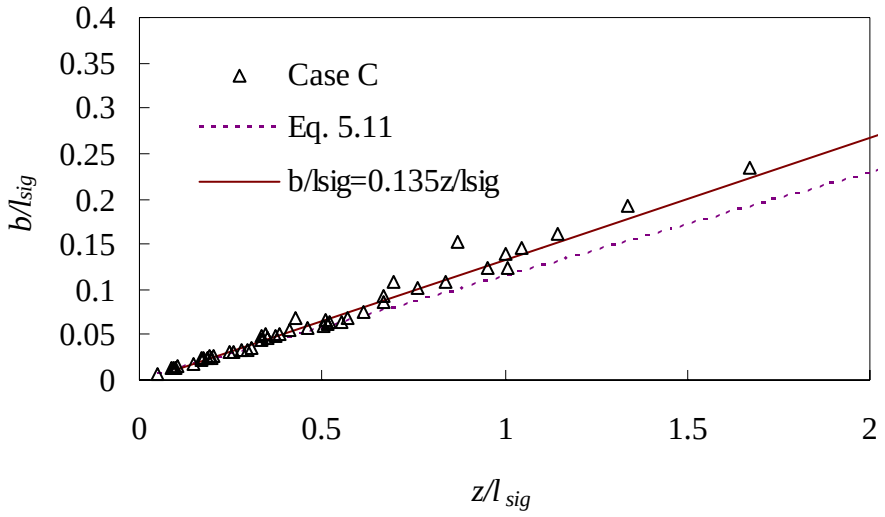

(c)

Figure 5.24. Variation of jet width against jet distance for (a) Case A; (b) Case B; and (c) Case C.

Figs 5.24 (a) – (c) show separate plots of the jet half-width (b) spreading rate for Cases A, B & C, respectively. Suggested equations to represent the jet spreading rate within the region of $0.1 < \frac{z}{l_w} \le 1$ as described in Eqs. 5.13(a), (b) & (c) are also included in figures.

$$\frac{b}{l_w} = 0.14\frac{z}{l_w} \quad \text{(Case A, } W_0\text{=0.8m/s)} \tag{5.13a}$$

$$\frac{b}{l_w} = 0.155\frac{z}{l_w} \quad \text{(Case B, } W_0\text{=0.53m/s)} \tag{5.13b}$$

$$\frac{b}{l_w} = 0.135\frac{z}{l_w} \quad \text{(Case C, } W_0\text{=1.038m/s)} \tag{5.13c}$$

The greater the jet discharge velocity is imposed, the smaller the jet width spread rate is obtained. This is because when the jet momentum is comparatively stronger than the wave momentum, the jet driving force is sufficiently strong to maintain the

general jet properties and to avoid the jet body from large deflection and deformation. The jet spreading coefficient obtained in the random wave environment should be dependent on the jet discharge velocity.

5.6 Turbulence intensity

Physically the time dependent motion of the present problem consists of the motion due to jet turbulence and the motion due to waves. A method has been proposed to separate these two types of motion quantitatively. Particularly the measured vertical velocity fluctuation component $\tilde{w}$, consists of 2 components, the jet induced velocity fluctuation, w', and the wave induced velocity variation, w_{wave}. These velocity components are defined by Eqs. 5.14 & 5.15 below

$$\tilde{w} = w - \overline{w} \tag{5.14}$$

$$\tilde{w} = w_{wave} + w' \tag{5.15}$$

where w = measured vertical velocity, $\tilde{w}$ = measured vertical velocity fluctuation, $\overline{w}$ = time-averaged vertical velocity, w_{wave} = wave-induced velocity variation in vertical direction and w' = jet-induced vertical velocity fluctuation.

The turbulence intensity is usually represented in terms of the root mean square velocity fluctuation. The squaring of Eq. 5.15 leads to Eq. 5.16. In general the wave induced vertical motion and the turbulent fluctuations are uncorrelated (Mossa 2004b), so $\overline{w_{wave}w'}$ is equal to zero. Eq. 5.16 is then simplified to obtain Eq. 5.17.

$$\overline{\tilde{w}^2} = \overline{\left(w_{wave}^2 + 2w_{wave}w' + w'^2\right)} \tag{5.16}$$

$$\sqrt{\overline{w'^2}} = \sqrt{\overline{\tilde{w}^2} - \overline{w_{wave}^2}} \tag{5.17}$$

5.6.1 *Wave-induced velocity fluctuation*

To eliminate the wave-induced effect generated by the presence of random waves, two approaches are proposed to compute the mean square value of wave-induced velocity variation.

Method 1

Assuming a time series of random waves is composed of a number of regular waves with different wave periods and wave heights as presented in Fig. 5.25, it is possible to calculate the wave induced velocity fluctuation by calculating the wave induced velocity for all waves.

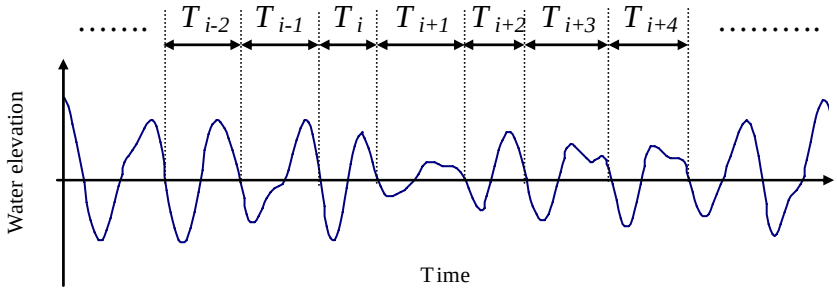

Figure 5.25. A series of random waves recognizes as many regular waves for calculating the wave induced velocity fluctuation.

Referring to the linear wave theory, the vertical component of the water particle velocity is described by the following equation (Eq. 5.18).

$$w_{wave} = \frac{H}{2}\frac{gT}{L}\frac{\sinh(kZ)}{\cosh(kh)}\sin(kx-\omega t) \tag{5.18}$$

where H = wave height, k = wave number, L = wave length, T = wave period, t = time phase, Z = flow depth measured from bottom to the free surface and ω = angular

frequency. The expression is then integrated over time to give the mean square values of w_{wave} by Eqs. 5.19 – 5.22.

$$\overline{w_{wave}^2} = \frac{1}{T_{total}} \sum_{i=1}^{N} \int_0^{T_i} \left[\frac{\pi H_i}{T_i} \frac{\sinh(k_i Z)}{\sinh(k_i h)} \sin(k_i x - \omega t) \right]^2 dt \tag{5.19}$$

$$\overline{w_{wave}^2} = \frac{1}{T_{total}} \sum_{i=1}^{N} \frac{\pi^2 H_i^{\,2}}{T_i^{\,2}} \frac{\sinh^2(k_i Z)}{\sinh^2(k_i h)} \int_0^{T_i} \frac{1}{2} \left(1 - \cos 2(k_i x - \omega t)\right) dt \tag{5.20}$$

$$\overline{w_{wave}^2} = \frac{1}{T_{total}} \sum_{i=1}^{N} \frac{\pi^2 H_i^{\,2}}{2T_i^{\,2}} \frac{\sinh^2(k_i Z)}{\sinh^2(k_i h)} \left[t + \frac{\sin 2(k_i x - \omega t)}{2\omega} \right]_0^{T_i} \tag{5.21}$$

$$\overline{w_{wave}^2} = \frac{1}{T_{total}} \sum_{i=1}^{N} \frac{\pi^2 H_i^{\,2}}{2T_i} \frac{\sinh^2(k_i Z)}{\sinh^2(k_i h)} \tag{5.22}$$

where H_i = wave height for the i^{th} wave, T_i = wave period for the i^{th} wave, k_i = i^{th} wave number, N = number of waves and T_{total} = total sampling time, The jet turbulence considering the vertical velocity component can then be calculated by Eq. 5.23 obtained by substituting Eq. 5.22 into Eq. 5.17. The horizontal component of the jet velocity fluctuation is given by Eq. 5.24 using similar analysis.

$$\sqrt{\overline{w'^2}} = \sqrt{\overline{\tilde{w}^2} - \frac{1}{T_{total}} \sum_{i=1}^{N} \frac{\pi^2 H_i^{\,2}}{2T_i} \frac{\sinh^2(k_i Z)}{\sinh^2(k_i h)}} \tag{5.23}$$

$$\sqrt{\overline{u'^2}} = \sqrt{\overline{\tilde{u}^2} - \overline{u_{wave}^2}} \tag{5.24a}$$

$$\overline{u_{wave}^2} = \frac{1}{T_{total}} \sum_{i=1}^{N} \frac{\pi^2 H_i^{\,2}}{2T_i} \frac{\cosh^2(k_i Z)}{\sinh^2(k_i h)} \tag{5.24b}$$

where $\tilde{u}$ = measured horizontal velocity fluctuation, u' = the jet velocity fluctuation and u_{wave} = wave induced velocity in horizontal direction.

Method 2

Considering the wave energy density spectrum, the wave-induced velocity at any time, *t*, can be generated by Fourier series using Eq. 4.23:

$$w_{wave}(t) = \sum_{n=1}^{N} \frac{\pi H(n)}{T(n)} \frac{\sinh[k(n)Z]}{\sinh[k(n)h]} \sin\left[\frac{2\pi}{T(n)} t - \varepsilon(n)\right] \qquad (4.23)$$

where H = wave height, h = water depth, T = wave period, t = time, k = wave number, Z is the flow depth measure from the bottom to the free surface, ε = random term for phase angle and n is the n^{th} wave component.

The mean square value of the variation of wave-induced vertical velocity by using a known wave energy spectrum is given by Eq. 5.25.

$$\overline{w_{wave}^2} = \frac{1}{T_{total}} \int_0^{T_{total}} \left(\sum_{n=1}^{N} \frac{\pi H(n)}{T(n)} \frac{\sinh[k(n)Z]}{\sinh[k(n)h]} \sin\left[\frac{2\pi}{T(n)} t - \varepsilon(n)\right] \right)^2 dt \qquad (5.25)$$

where T_{total} = total sampling time. Similarly, the mean square value of the wave-induced horizontal velocity is then given by Eq. 5.26

$$\overline{u_{wave}^2} = \frac{1}{T_{total}} \int_0^{T_{total}} \left(\sum_{n=1}^{N} \frac{\pi H(n)}{T(n)} \frac{\cosh[k(n)Z]}{\sinh[k(n)h]} \cos\left[\frac{2\pi}{T(n)} t - \varepsilon(n)\right] \right)^2 dt \qquad (5.26)$$

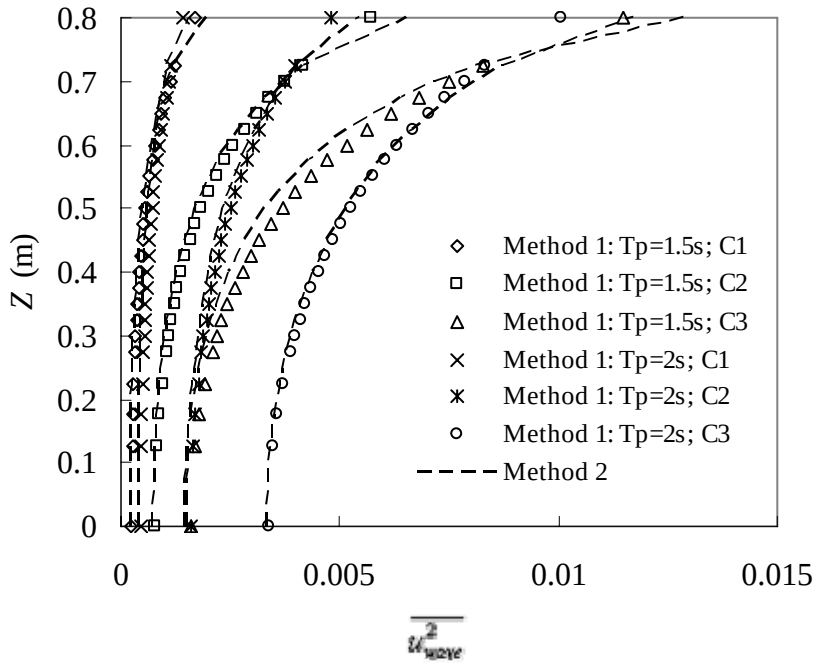

Figure 5.26. The mean square values of u_{wave} at various depths.

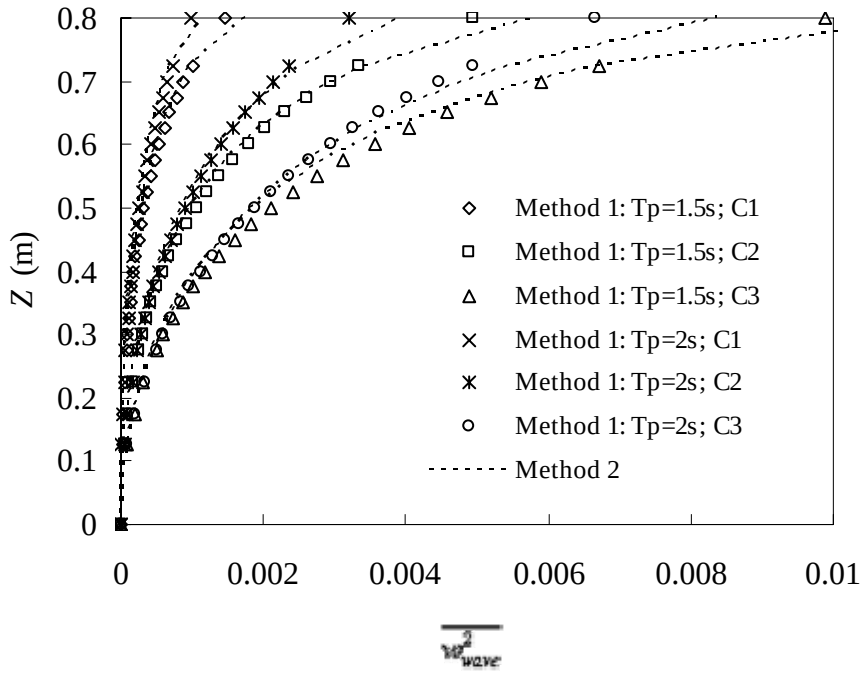

Figure 5.27. The mean square values of w_{wave} at various depths.

To show the difference in velocity fluctuation by the above derived methods, the experimental results obtained in Case D are used. The recorded water surface

fluctuation was used to compute the wave height, wave period and the wave number for *Method 1* while the spectrum generated by the wave synthesizer was used in the computation using *Method 2*. Results for the mean square values of u_{wave} and w_{wave} obtained in different depths of Case D are presented in Figs. 5.26 and 5.27, respectively. The depth dependence of the mean square values is clearly observed. A roughly exponential variation of the mean square values with depth is obtained. Both *Methods 1* and *2* give close values of the mean square wave-induced velocity at various depths. *Method 2* is used subsequently to calculate the mean square value of the wave-induced velocity as the method is more rigorous.

5.6.2 *Turbulence intensity profile along jet centerline*

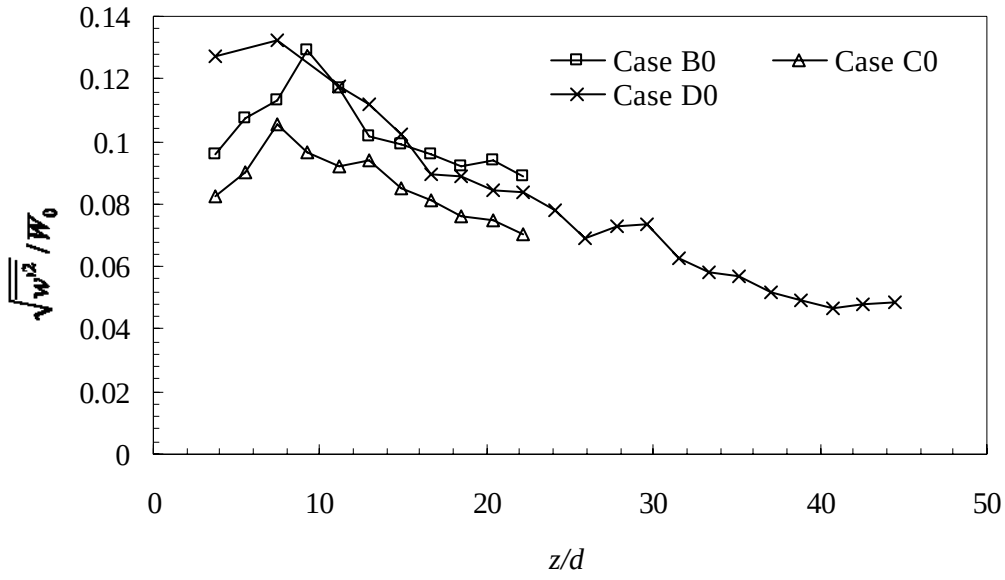

Figure 5.28. Turbulence intensity profile (scaled with the source velocity) along jet centerline obtained in stagnant environment.

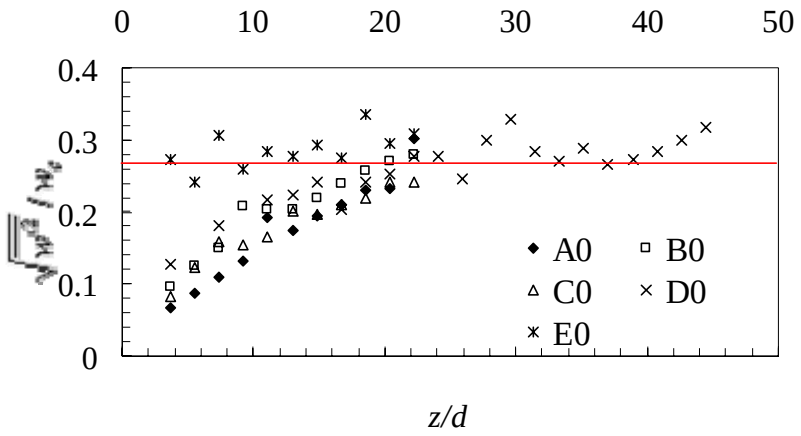

Figure 5.29. Turbulence intensity profile (scaled with the velocity at the corresponding level) along jet centerline obtained in stagnant environment.

The centerline profiles of the jet turbulence intensity obtained in stagnant ambient condition are shown in Fig. 5.28. In stagnant ambience the peak turbulence intensity of around 0.13 is observed at $z \sim 9d$ and the turbulence level then decreases gradually. These results show a good agreement with the data obtained by Fischer et. al (1979). More recent literatures (i.e. Wang and Law 2002) have shown that the turbulence intensity regarding the jet discharge in stagnant ambience is around 0.25. This seems to be inconsistent with the experimental results as shown in Fig. 5.28. However, most of these studies used the centerline velocity (w_c) to be the scaling velocity in the calculation of the jet turbulence intensity. The resulting turbulence level will be different from that using the source velocity or the discharge velocity (W_0) as the scaling velocity. Fig. 5.29 displays the turbulence intensity, scaled with w_c, obtained in this study. The resulting turbulence intensity is close to the empirical value of

0.25. Thus, the present results obtained in stagnant ambience are consistent with those from the literatures.

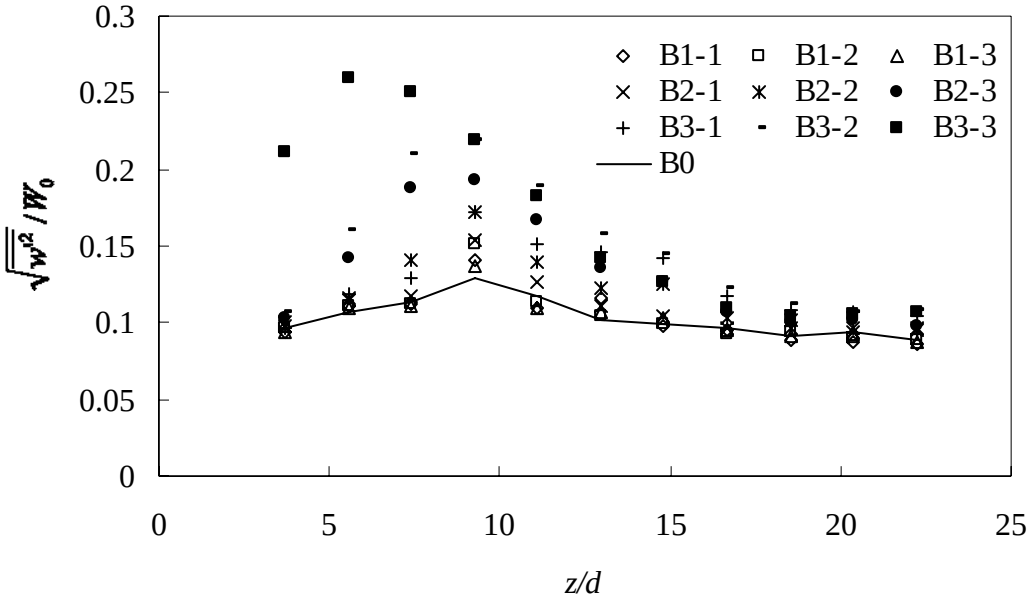

(a)

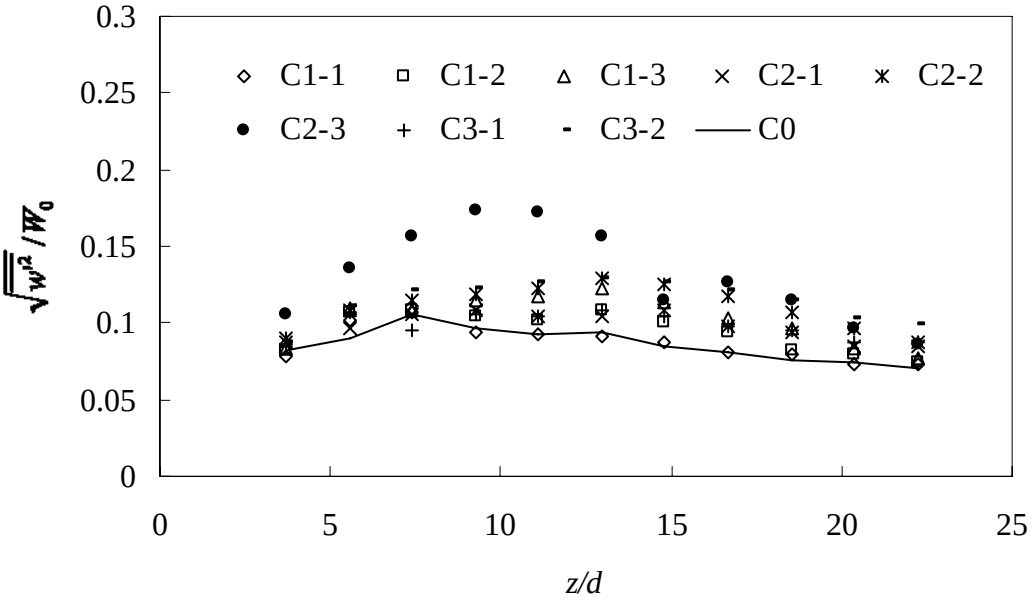

(b)

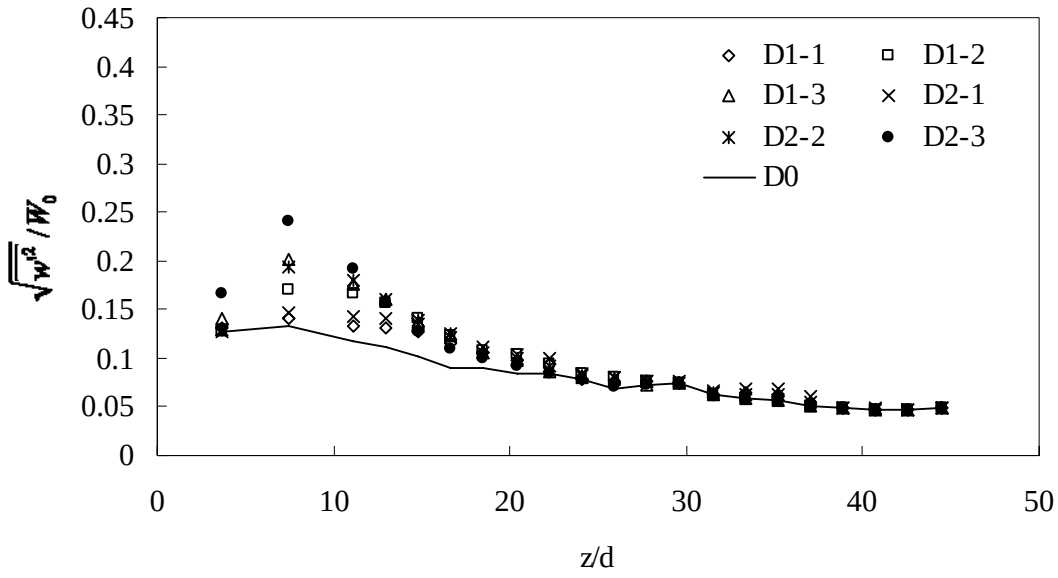

(c)

Figure 5.30. Turbulence intensity profiles along the jet axis for (a) Case B; (b) Case C; and (c) Case D.

The centerline velocity is dependent on the wave strength as shown in the previous results. So, though the use of centerline velocity is commonly used as the turbulence scaling velocity, it would be very difficult to determine the change of turbulence properties purely due to the presence of random waves. Consequently, the discharge velocity is used as the scaling velocity in calculating the longitudinal turbulence intensity.

The longitudinal turbulence intensity profiles obtained in Cases B, C and D are shown in Figs. 5.30(a), (b) and (c), respectively. The degree of turbulence is larger for the jet discharge in random waves than that of jets in stagnant ambience. However, the general trend of the turbulence intensity profile is similar to that obtained in

stagnant ambience which the turbulence intensities decrease gradually after reaching the peak values. In addition, the increase in turbulence is apparent in the jet near field under the propagation of waves with longer periods and larger amplitude. As discussed before, the length of the potential core is shorter in wave environment. The jet flow is to reach the fully turbulent flow condition earlier particularly in jet discharge to the relatively strong wave field. This explains why the peak turbulence reading was noticed to move closer to the jet outlet for case B3-3.

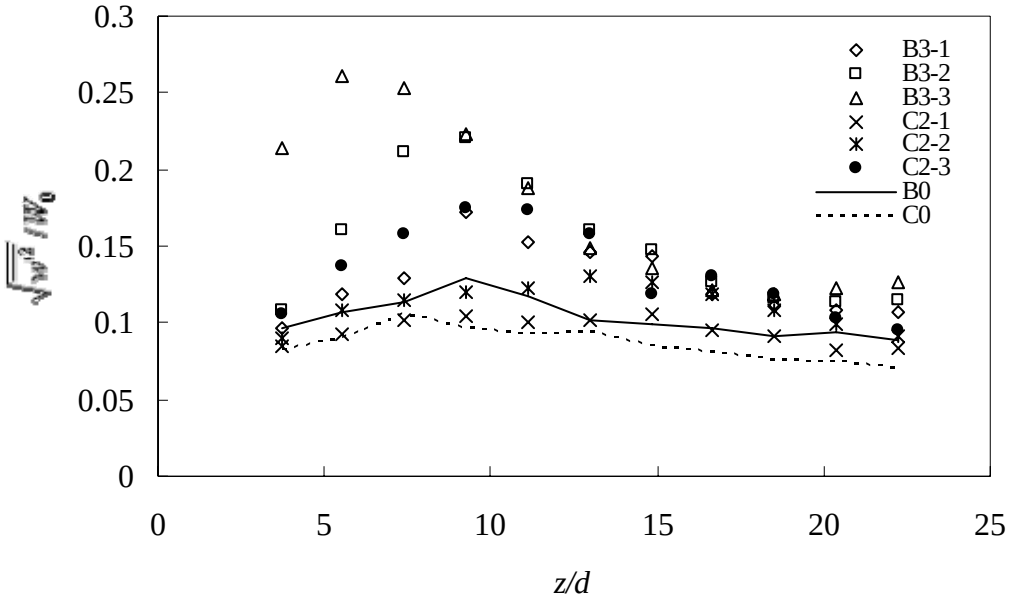

Figure 5.31. Turbulence intensity profiles obtained in Case B and C, T_p=2s experiments.

Most of the results obtained in this study show that the peak turbulence intensity still occurred at $z \sim 9d$, similar to that for jet in stagnant ambience. Case B3-3 is exceptional in which the jet trajectory is affected significantly by the strong wave field and becomes discontinuous. The magnitude of the wave-induced horizontal velocity

at the bottom boundary is large enough to split the jet trajectory frequently. The flow pattern was altered and the wave-induced horizontal velocity fluctuation may assist the formation of turbulent entrainment. Consequently, the location of peak turbulence shifts towards the jet outlet. Also the jet discharge velocity may be one of the factors leading to the shifting of location of the occurrence of peak turbulence as shown in Fig. 5.31.

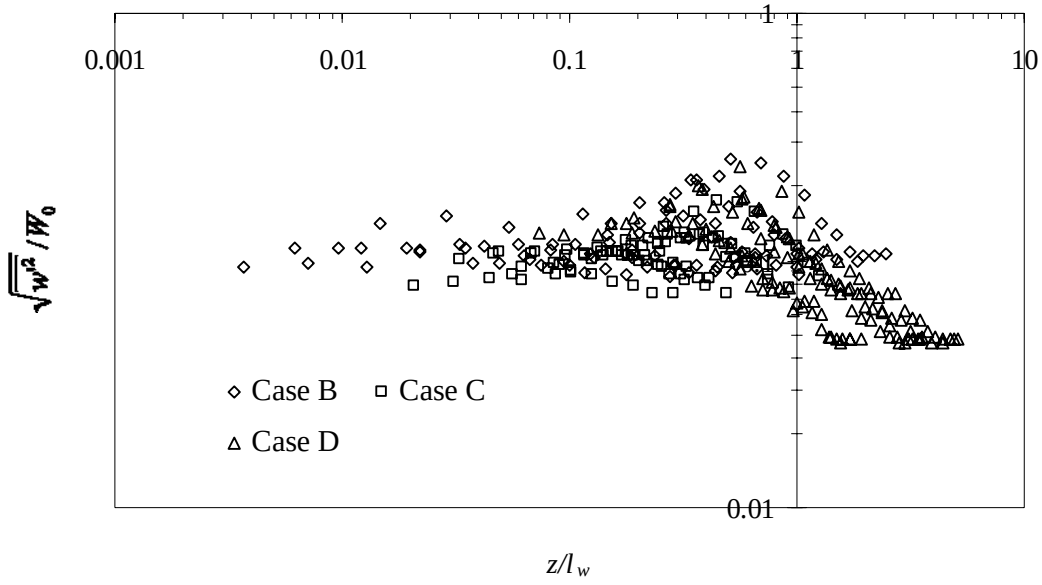

(a)

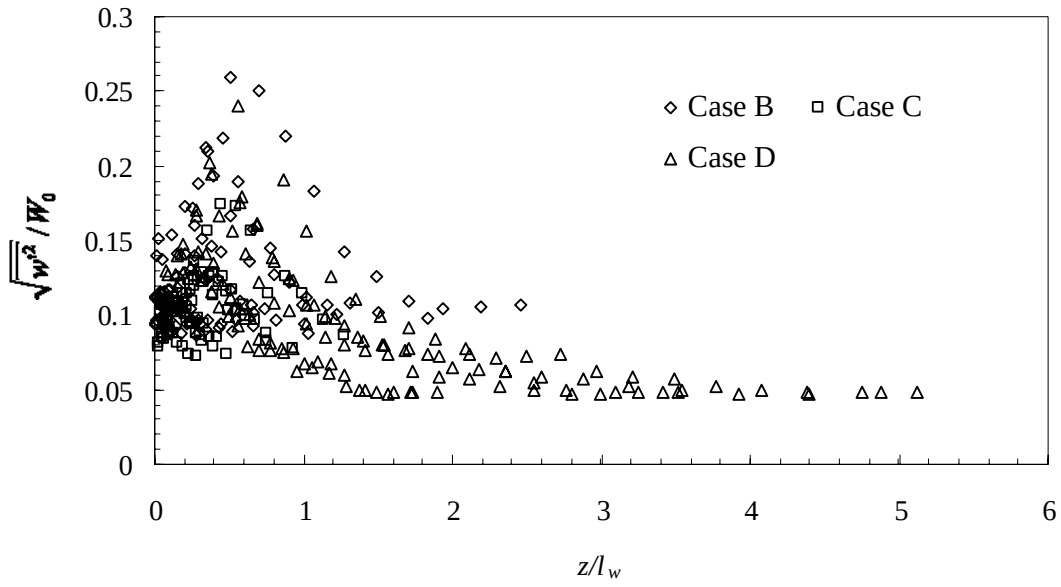

(b)

Figure 5.32 Variation of turbulence intensity with z/l_w in (a) logarithmic form and; (b) normal form.

Using the wave-induced momentum characteristic length, $l_w = \frac{\sqrt{M_0}}{u_w}$, as the length scale of the jet centerline distance, the results are plotted in Fig. 5.32 (a) (in log scale) and (b) (in normal scale). The figures show clearly that the turbulence intensity increases significantly when $z/l_w > 0.1$ and almost reaches the maximum value at the region of $z/l_w \sim 1$. This significant increase in turbulence conforms to the discussions about the formation of additional turbulent entrainment due to the wave-induced cross-currents, resulting in the greater jet spreading rate. The energy lost to the turbulence causes faster decay of centerline velocity.

As shown in Fig. 5.32 (b), the degree of scattering of the turbulence intensity data decreases at $z/l_w >> 1$ and closed to those values in jet far field (i.e. close to the

impinging region) obtained in stagnant ambient. The jet velocity is small in the far field and the jet will behave as a passive tracer advected to and fro by the wave motion. There is relatively little interference between the jet turbulence and the ambient wave motion.

5.6.3 *Cross-sectional profiles of turbulence intensity*

The radial profiles of axial turbulence intensity are displayed in Figs. 5.33(a) – (c). The root mean square jet velocity fluctuations are scaled with the time-averaged centerline velocity obtained in stagnant ambient (w_{c_pure}) corresponding to the same flow depth. In general, the shape of the turbulence intensity profile obtained in wave environment is similar to that obtained in stagnant ambience. However, the peak turbulence values in wave environments are increased by approximately 20%.

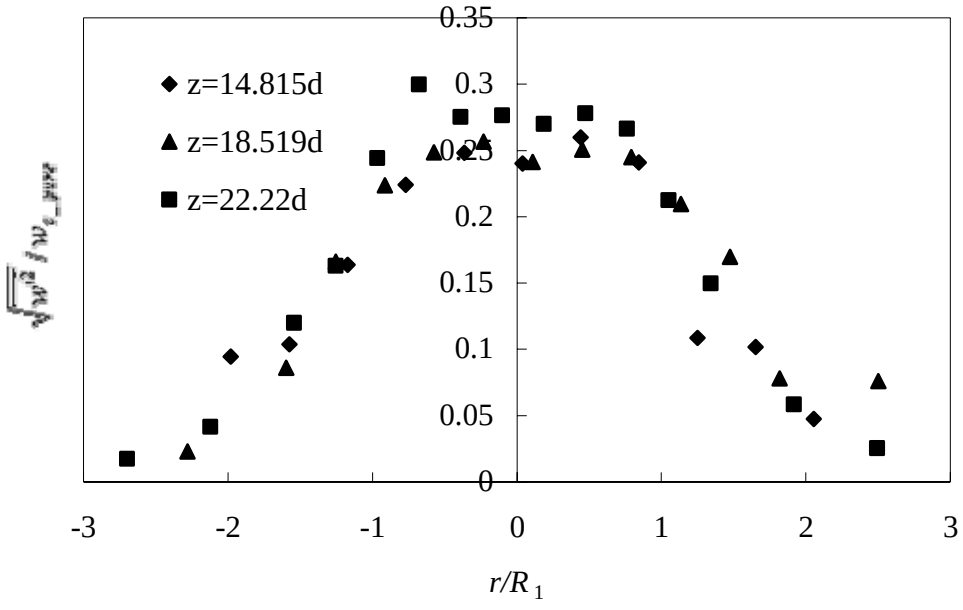

(a)

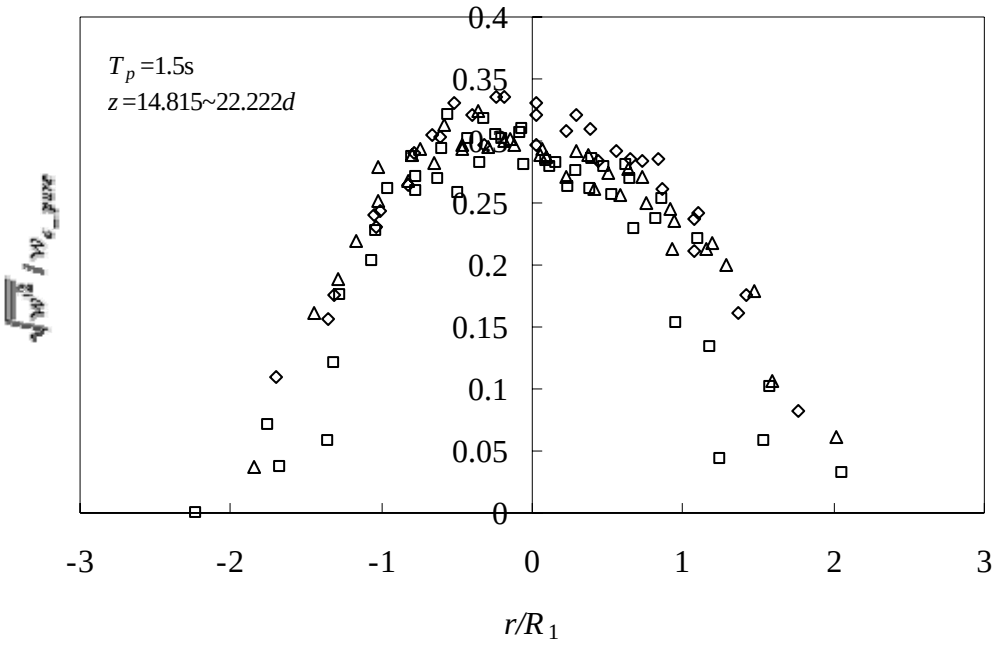

(b)

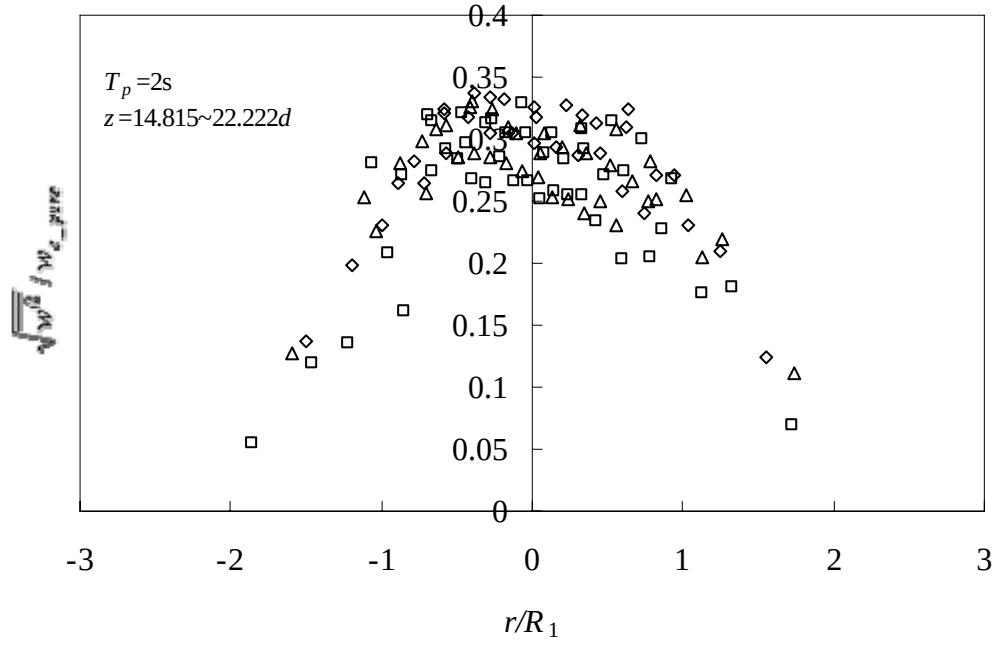

(c)

Figure 5.33. Radial turbulence intensity profiles obtained in (a) Case D0 (no wave); (b) Case D1 (T_p=1.5s); and (c) Case D2 (T_p=2s)

6 JET-RANDOM-WAVE LAGRANGIAN INTEGRAL MODEL

6.1 Introduction

The Lagrangian integral model used to compute the properties of jet discharge in wave environments is introduced. The model generated results are compared with the experimental results. Finally, the centerline dilution in Hong Kong coastal area is predicted based on the integral model and the empirical formulas derived in this study.

6.2 Formation of integral model

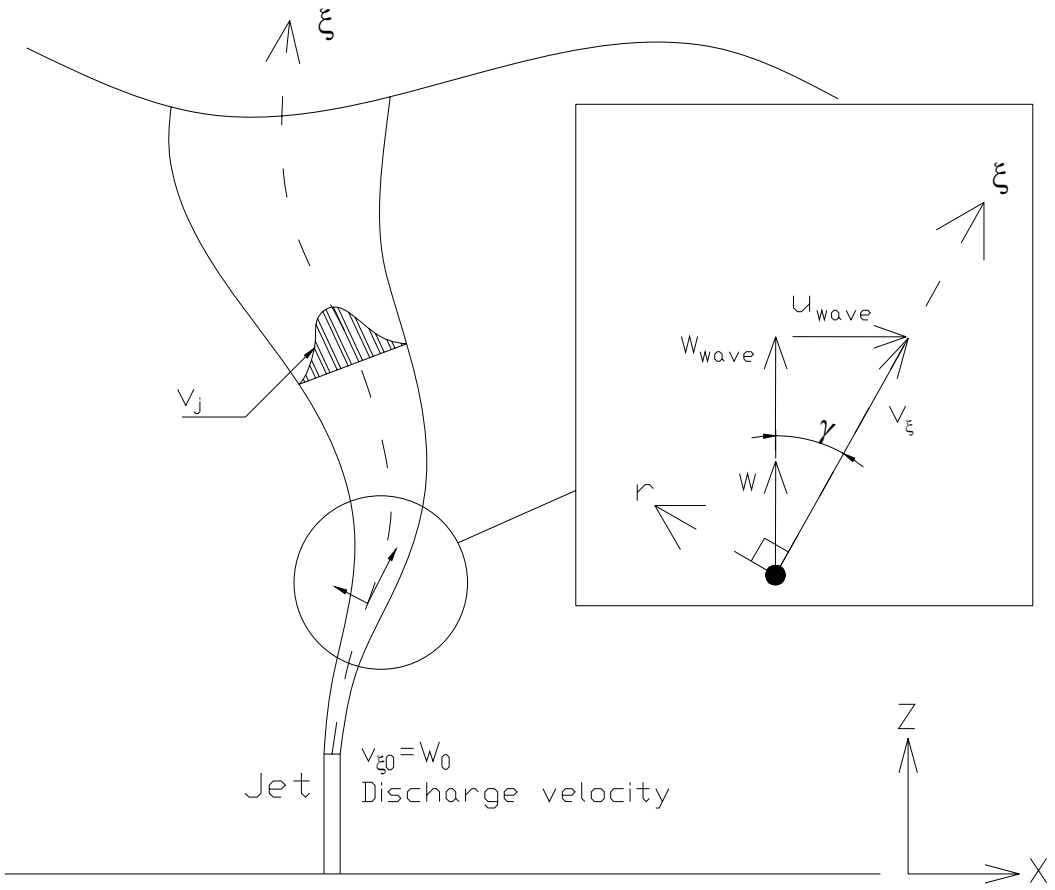

Figure 6.1. Motion of the fluid element of a jet discharge vertically to the wave environment.

The Lagrangian integral model developed by Chin (1998) for buoyant jet discharged in regular waves is being modified to predict the flow characteristics of a submerged vertical jet discharged in random waves. The diagram illustrating the problem is shown in Fig. 6.1.

The model in essence solves the following governing equations for the motion of the jet relative to the ambience.

Conservation of axial momentum:

$$\frac{\partial}{\partial \xi}\int_0^{\infty}(v_j \cos\gamma)^2 dr = 0 \tag{6.1}$$

Conservation of mass:

$$\frac{\partial}{\partial \xi}\int_0^{\infty} v_j \cos\gamma r dr = b\alpha v_{\xi}\cos\gamma + \frac{b\beta v_{\xi}\sin\gamma}{\pi} \tag{6.2}$$

$$\gamma = \tan^{-1}\left(\frac{u_{wave}}{w_{\xi} + w_{wave}}\right) \tag{6.3}$$

$$w_{\xi} = \frac{v_{\xi}}{\cos\gamma} \tag{6.4}$$

where ξ = axial direction ordinate, r = radial direction ordinate, v_{ξ} = centerline velocity of the jet element relative to the ambience, v_j = jet velocity relative to the ambience, w_{ξ} = vertical component of v_j, γ = angle that v makes with the jet axis, b = jet half-width, α = radial entrainment coefficient, β = forced entrainment coefficient and u_{wave} and w_{wave} are the wave induced velocity component regarding the horizontal and vertical direction, respectively. Since the model is used to simulate the random wave condition particularly for the waves in the form of JONSWAP spectrum, the wave particle velocity based on the linear wave theory is not in accordance with the current study. However, the wave velocity achieved in random wave condition can be re-simulated with the used of a known wave energy spectrum as discussed previously. The wave fluid velocity in random wave conditions can be

achieved based on the simulated surface elevation and the equations for both the horizontal and vertical components are presented in Eqs. 6.5 and 6.6, respectively.

$$u_{wave}(t) = \sum_{n=1}^{N} \frac{\pi H(n)}{T(n)} \frac{\cosh[k(n)Z]}{\sinh[k(n)h]} \cos\left[kX - \frac{2\pi}{T(n)} t + \varepsilon(n) \right] \tag{6.5}$$

$$w_{wave}(t) = \sum_{n=1}^{N} \frac{\pi H(n)}{T(n)} \frac{\sinh[k(n)Z]}{\sinh[k(n)h]} \sin\left[kX - \frac{2\pi}{T(n)} t + \varepsilon(n) \right] \tag{6.6}$$

where t = time, X = horizontal co-ordinate and Z = flow depth measured from bottom to top.

6.3 Solution method

The equations listed above can be solved by using the finite difference method. Eqs. 6.1 and 6.2 are discretized by forward difference as follow.

$$\frac{v_{i+1} - v_i}{\Delta\xi} = -\frac{2v_i}{b_i}\left(\alpha + \frac{\beta \tan\gamma}{\pi} \right) \tag{6.7}$$

$$\frac{b_{i+1} - b_i}{\Delta\xi} = 2\left(\alpha + \frac{\beta \tan\gamma}{\pi} \right) \tag{6.8}$$

$$v = v_\xi / v_{\xi 0} = v_\xi / W_0 \tag{6.9}$$

$$\Delta\xi = v_\xi \Delta t \tag{6.10}$$

where v = non-dimensional jet velocity, Δt = time increment and $\Delta\xi$ is the segment of the jet axis with respect to Δt.

The ordinate of the instantaneous jet axis, ξ, is resolved into the horizontal (X) and the vertical (Z) components. The associated equations are given below.

$$X_{i+1} - X_i = \sin\gamma\Delta\xi + u_{wave}\Delta t \tag{6.11}$$

$$Z_{i+1} - Z_i = \cos\gamma\Delta\xi + w_{wave}\Delta t \tag{6.12}$$

The time increment Δt should be decreased with the increase in discharge velocity to achieve an accurate result. In addition, the length of the potential core has to be adjusted appropriately for simulating the real situation. The initial conditions and those required parameters used in the computation are listed below:

$b_0 = \frac{\sqrt{2}}{2}$ d, $v_0 = 1$, $\alpha = 0.057$ & $\beta = 1$.

6.4 Lagrangian integral model results

The path of the jet trajectory at different period of time is different due to the passing waves with irregular waveform various frequency. Hence, the jet trajectory and the associated properties are needed to obtain for time-averaged analysis. Around a hundred waves were simulated to interact with the jet and the time-averaged centerline velocities are showed in Figs. 6.2(a) and (b). The results computed by the present Lagrangian integral model are generally in good agreement with the experimental results. Both the experimental and model simulation results are very close except the velocity values within or very near to the jet potential core. The model predicts a higher velocity in the jet potential core region. However, it is not certain whether the overestimation of the centerline velocity is owing to the

Lagrangian model limitation. This is because the velocity measured across the jet orifice can vary significantly particularly at the region where the jet cross-sectional velocity profile changes from “top-hat” to Gaussian shape. The sampling size of the ADV probe may be too large and may underestimate the jet velocity at the zone of flow establishment during sampling.

Koole and Swan (1994) and the results of this study suggested that the jet potential core is influenced by the propagation of the surface waves. The additional fluid motion owing to the presence of wave mechanism may speed up the formation of jet fully turbulent flow resulting in a shorter potential core is achieved. In such a scenario, the length of the potential core is necessary to re-adjusted in order to obtain an accurate simulation results with the use of the Lagrangian integral model.

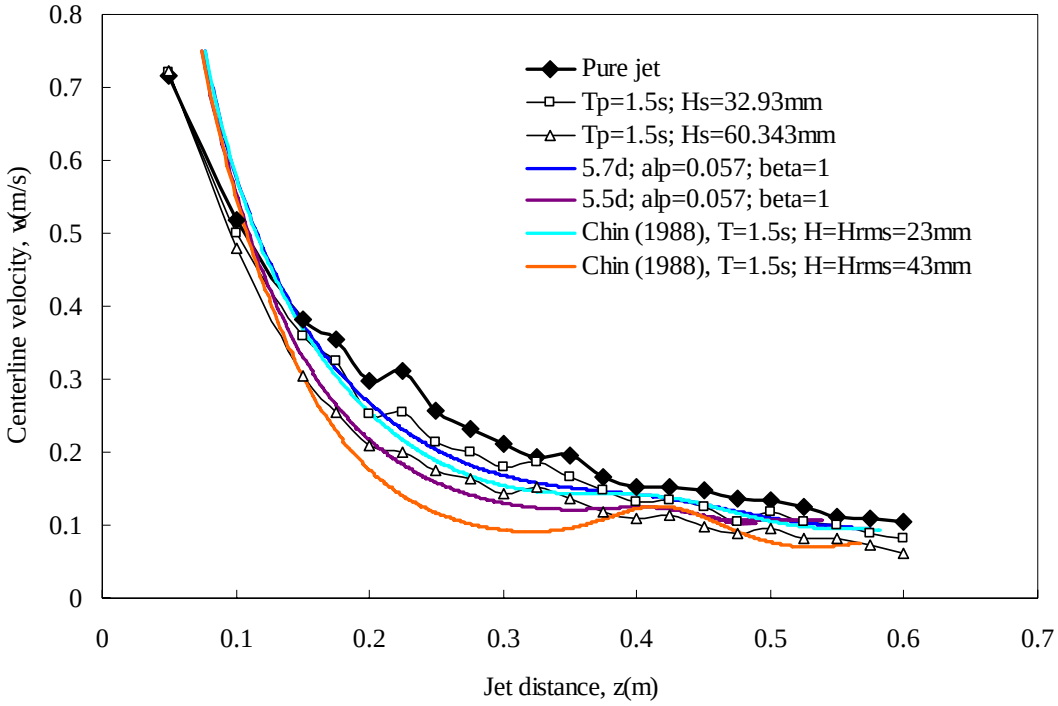

(a)

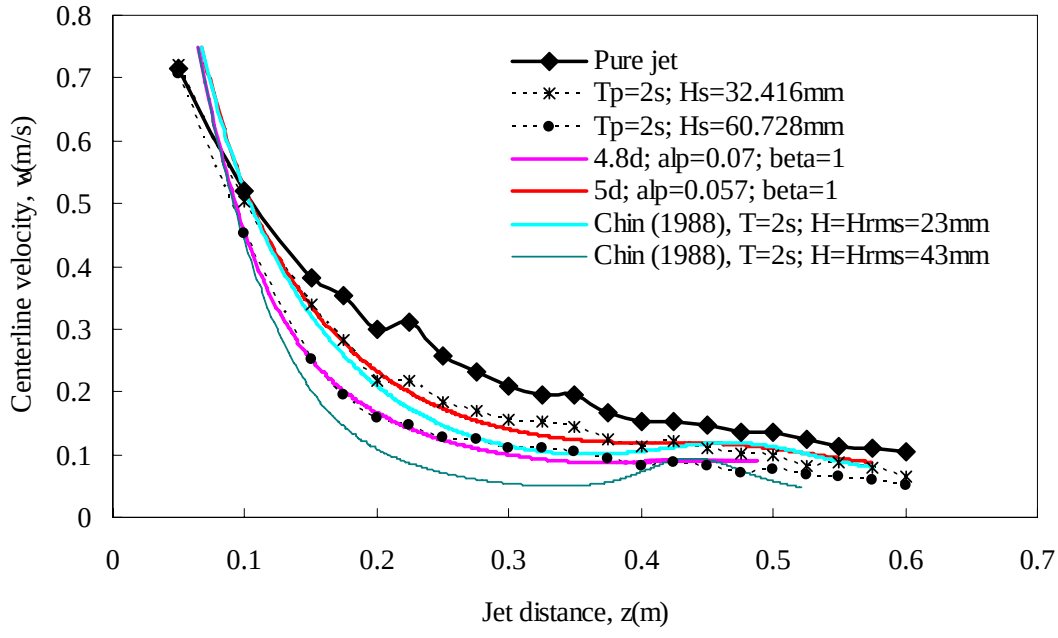

(b)

Figure 6.2. The results obtained from this study modified Lagrangian integral model, Lagrangain integral model by Chin (1988) and the experimental results for (a) Cases D1-1 and D1-2; and (b) Cases D2-1 and D2-2.

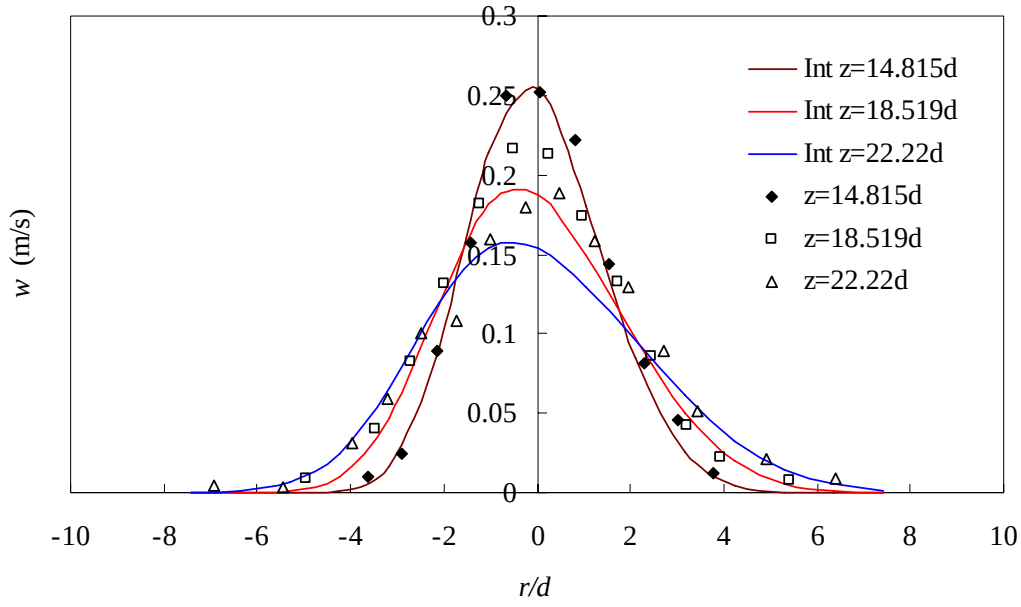

Figure 6.3. The radial velocity profile obtained by jet-random wave Lagrangian integral model modified in this study with T_p=1.5s and H_s=33mm and validated with the experimental results obtained in Case D1-1.

In addition, the radial profile of the axial velocity, especially for the width, obtained by the integral model agrees quite well with that obtained experimentally as shown in Fig. 6.3. This confirms the validity of the choice of the entrainment coefficients. In the Lagrangian integral model, a forced entrainment coefficient, β, is introduced to account for the entrainment due to ambient flow, in addition to the jet entrainment coefficient, α. Chin (1988) recommended $\beta \sim 1$ based on past results of plume in crossflows. This is reasonable since the wave-induced fluid motion can be recognized as an oscillatory cross current. Thus, the use of the entrainment coefficients of pure turbulent jet α=0.057 (Lee & Chu 2003, pp40) and β=1 are considered reasonable in this study.

6.5 Comparisons with Chin's model (1988)

In the previous chapter the root mean square wave height (H_{rms}) was proposed as the wave height (H) and the period wave period (T_p) as the wave period (T) for analysis. In an attempt to find out the differences of flow behaviours for jet in regular waves and jet in random waves, the corresponding values of H_{rms} and T_p, used in the experiments of the present study are employed to simulate the results with the jet-regular-wave integral model by Chin (1988). The simulated centerline velocity for Cases D1-1, D1-2, D2-1 and D2-2 are also displayed in Figs. 6.2(a) and (b). Apparently the results from Chin's model are not as good as those from the modified jet-random-wave Lagrangian model, particularly for those cases in which the jets were discharged into relatively strong waves, i.e. T=T_p=2s or H=H_{rms}=43mm. The centerline velocity results obtained by Chin's model are close to the experimental results only in the jet downstream region while the computed results display a steeper descent of the velocity along the jet flow direction and underestimate the velocity in the jet upstream region. Lower centerline velocities were simulated by the regular wave model. This can be explained together with the cross-sectional vertical velocity profiles simulated by Chin's model in Fig.6.4. Twin-peak or top-hat velocity profiles are shown in Fig. 6.4 for the simulation of jet discharge in a regular wave environment. As mentioned in Section 5.3.1, the formation of twin-peak

velocity profile should be dependent on the jet discharge velocity, waves with long wave length (i.e. long period waves) or high fluid particle velocity. The jet body is easily advected under certain wave conditions and resulted in wider, flatter axial velocity profiles, and occasionally top-hat or twin-peak velocity profiles appear as shown in Fig. 6.4. Thus, the jet centerline velocity simulated by Chin's integral model, considering only the jet-regular-wave interaction, may not be as good as the jet-random-wave model proposed in this study.

Although twin-peak velocity profiles may be obtained from the jet-regular wave model for jet under relatively strong, the results, obtained by the jet-regular-wave Lagrangian integral model by Chin (1988), are still satisfactory for cases of jet discharged into relatively weak wave conditions, i.e. Case D1-1, $T=T_p$=1.5s, $H=H_{rms}$=23mm, as shown in Fig. 6.2(a). This strongly supports that the degree of influence of jet, due to different form of waves, should be the same under the same level of wave energy.

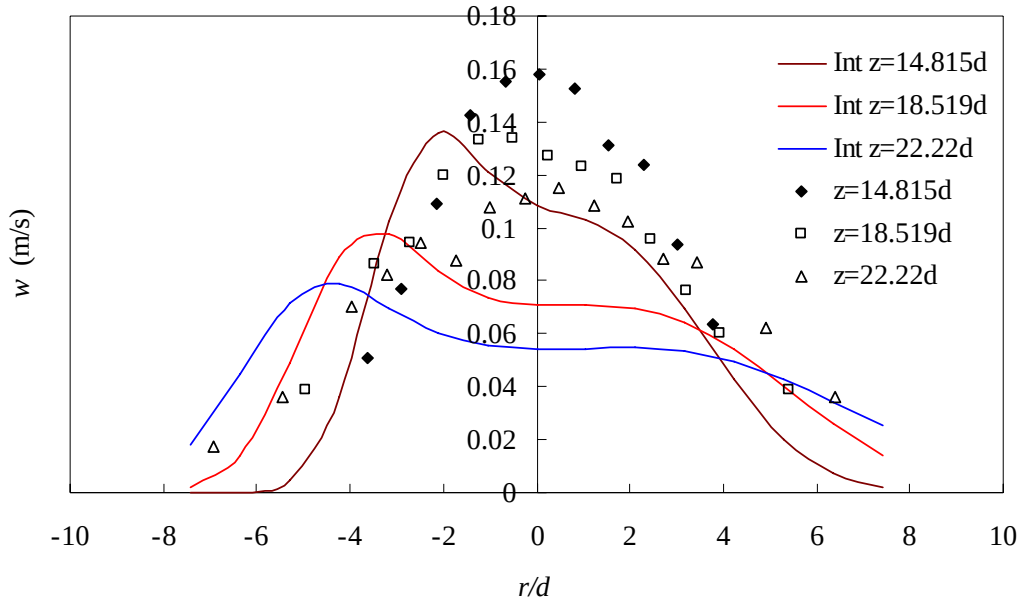

Figure 6.4. The radial velocity profile obtained by Chin's Lagrangian integral model [Chin (1988)] with $T=T_p$=2s and $H=H_{rms}$=43mm and validated with the experimental results obtained in Case D2-2.

6.6 Model limitations

The jet-random-wave Lagrangian integral model in this study gives quite well estimations on the jet centerline velocity and the jet cross-sectional velocity profiles with the commonly used entrainment coefficient values. Koole and Swan (1994) validated Chin's model with the use of α=1.56 and β=1. This may be related to the difference in the experimental setup. In their work a submerged horizontal non-buoyant plane jet under regular waves was studied. Since the jet discharge counteracted the surface wave propagation directly, a greater value of the coefficient may be required to represent the rate of entrainment.

The jet-random-wave Lagrangian integral model is shown to accurately predict the jet centerline velocity for jet discharge in the random wave environments. However, the jet turbulent intensity can be strong for jet with a relatively low discharge velocity, i.e. Case B, W_0=0.53m/s. The presence of waves may enlarge the effect on turbulent diffusion resulting in a greater jet cross-sectional area. The jet spreading rate contributed by the turbulent diffusion with the presence of waves may consider to be more significant in low discharge velocity. Thus, the prediction on jet spreading rate and the jet cross-sectional velocity or concentration profiles in wave conditions may result a lesser degree of accuracy as shown in Fig. 6.5.

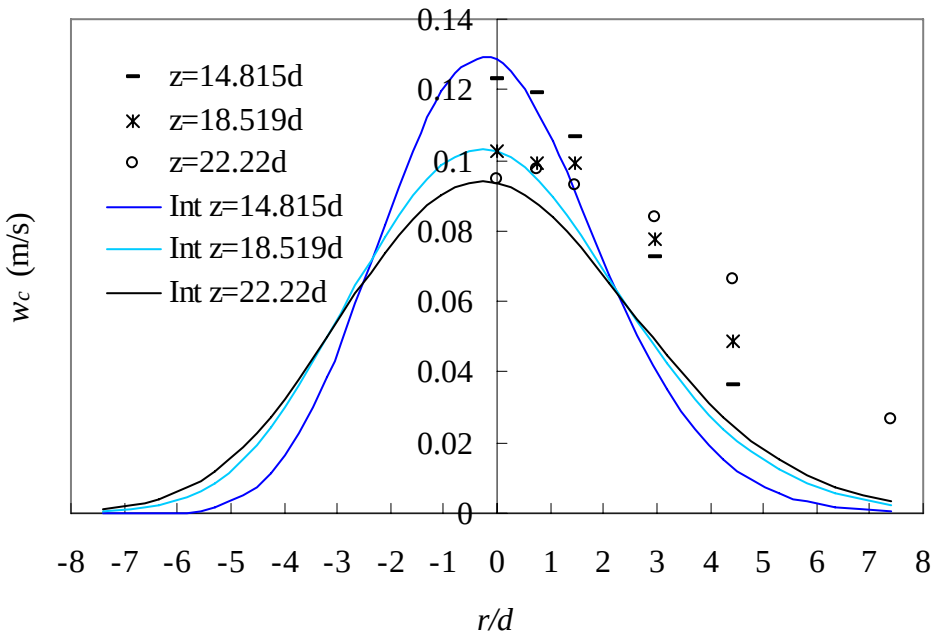

Figure 6.5. The radial velocity profile obtained by jet-random wave Lagrangian integral model modified in this study with T_p=2s and H_s=29mm and validated with the experimental results obtained in Case B3-2.

As discussed in the previous chapter, the discontinuous jet trajectory may happen when the wave motion is relatively strong compared to the jet momentum. The jet-wave model is developed based on the continuous form of the deflected jet trajectory. The discontinuous motion is not accounted for by the integral model, even though the applied wave field is considered to be shallow water waves and should be sufficiently strong to split the jet trajectory. Because the degree of influence due to the discontinuous motion cannot be simulated, the proposed jet-random-wave model should be limited to the categories of symmetric and asymmetric motions and for the presence of deep water and transitional water waves (i.e. Shallow water waves have greater possibility to generate discontinuous motion because the wave-induced fluid movement is considerably significant)

Although the jet trajectory may be deflected significantly away from the vertical centerline of the jet outlet under strong waves, the fluid around the jet outlet centerline will be still in motion owing to the jet induced turbulent eddies as well as the wave induced motion. The Lagrangian model by Chin (1988) determined only the velocity within the jet body but has not considered the rest of the fluid motion which may take place. Consequently, the jet centerline velocity computed by the Lagrangian integral model may have intermittency when strong waves are present. The Eulerian time-averaged jet centerline velocity predicted by this model may be smaller than that

occurs in reality. This explained why the computed results show better agreement with the experiments for cases with small energy waves (i.e. shorter wave period or smaller wave height).

The Lagrangian integral model is limited by the empiricism involved in the choice of the length of the potential core. However, the fluid motion at the bottom boundary for deep water wave is relatively small. The influence towards the formation of zone of flow establishment (ZFE) of the submerged jet is considered to be very limited by deep water wave. Hence, the length of the potential core can be considered to be the same as that in stagnant environment if deep water waves are imposed to interact with the jet body.

6.7 Centerline velocity and dilution ratio in prototype

The wave data obtained in Kau Yi Chau, one of the long term wave monitoring stations maintained by the Civil Engineering and Development Department (CEDD), the Government of HKSAR, are used as an example to estimate the improvement in centerline dilution of jet discharge in the Hong Kong coastal area when the effect of waves are considered. The averaged peak wave period and the averaged significant wave height inferred from the data collected in 2003 at Kau Yi Chau monitoring station are used together with the commonly used wastewater discharge parameters. The data are listed in Table 6.1.

Table 6.1. The parameters used for the prediction of centerline velocity ratio.

Case	Jet parameters				Wave parameters		
	Q_0 (m^3/s)	W_0 (m/s)	d (m)	h (m)	T_p (s)	H_s (m)	H_{rms} (m)
I	0.157	3.2	0.25	9	6.4	0.28	0.198

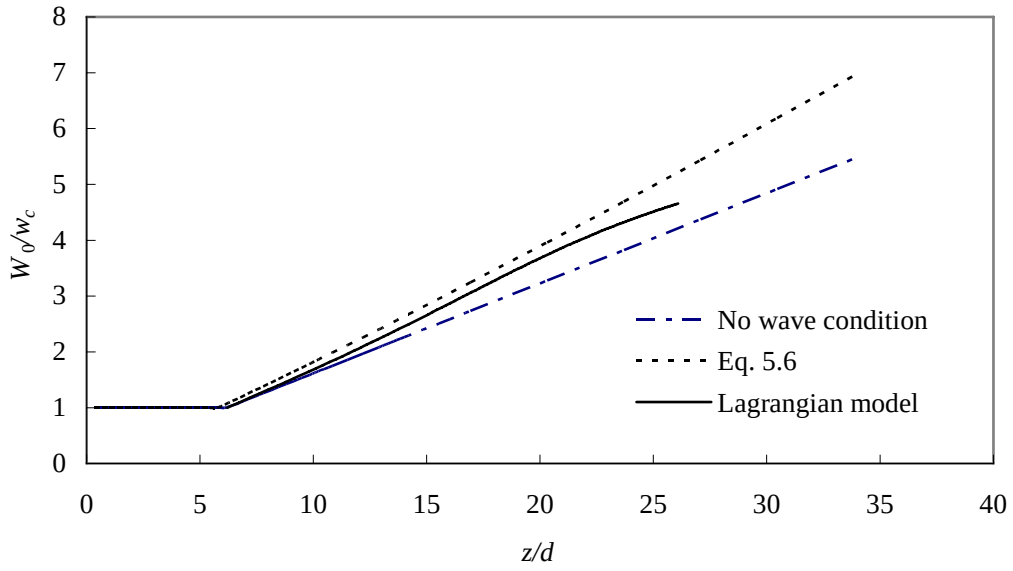

Figure 6.6. The prediction of centerline velocity ratio.

The wave-induced velocity for the wave conditions as shown in Table 6.1 can be calculated based on Eq. 5.8: $u_{w\_simp} = \frac{\pi H_{rms}}{T_p} \frac{\cosh(k_a Z_a)}{\sinh(k_a h)}$ where Z_a=h/2, assuming the riser length =0. The centerline velocity along the jet axis is predicted with the use of formulas proposed in Eqs. 5.6(a), (b) & (c) and also the Lagrangian integral model. The results for the two proposed cases listed in Table 6.1 are presented by plotting the velocity ratio W_0/w_c against z/d in Fig. 6.6. The centerline velocity ratio predicted in stagnant ambience is also included for comparison. The value of W_0/w_c obtained in wave environments is higher than that obtained in stagnant ambience under the same discharge parameters. It is observed that the lower the initial jet velocity used in jet discharge, the higher the centerline velocity ratio is obtained. Because the velocity jet width is inter-related with the concentration jet width with a scale parameter of

$\lambda = 1.2$ as suggested by Papanicolaou and List (1988), the centerline dilution ratio of the proposed scenario can be predicted based on the results presented in Fig. 6.6. Thus, under the presumed conditions, the centerline dilution ratio will be increased. When the jet body is about to impinge the water surface, the dilution ratio will be 125% of that in stagnant ambient for Cases I.

The above results are only indicative as in the real situation, many other factors need to be considered. For instance, the waves will be 3-dimensional, which will possibly further enhance the jet mixing. Also the effluent will have a different density from that of sea water (usually lighter). Buoyancy force thus will exist which will enhance the dilution process. More accurate prediction can be achieved only after the above factors have been thoroughly investigated.

7 CONCLUSIONS

An experimental study of vertical jets discharged under random surface waves with JONSWAP spectra has been carried out. A total of 42 set of experiments for jets in stagnant or random wave environments were conducted. Time-averaged jets characteristics such as centerline velocity, jet width spreading rate, cross-sectional velocity profile and the turbulence intensity were obtained from the time-varying data measured by an acoustic Doppler velocimeter (ADV). Flow visualization was conducted to investigate the difference in the flow behaviours for jet discharge in stagnant ambience and in random wave environment. The Lagrangian integral model based on jets discharge in regular waves was modified and gave satisfactory results.

7.1 Summary of findings

Three different types of jet motions, symmetric, asymmetric and discontinuous were observed in the flow visualization. As the submerged vertical jet was used, the type of motion should be dependent on the water depth and the velocity ratio of jet discharge to the wave induced current. For each flow scenario, three flow regions of deflection, transition and developed regions were also identified.

The cross-sectional axial velocity profiles in waves and in stagnant ambience were achieved. All the obtained profiles followed the Gaussian distribution curve

while the multi-peak profiles occasionally occurred. This was explained by the strong wave-induced horizontal movement which oscillated the jet body periodically.

The total wave energy given by the significant wave height (H_s) is only half of the energy given by the same value of wave height (H) obtained in regular waves. Hence, the period and the wave height used in linear wave theory cannot be directly replaced by the peak wave period (T_p) and the significant wave height. With the use of the wave energy spectrum, the free surface fluctuation can be re-simulated and the wave-induced velocity can be computed. The derivation of the wave-induced characteristic velocity and the wave significant velocity has been briefly discussed in Chapter 4. In accordance with the concept of crossflow length scales, the wave-induced characteristic length was also obtained.

The experimental measurements showed the centerline velocity decays faster in random waves than that in stagnant ambience. This phenomenon is related to the enhancement of jet spreading rate in wave environment. In addition, the wave-induced cross-current entrains more ambient water into the jet body. More energy is consumed into the turbulent entrainment process, resulting in the faster centerline velocity decay rate in wave environment than that in stagnant environment. The non-dimensional jet centerline velocity and the jet-axial distance were formed based on the characteristic wave velocity and the wave-induced

momentum characteristic length. The results showed that the jet discharge with $z/l_w \le 0.1$ experiences a similar velocity decay rate as those obtained in stagnant ambience. This suggests that the jet flow characteristics are still governed by the jet driving force. A pure jet region thus exists for $z/l_w \le 0.1$. However, the degree of velocity data scattering increases when $z/l_w > 0.1$. The degree of scattering seems to reach the maximum at $z/l_w \sim 1$ and then decreases gradually for $z/l_w > 1$. This result strongly suggested that the momentum exchange between the jet and the wave field exists, resulting in the jet-wave interaction region located at $0.1 < z/l_w < 10$.

The wave-induced significant velocity is also used to scale the jet centerline velocity. The velocity data follow a separate piecewise linear relationship when the non-dimensional jet distance, $z/l_{sig} > 0.1$. A set of equations is suggested to describe the rate of decay of velocity with the use of the scaling parameters (u_{sig}, l_{sig}). This study finds that the wave-induced significant velocity can be calculated using the linear wave theory, the root mean square wave height and the peak wave period. This would be easier and convenient computationally to estimate the decay of jet centerline velocity in the presence of random wave environment.

The formation of the potential core is noticed to be shortened when JONSWAP random waves are present. The results showed that the smaller the ratio of jet discharge velocity to the wave-induced characteristic velocity $R = W_0/u_w$, the

shorter the potential core is obtained, which is reflected by the reduction of the jet velocity corresponding to the same jet distance.

The jet half-width achieved in the direction of waves shows a non-linear spread rate with the jet-axial distance. The presence of non-linear spreading rate can be related to the deflection of jet trajectory in the presence of wave motion. In addition, the wave-induced cross-currents entrain more ambient water into the jet body resulting in a further expansion of the jet cross-sectional area particular in the direction of the wave propagation. As the two-dimensional irregular surface waves are applied, the circular jet flow sectional area is changed to elliptical shape. The jet half-width (b), used to account for the jet flow area, is then suggested to be calculated by $b = \sqrt{R_1 R_2}$ where R_1 and R_2 are the jet half-width measured along the wave direction and normal to the wave direction (Chapter 4). By plotting the non-dimensional jet width against the non-dimensional jet distance, the jet width data were cluster at $z/l_{sig} < 0.1$. The degree of scatter increase when $z/l_{sig} > 0.1$. A formula is obtained by curve-fitting, which shows that the jet spreading rate in JONSWAP random waves is enhanced by approximately 30% ($\beta_g = \frac{\partial b}{\partial z} \sim 0.145$) for $z/l_{sig} > 0.1$. This study also shows the discharge velocity is one of the factors affecting the jet spreading rate.

The jet turbulence intensity was also considered in this study. The measured turbulence intensities along the jet axis, were in agreement with those in Fischer et al. (1979) for the case of stagnant ambience. To analyse the turbulence intensity of jet discharge in wave conditions, two simple methods are proposed (*Method 1* developed based on linear wave theory or *Method 2* developed based on the wave energy spectrum) to eliminate the wave induced velocity fluctuation from the measured data. The peak turbulence intensities in wave environments occurred roughly at the same position as those in stagnant water at $z \sim 9d$. However, the jet turbulence intensity increases significantly within the region of $0.1 < z/l_w < 10$, which is related to the additional turbulent entrainment due to the presence of wave-induced cross-current.

To predict the jet characteristics, the Lagrangian integral model of jet-random-wave interaction is proposed based on the one developed by Chin (1988) . This is used to compare with the data obtained exeperimentally in this study. The root mean square wave heights and the peak wave periods were used as the wave parameters in the model. The generated results showed agreements with the experimental data obtained in random waves. However, the model performance depends on the values of the entrainment coefficients used.

Wave data based on long term field measurement were used together with the empirical formulas, derived in this study, to estimate centerline dilution of wastewater

discharge in Hong Kong coastal waters. The results indicated the centerline dilution, dependent on the jet initial velocity, can be increased by 25% more than the estimation obtained in stagnant water.

7.2 Recommendations

In this study experiments were carried out to investigate the jet behaviour in random waves and obtain some empirical formulae based on the measurements. Although a great deal of experimental data on jets discharge in random waves is collected, the data are limited to momentum dominated turbulent jets. They may not completely account for the mixing of wastewater discharge in natural coastal water. This is because the discharge effluent usually has a different density from the ambient water. Additional buoyancy force thus exists and further complicates the mixing mechanism. Hence, it is necessary to study the buoyant jet discharge in irregular wave environments in order to complete the picture of jet-wave interaction.

Multiport diffusers are broadly employed in the wastewater disposal scheme. It is likely that the dilution ratio of multiple jets discharge into random waves will be enhanced while the degree of improvement is not yet determined. In addition, the strong wind created by typhoons would build up a strong wave motion in rivers. The jet interaction with random waves and currents has never been studied. A numerical model for jet discharge in wave environments should also be developed. These

works will be useful for engineers and environmentalists to carry out environmental impact assessment.

REFERENCES

1. Abramovich, B.N. (1963). *The theory of turbulent jets*, MIT Press, Cambridge, Mass.
2. Albertson, M.L., Dai, Y.B., Jensen, R.A., and Rouse, H. (1950). "Diffusion of submerged jets." *Trans. ASC*E, Vol. 115, 639-644.
3. Andreopoulos, J. (1982). "Measurements in a jet-pipe flow issuing perpendicularly into a cross stream." *J. Fluids Engrg*, ASME, 104, 493-499.
4. Andreopoulos, J. (1983). "Heat transfer measurements in a heated jet-pipe flow issuing into a cold cross stream." *Phys. Fluids*, 26(11), 3201-3209.
5. Andreopoulos, J. and Rodi, W. (1984). "Experimental investigation of jets in a crossflow." *J. Fluids Mech*., 138, 93-127
6. Andreopoulos, J. (1985). "On the structure of jets in a crossflow." *J. Fluids Mech*., 157, 163-197.
7. Becker, H.A. and Massaro, T.A. (1968). "Vortex evolution in a round jet." *J. Fluid Mech.*, 31, 435-448.
8. Chen, Y.P., Li, C.W., Lee, J.H.W. (2003). "Measurement of a round jet under random waves." *Proc. 30th IAHR Congress*, Greece, Theme C, Vol. 1, 287-292.
9. Chen, Y.P., Li, C.W. and Zhang, C.K. (2004). "LES of 2D and 3D vertical jets impinging on free surface." *Proc. 4th Int. sym. Envir. Hydr*., HK, 367-373.
10. Chin, D.A. (1987). "Influence of surface wave on outfall dilution." J. Hydr. Engrg., ASCE, 113(8), 1006-1017.
11. Chin, D.A., (1988). "Model of buoyant-jet-surface-waves interaction." *J. Waterway, Port, Coastal and Ocean Eng*., ASCE, 114(3), 331-345.
12. Chu, P.C.K., Lee, J.H.W. and Chu, V.H. (1999). "Spreading of turbulent round jets in coflow." *J. Hydr. Engrg.*, ASCE, 125 (2), 193-204.
13. Chu, V.H. and Lee, J.H.W. (1996). "General integral formulation of turbulent buoyant jets in

cross-flow." *Journal of Hydraulic Engineering*, ASCE, 122, 27-34.

14. Chyan, J.M. and Hwung, H.H. (1993). "On the interaction of turbulent jet with waves." *J. Hydr. Res*., 31(6), 791-810.

15. Davidson, M.J. and Pun, K.L. (1998). "Hybrid model for prediction of initial dilutions from outfall discharges." *J. Hydr. Engrg*., ASCE, 124(12), 1188-1197.

16. Davidson, M.J. and Pun, K.L. (1999). "Weakly advected jets in cross-flow." *J. Hydr. Engrg*., ASCE, 125(1), 47-58.

17. Davidson, M.J. and Wang. H.J. (2002). "Strongly advected jet in a coflow." *J.Hydr. Engrg.*, ASCE, 128(8), 742-752.

18. Fischer, H.B., List, E.J., Koh, R.C.Y., Imberger, J. and Brooks, N.H. (1979). *Mixing in Inland and Coastal Waters*. Academic.

19. Ger, A.M. (1979). "Wave effects on submerged buoyant jets." *Proc. 8th Congress Int. Ass. for Hydr. Res*., New Delhi, Part C, 295-300.

20. Hasselmann, K. & al. (1973). "Measurements of wind-wave growth and sewll decay during the Joint Nosth Sea Wave Project (JONSWAP)." *Detsche Hydrographische Zeitschrift*, Reihe A (8^0), No. 12.

21. Hodgson, J.E., Rajaratnam, N. and Moawad, A.K. (1999). "Circular jets in crossflows of finite depth." *Proc. Instn Civ. Engrs Wat., Marit. & Energy*, 136, 35-42.

22. Jones, W.P. and Wille, M. (1996). "Large eddy simulation of a round jet in a cross-flow." In *Engineering Turbulence Modelling and Experiment 3* (Ed. by W. Rodi & G. Bergeles), 199-208. Elsevier.

23. Keffer, J.F. and Baines, W.D. (1963). "The round turbulent jet in a cross wind." J. Fluid Mech., 15, 481-496.

24. Kelso, R.M., Lim, T.T. and Perry, A.E. (1996). "An experimental study of round jets in cross-flow." *J. Fluid Mech*., 306, 111-144.

25. Kinsman, B. (1965). *Wind Waves*, Prentice-Hall, Englewood Cliffs, NJ.

26. Koole, R. and Swan, C. (1994). “Measurements of a 2-D non-buoyant jet in a wave environment.” *Coastal Engrg*., 24, 151-169.

27. Koole, R. and Swan, C. (1995). “Dispersion of pollution in a wave environment.” Proc. 24th Int. Conf. Coastal Engrg, Kobe, Japan 1994, 3, 3071-3085..

28. Kuang, J., Hsu, C.T., Qiu, H. (2001). “Experiments on vertical turbulent plane jets in water of finite depth.” *J. Hydr. Engrg.*, ASCE, 127(1), 18-26.

29. Kwan, K.H. and Swan, C. (1997). “Near-field measurements of a buoyant jet in waves and currents.” Proc. Coastal Engrg Conf., ASCE, NY, USA, v4, Part 4, 4569-4582.

30. Kwan, S.H. and Swan, C. (1998). “Numerical simulations of a jet in a wave-induced oscillatory flow.” *Proc. 2nd Int. Sym. Environmental Hydraulics*, Hong Kong, 173-178.

31. Lam, K.M. and Chan, C.H.C. (2002). “Time-averaged mixing behaviour of circular jet in counterflow: velocity and concentration measurements.” *J. Hydr. Engrg.*, ASCE, 128(9), 861-865.

32. Lam, K.M. and Xia, L.P. (2001). “Unsteady effluent dispersion in a round jet interacting with an oscillating cross-flow.” *J. Hydr. Engrg.*, ASCE, 130(7), 667-677.

33. Lee, J.W.H. and Chu, V.H. (2003). *Turbulent Jets and Plumes*, Kluwer Academic Publishers.

34. Li, C.W. and Lee, J.H.W. (1991). “Line momentum source in cross-flow.” *Int. J. Engrg. Sci*., 29(11), 1409-1418.

35. Lim, T.T., New, T.H., Luo, S.C. (2001). “On the development of large-scale structures of a jet journal to a cross flow.” *Phys. Fluids*, 13(3), 770-775.

36. List, E.J. (1982). “Mechanics of turbulent buoyant jets and plumes.” *Turbulent buoyant jets and plumes*, Pergamanon, 1-68, Ed. Rodi, W.

37. Mollϕ-Christensen, E. (1967). “Jet noise and shear flow instability seen from an experimenter’s viewpoint.” *J. Appl. Mech., Trans. ASME*, 34, 1-7.

38. Mori, N. and Chang, K.A. (2003). “Experimental study of a horizontal jet in a wavy environment.” *J. Engrg. Mech*., ASCE, 129(10), 1149-1155.

39. Morton, B.R. and Ibbetson, A. (1996). “Jets deflect in a crossflow.” *Experimenal Thermal and Fluid Science*, 12, 112-133.

40. Morton, B.R., Taylor, G.I. and Turner, J.S. (1956). “Turbulent gravitational convection from maintained and instantaneous sources.” *Proc. Royal Soc., London*, Vol. A234, 1-23.

41. Mossa, M. (2004a). “Experimental study on the interaction of non-buoyant jets and waves.” J. *Hydr. Res*., 42(1), 13-28.

42. Mossa, M. (2004b). “Behavior of nonbuoyant jets in a wave environment.” *J. Hydr. Engrg*., ASCE, 130(7), 704-717.

43. Papanicolaou, P. and List, E.J. (1988). “Investigations of round vertical turbulent buoyant jets.” *J. Fluid Mech*., 195, 341-391.

44. Pratte, W. and Baines, W.D. (1967). “Profiles of the round turbulent jets in a crossflow.” *J. Hydr. Div*., ASCE, 92, 53-54.

45. Rajaratnam, N. (1976). *Turbulent Jets*. Elsevier, Amsterdam, The Netherlands.

46. Ricou, F.P. and Spalding, D.B. (1961). “Measurements of entrainment by axisymmetrical turbulent jets.” J. Fluid Mech., 11, 21-32.

47. Sharp, J.J. (1986). “The effect of waves on buoyant jets.” *Proc. Inst. Civ. Eng*. Part 2, 81, 471-475

48. Shuto, N. and Ti, L.H. (1974). “Wave effects on buoyant plumes.” Proc. 14th Coastal Eng. Conf., pp. 2199-2209.

49. Sverdrup, H.U. and Munk, W.H. (1947). *Wind, Sea and Swell: Theory of Relations for Forecasting*, U.S. Navy Hydro. Office, Publication No. 601.

50. Wright, S.J. (1977). “Mean behaviour of buoyant jets.” *J. Hydr. Div*., 103(HY5), 499-513.

51. Xia, L.P. and Lam, K.M. (1997). “A vertical round jet issuing into an unsteady corsslfow consisting of a mean current and a sinusoidal fluctuating component.” *J. Wind Engrg & Industrial. Aerodyn*., 67-68, 843-857.

52. Xia, L.P. and Lam, K.M. (2004). “Unsteady effluent dispersion in a round jet interacting with

an oscillating cross-flow." *J. Hydr Engrg*., ASCE, 130(7), 667-677.

53. *Wastewater Engineering: Treatment, Disposal, and Reuse*. (1991). Metcalf and Eddy, NY, McGraw-Hill.

54. Yu, D., Ali, Md. S. and Lee, J.H.W. (2003). "Experiments on interaction of multiple jets in crossflow." *Proc. 16th ASCE Engrg. Mech. Conf*, Univ. of Washington, Seattle.

APPENDIX – Wave density spectrum

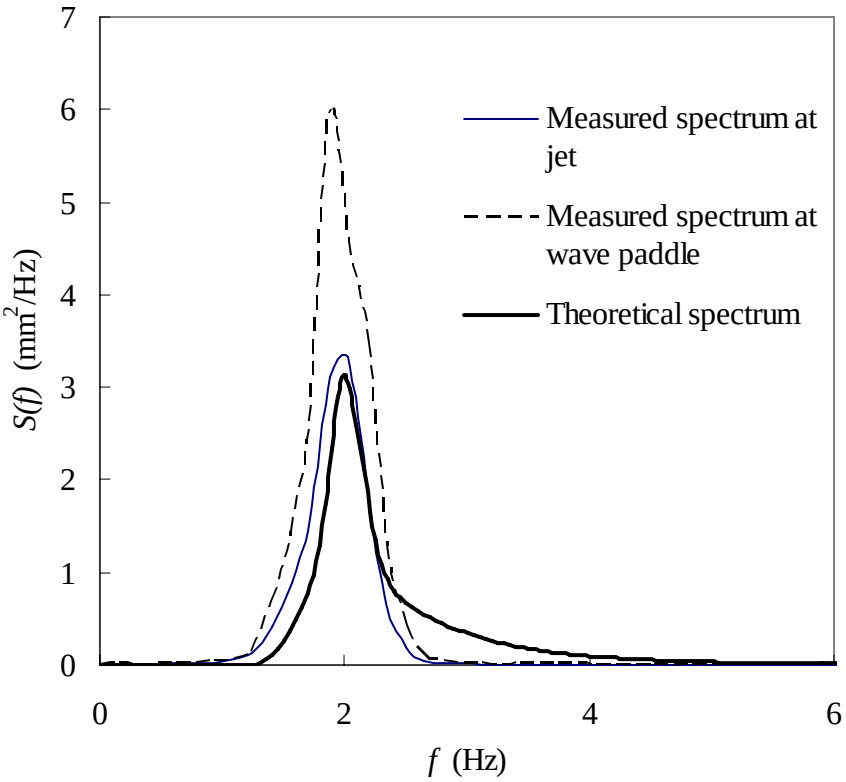

Wave condition: Case B1-1 (T_p=0.5s; H_s=5.702mm)

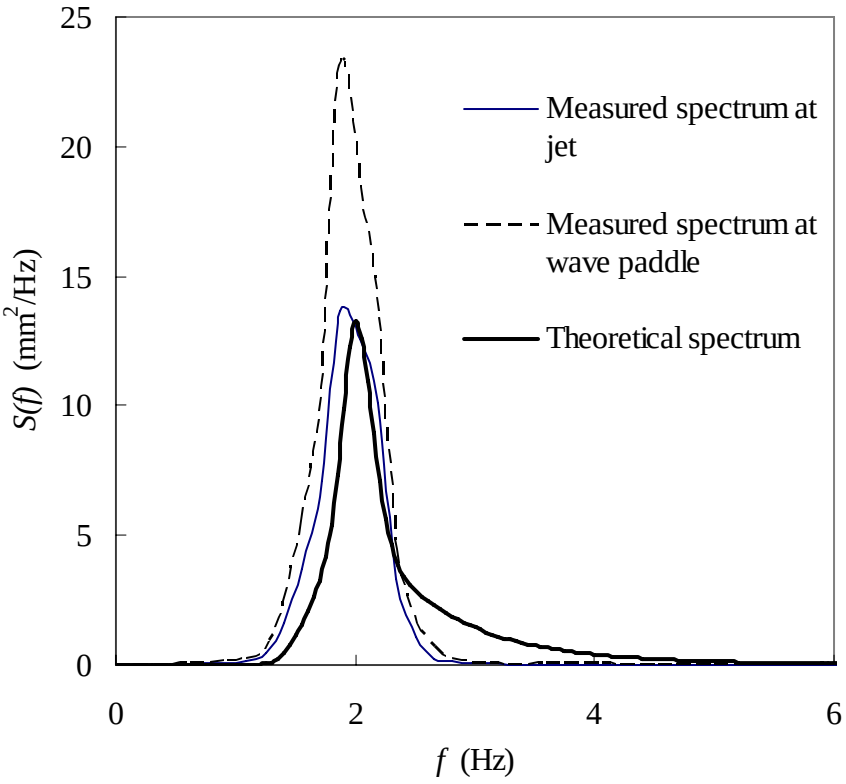

Wave condition: Case B1-2 (T_p=0.5s; H_s=11.72mm)

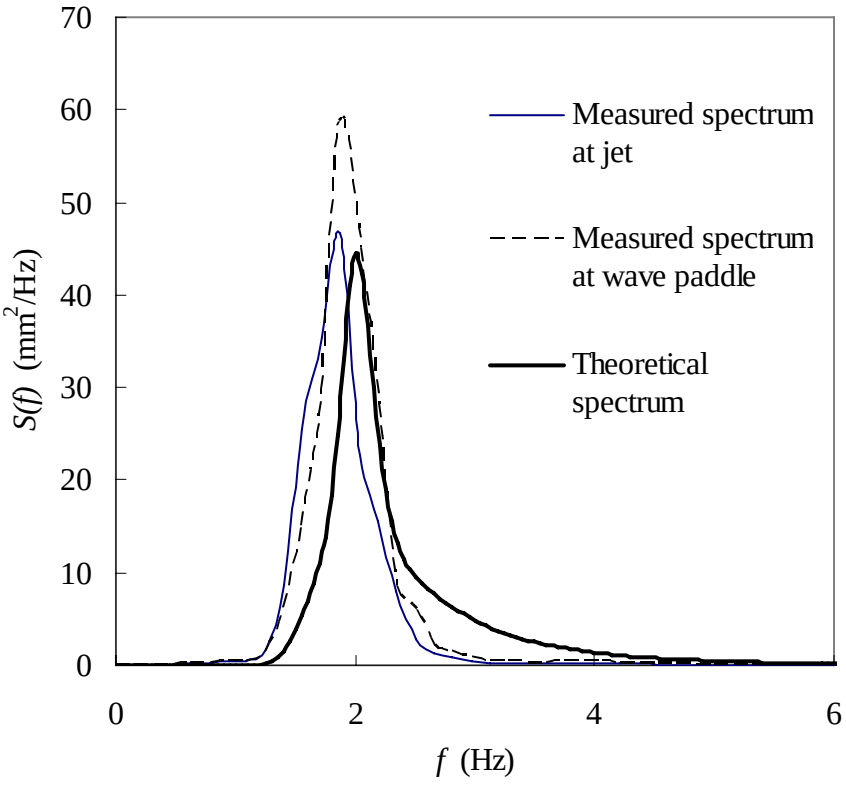

Wave condition: Case B1-3 (T_p=0.5s; H_s=21.484mm)

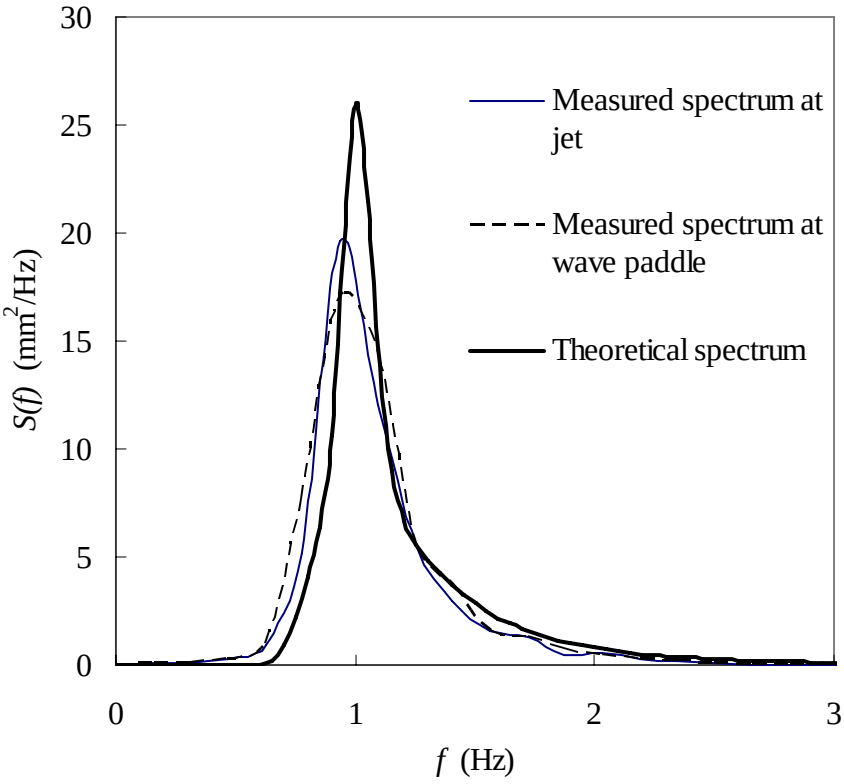

Wave condition: Case B2-1, C1-1 & E1-1 (T_p=1s; H_s=11.602mm)

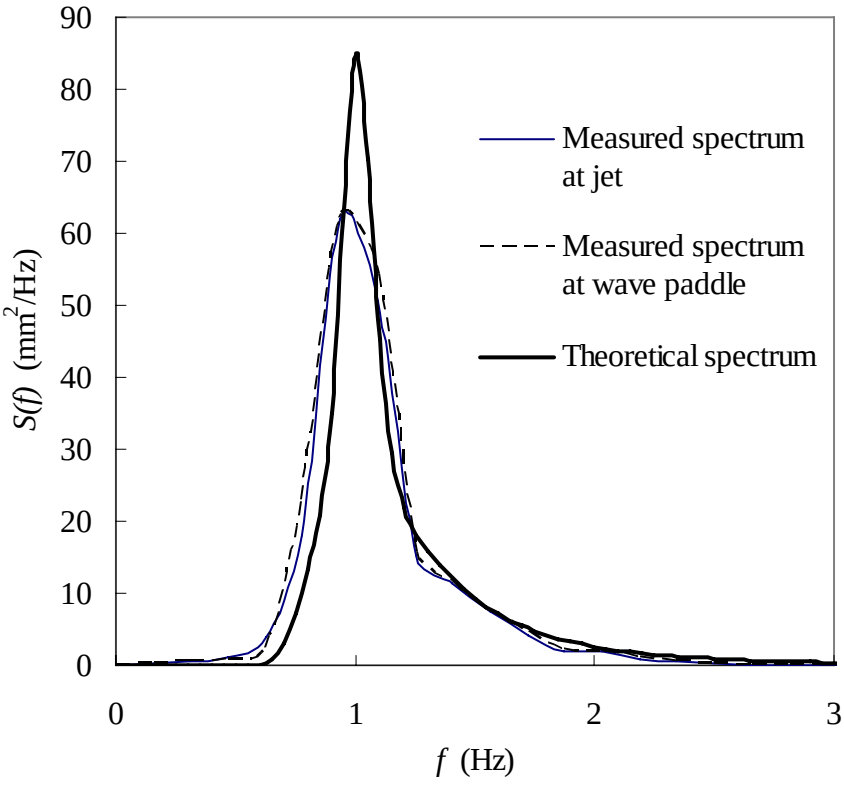

Wave condition: Case B2-2, C1-2 & E1-2 (T_p=1s; H_s=20.984mm)

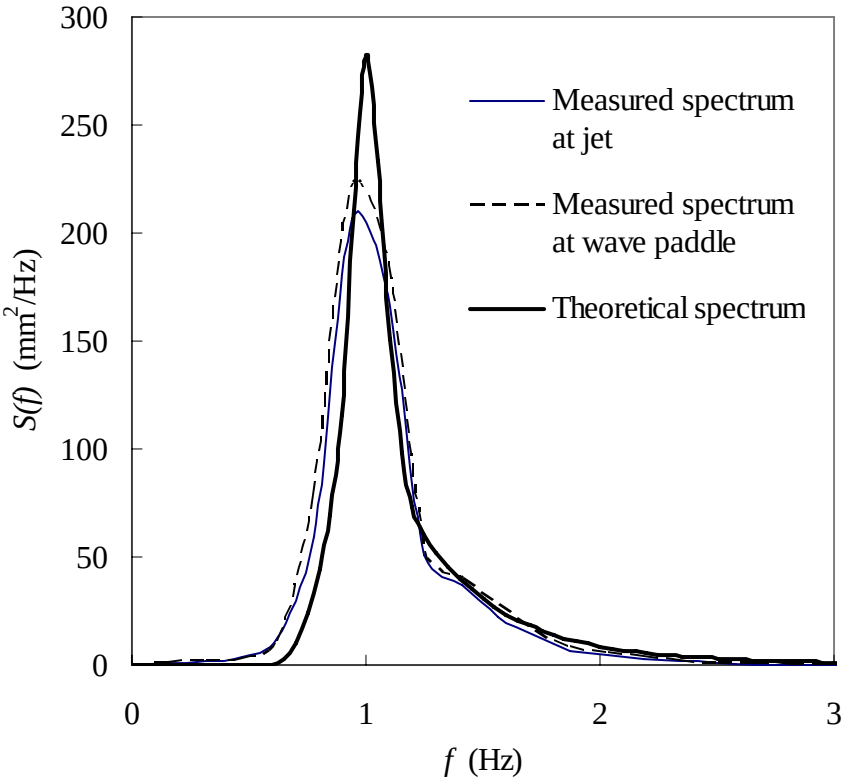

Wave condition: Case B2-3, C1-3 & E1-3 (T_p=1s; H_s=38.242mm)

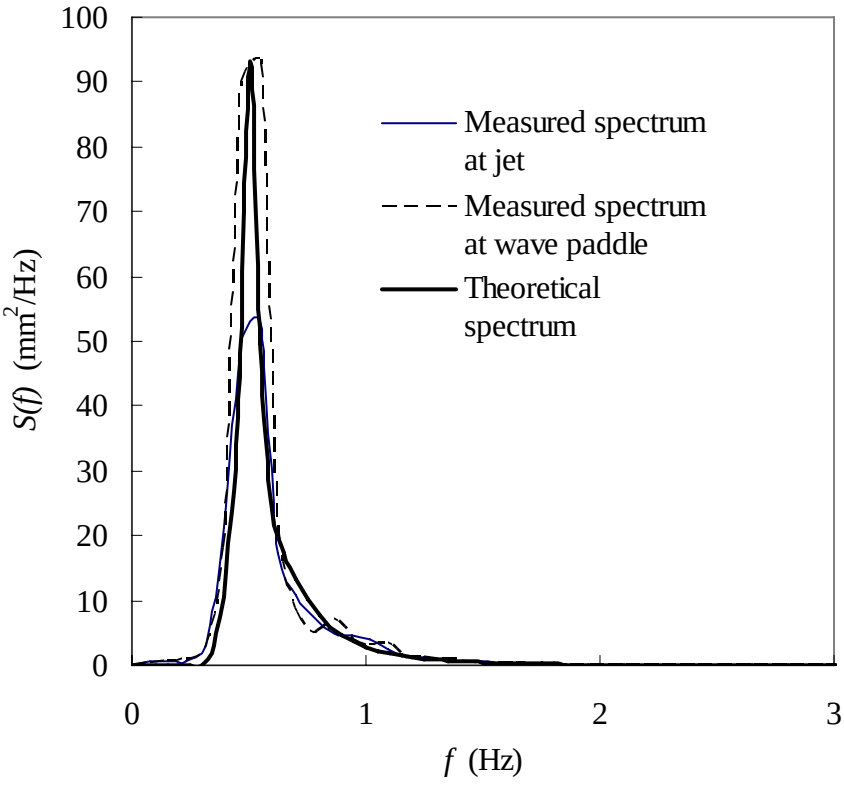

Wave condition: Case B3-1, C2-1 & E2-1 (T_p=2s; H_s=15.519mm)

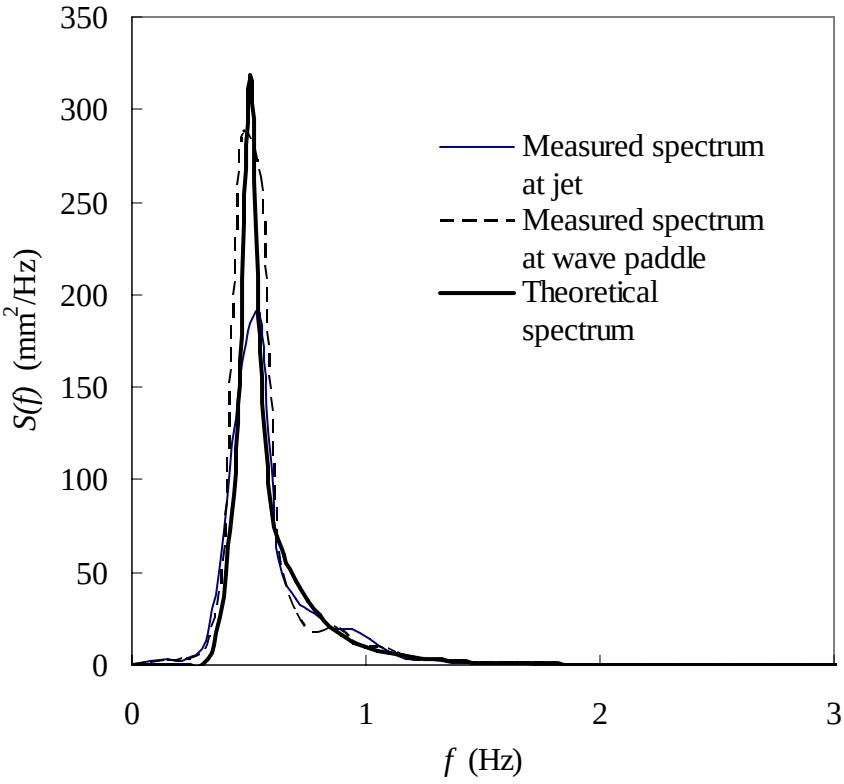

Wave condition: Case B3-2, C2-2 & E2-2 (T_p=2s; H_s=28.736mm)

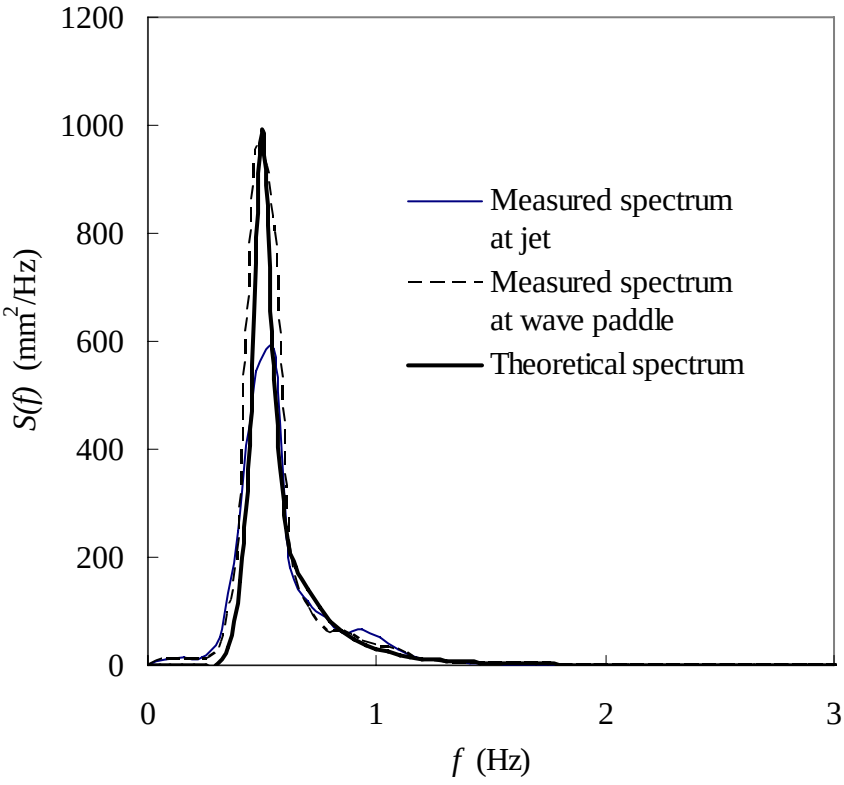

Wave condition: Case B3-3, C2-3 & E2-3 (T_p=2s; H_s=50.657mm)

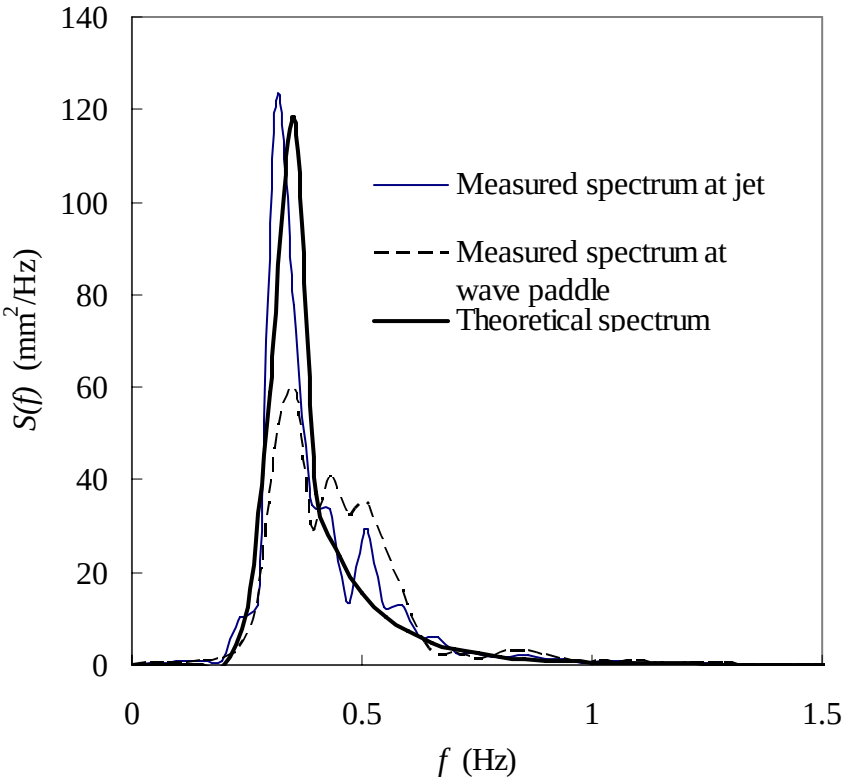

Wave condition: Case C3-1 (T_p=3s; H_s=15.745mm)

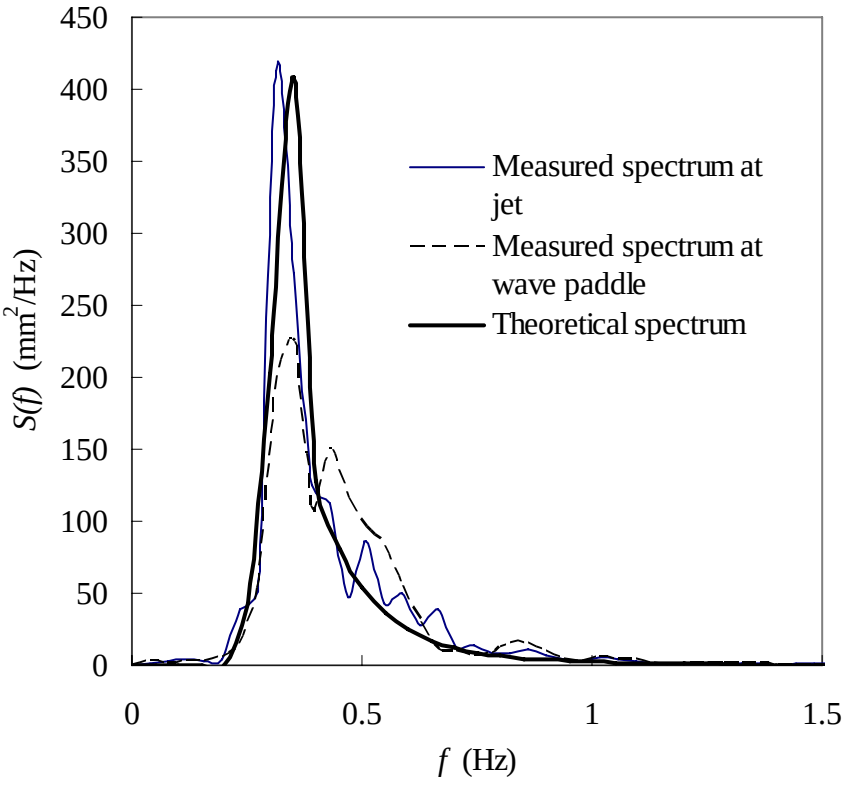

Wave condition: Case C3-2 (T_p=3s; H_s=29.212mm)

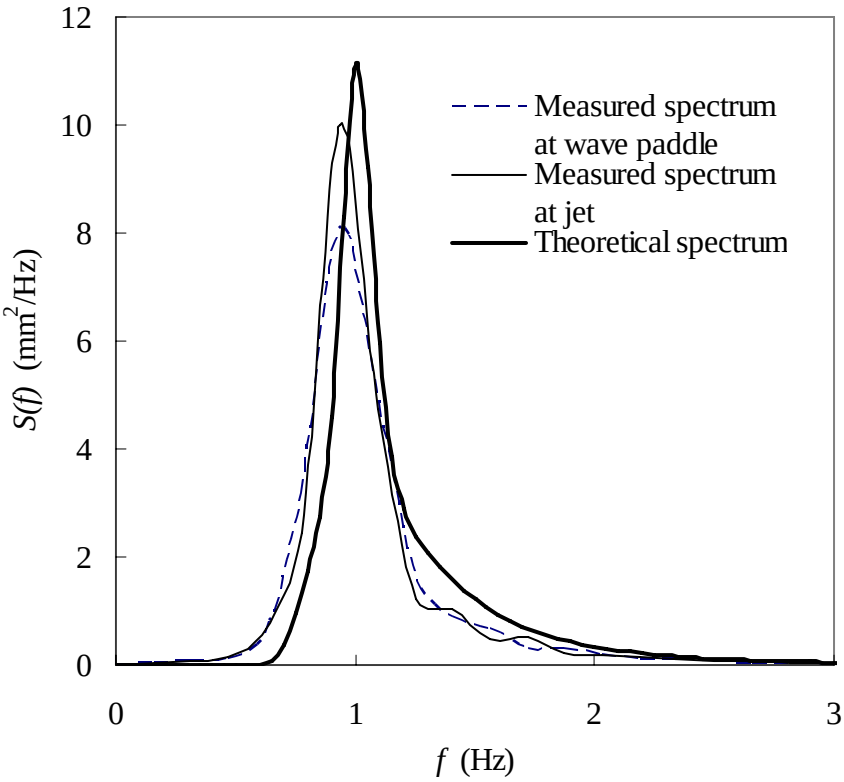

Wave condition: Case A1-1 (T_p=1s; H_s=7.601mm)

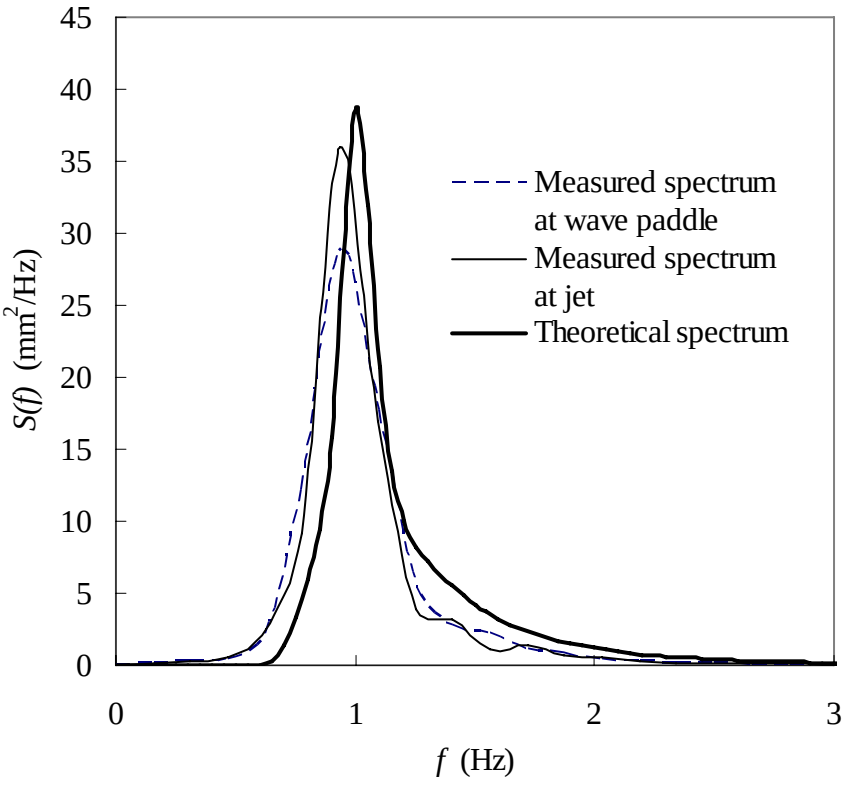

Wave condition: Case A1-2 (T_p=1s; H_s=14.167mm)

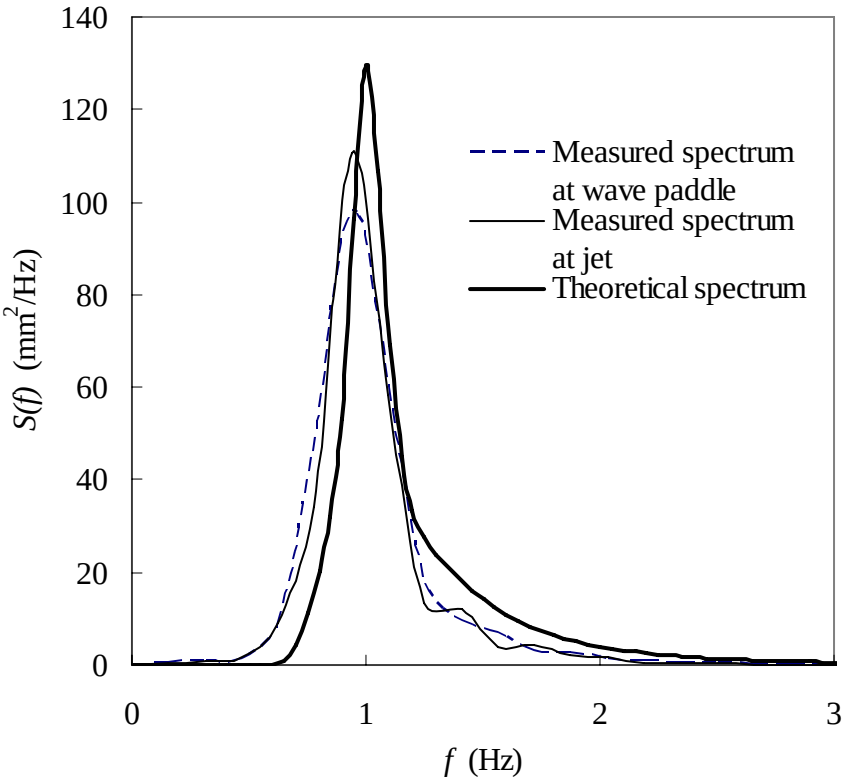

Wave condition: Case A1-3 (T_p=1s; H_s=25.905mm)

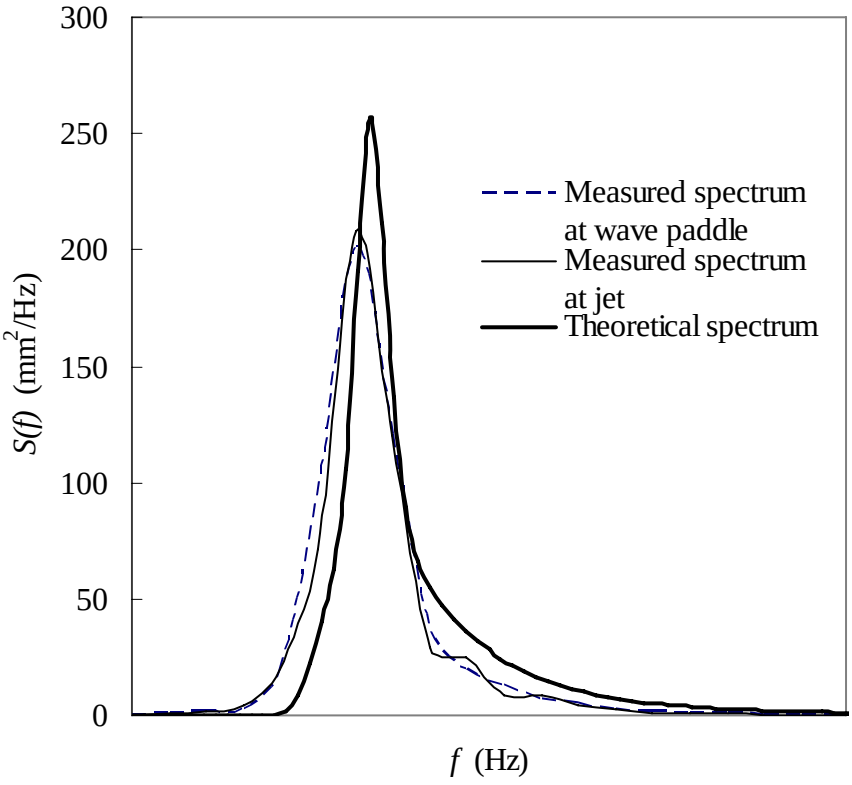

Wave condition: Case A1-4 (T_p=1s; H_s=36.465mm)

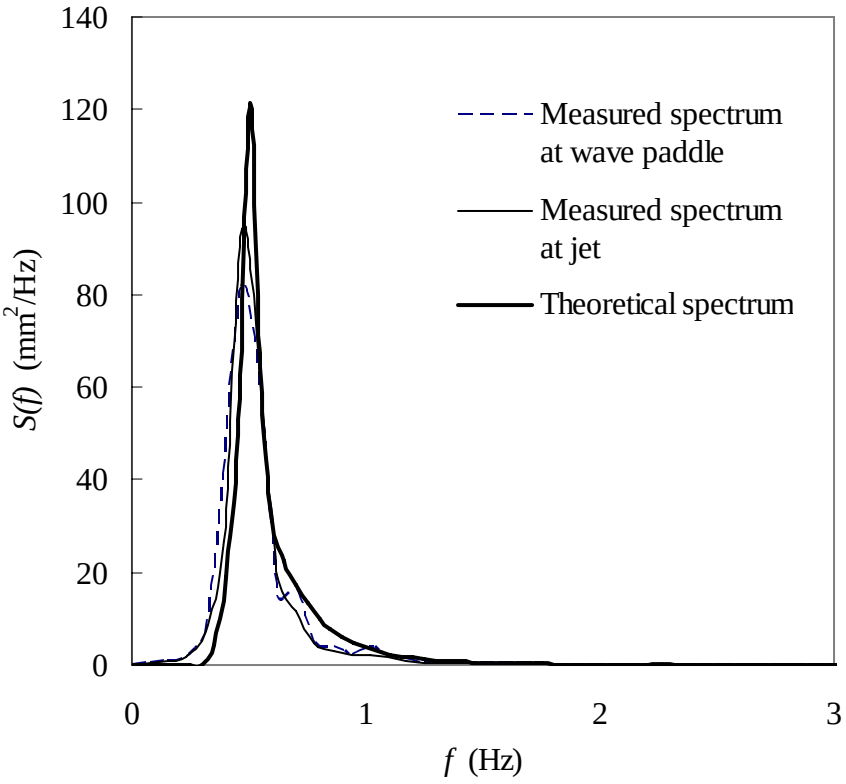

Wave condition: Case A2-1 (T_p=2s; H_s=17.716mm)

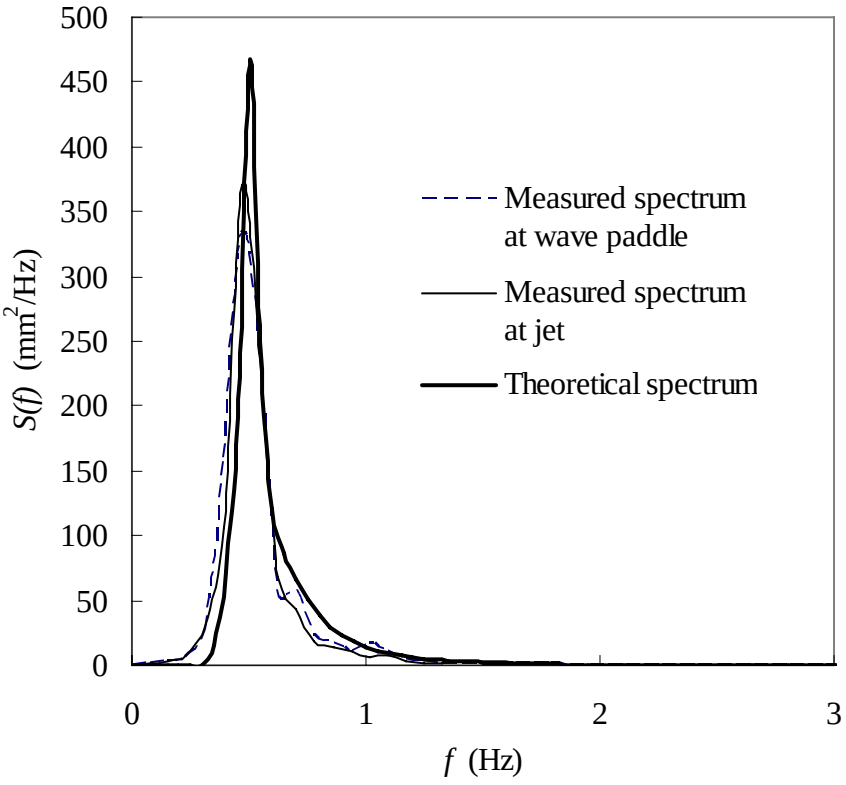

Wave condition: Case A2-2 (T_p=2s; H_s=34.805mm)

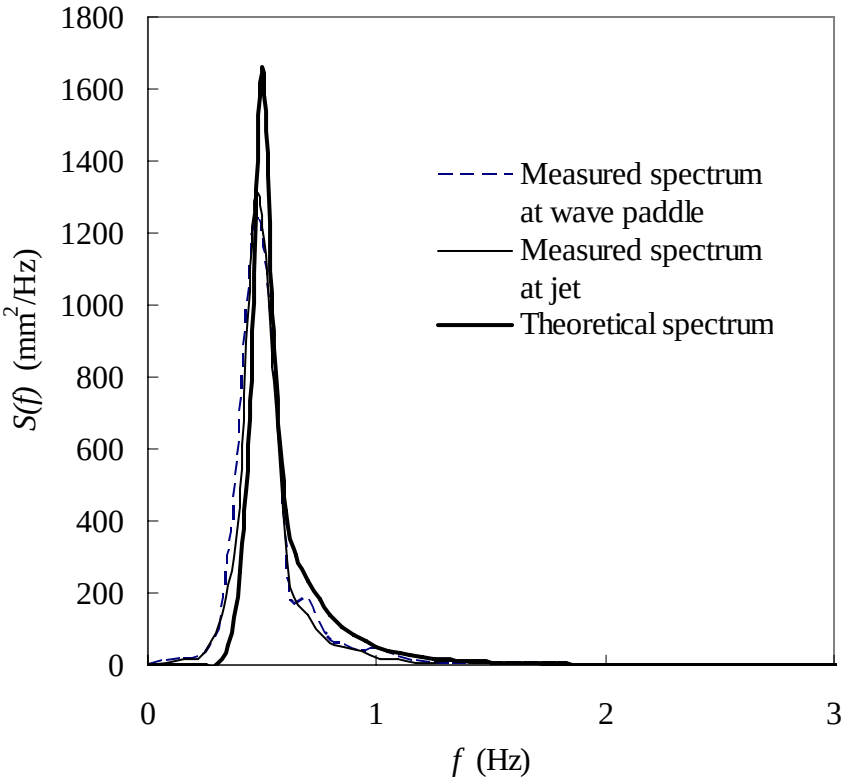

Wave condition: Case A2-3 (T_p=2s; H_s=65.577mm)

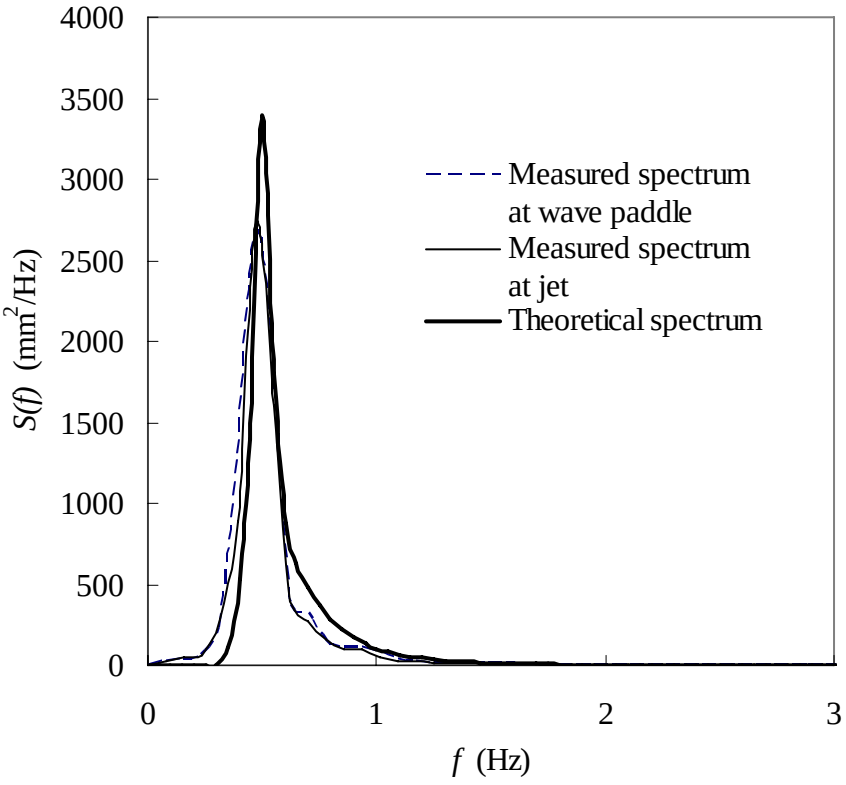

Wave condition: Case A2-4 (T_p=2s; H_s=93.707mm)

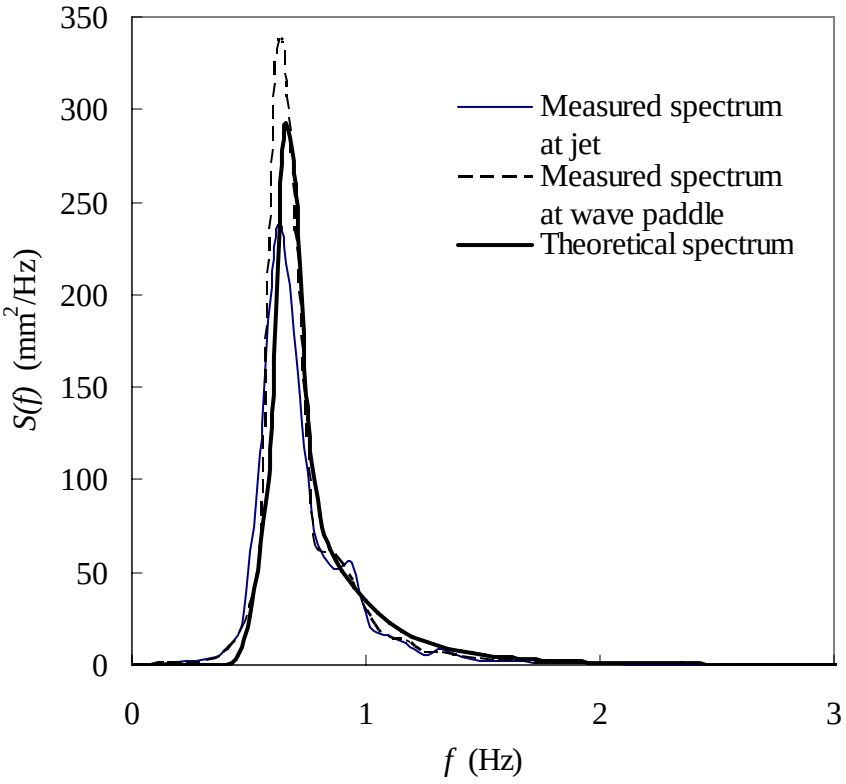

Wave condition: Case D1-1 (T_p=1.5s; H_s=32.93mm)

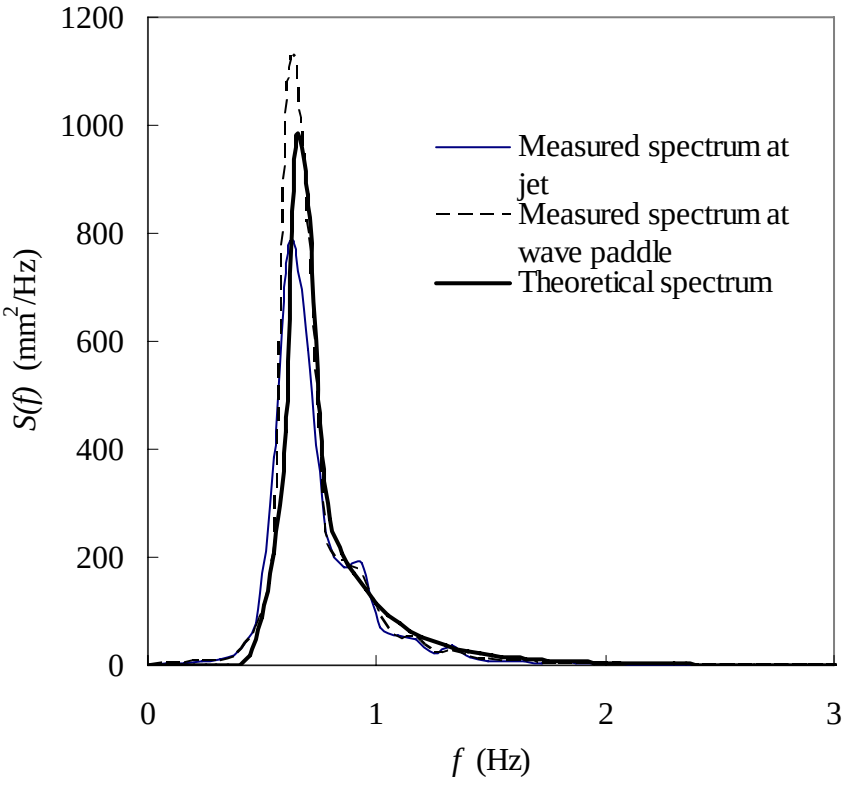

Wave condition: Case D1-2 (T_p=1.5s; H_s=60.343mm)

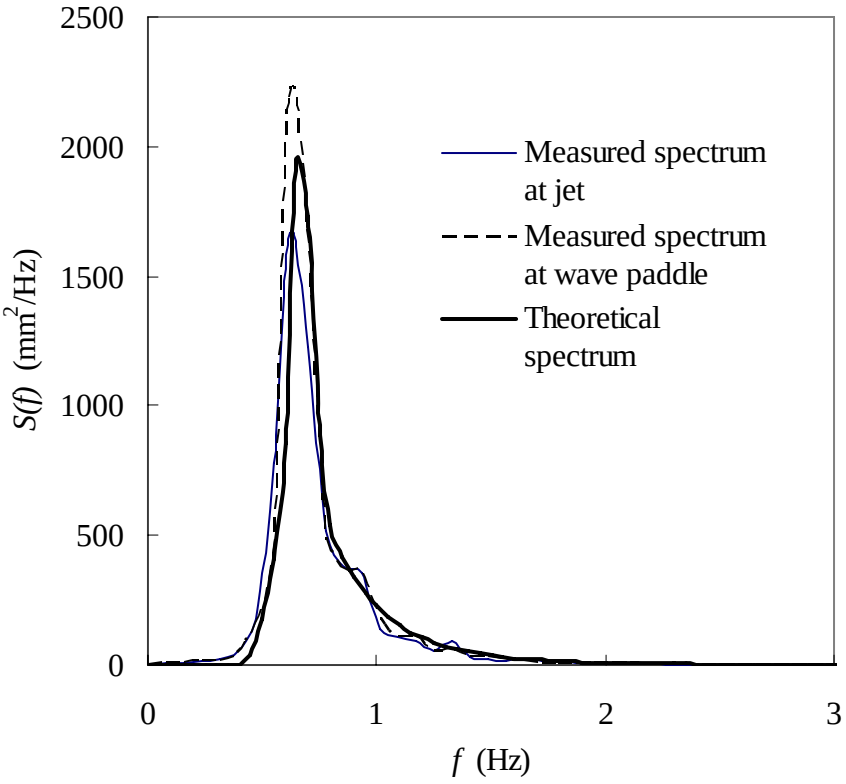

Wave condition: Case D1-3 (T_p=1.5s; H_s=85.048mm)

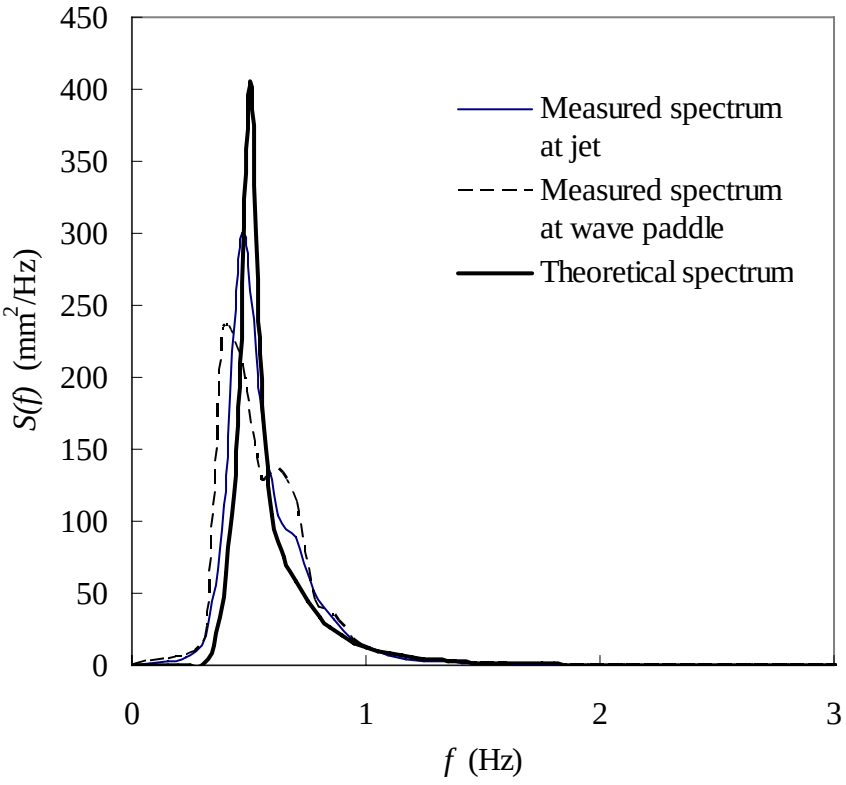

Wave condition: Case D2-1 (T_p=2s; H_s=32.416mm)

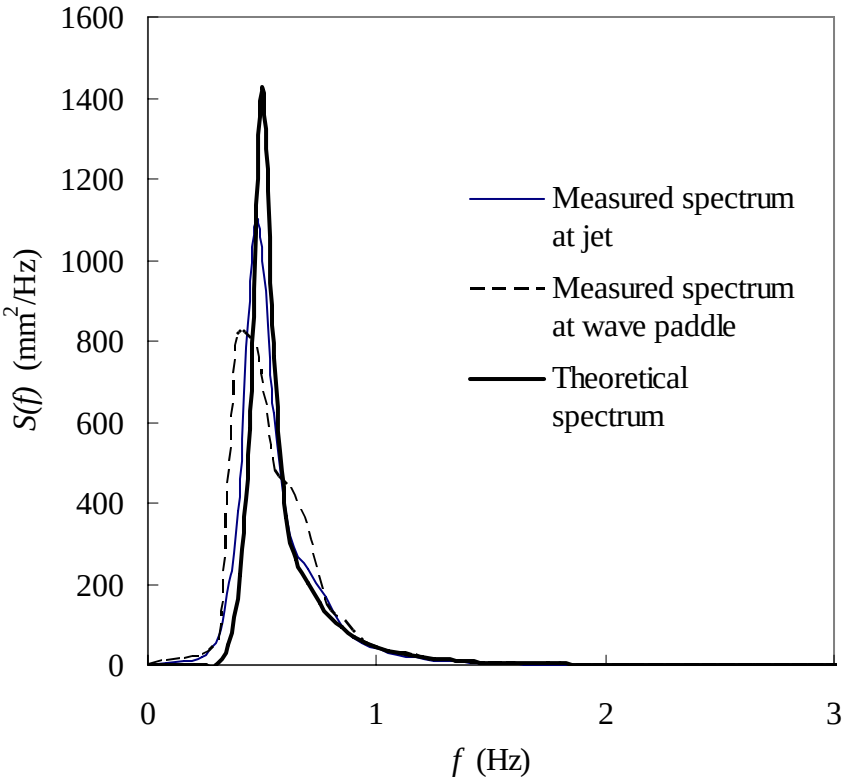

Wave condition: Case D2-2 (T_p=2s; H_s=60.728mm)

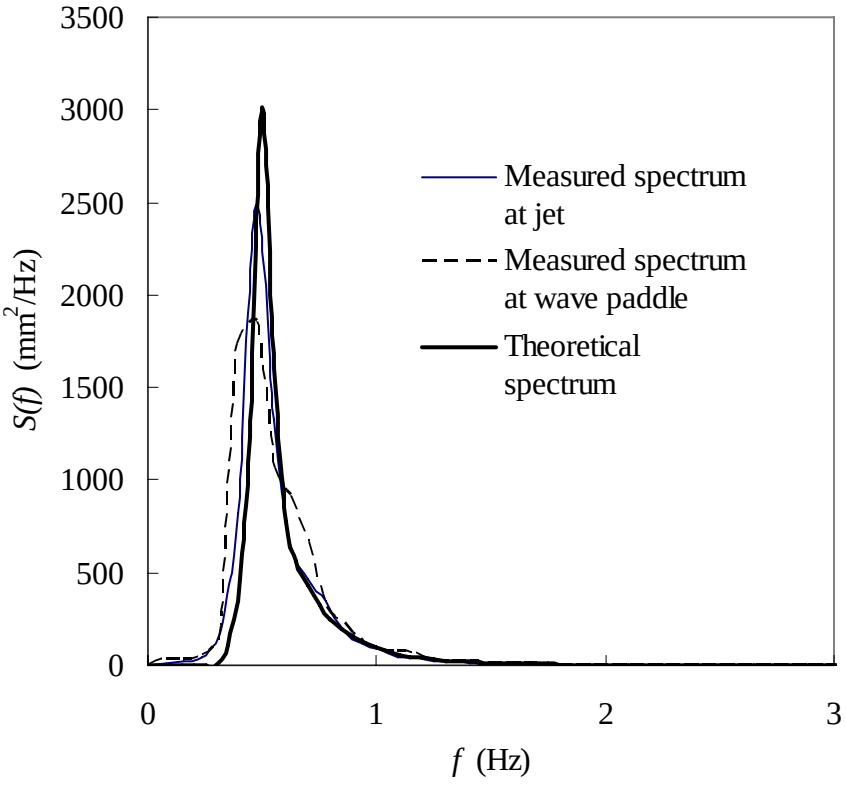

Wave condition: Case D2-3 (T_p=2s; H_s=88.35mm)